An algorithm for the reconstruction of the projected gravitational potential of galaxy clusters from galaxy kinematics

Eleonora Sarli-Waizmann

Dissertation

submitted to the

Combined Faculties of Natural Sciences and Mathematics

of the Ruperto-Carola-University of Heidelberg, Germany

for the degree of

Doctor of Natural Sciences

Put forward by

Eleonora Sarli-Waizmann

born in: Bergamo

Oral examination: December, 18th

An algorithm for the reconstruction of the projected gravitational
potential of galaxy clusters from galaxy kinematics

Referees: Prof. Dr. Matthias Bartelmann
                 Prof. Dr. Luca Amendola

A mia nonna,
che mi ha insegnato a contare

Keine Experimente!

K. Adenauer

Summary: In this work we develop a method to incorporate the information from galaxy kinematics into the reconstruction of the two-dimensional, projected gravitational potential of galaxy clusters. We start by deprojecting the observed line-of-sight velocity dispersions of cluster galaxies with an application of Bayes' theorem, the Richardson-Lucy method, requiring the assumption of a shape for the cluster. Assuming spherical symmetry, after the deprojection we obtain an effective galaxy pressure, i.e. the density-weighted radial velocity dispersions of the cluster galaxies, which is then related to the three-dimensional gravitational potential by using the tested assumption of a polytropic relation between the effective galaxy pressure and the density. The two-dimensional gravitational potential can finally be found by straightforward projection along the line of sight. We test the method with a numerically simulated tri-axial galaxy cluster and the galaxies identified therein and perform the reconstruction for three different lines of sight, initially assuming sphericity. Expanding the gravitational potential in the cluster's geometrical ellipticities yields second-order corrections to the spherical reconstruction. By comparing our results with the projected gravitational potential directly obtained from the simulation, we show that the deviation between the projected potential obtained with our reconstruction method and the potential directly extracted from the simulation is $\lesssim 10\,\%$ within approximately the virial radius ($1.5\,h^{-1}\mathrm{Mpc}$) from the cluster centre in the case of a spherical cluster and remains moderate (below $10\,\% - 25\,\%$) within the same radius in the case of an ellipsoidal cluster.

Zusammenfassung: In der vorliegenden Arbeit entwickeln wir eine Methode, um die Information aus der Kinematik der Galaxien in die Rekonstruktion des zweidimensionalen, projizierten Gravitationspotentials von Galaxienhaufen einzubeziehen. Wir beginnen mit der Deprojektion der beobachteten Geschwindigkeitsdispersionen der Haufengalaxien längs der Sichtlinie mithilfe einer Anwendung des Bayes'schen Theorems, der Richardson-Lucy-Methode, die eine Annahme über die Form des Galaxienhaufens voraussetzt. Unter der Annahme sphärischer Symmetrie ergibt die Deprojektion einen effektiven Druck der Haufengalaxien, d.h. deren Dichte-gewichtete radiale Geschwindigkeitsdispersion, die dann durch eine angenommene und überprüfte polytrope Relation zwischen dem effektiven Galaxiendruck und der Dichte mit dem dreidimensionalen Gravitationspotential in Beziehung gesetzt wird. Das zweidimensionale Gravitationspotential ergibt sich schließlich durch Projektion längs der Sichtlinie. Wir überprüfen die Methode anhand eines numerisch simulierten triaxialen Galaxienhaufens und darin identifizierter Galaxien und führen die Rekonstruktion entlang dreier verschiedener Sichtlinien durch. Indem wir das Gravitationspotential in den geometrischen Elliptizitäten entwickeln, leiten wir Korrekturen zweiter Ordnung an die sphärische Rekonstruktion ab. Ein Vergleich unserer Ergebnisse mit dem aus der Simulation bekannten Gravitationspotential zeigt, dass die Abweichung zwischen dem projizierten Potential aus unserer Rekonstruktionsmethode und dem bekannten Potential innerhalb des Virialradius ($1.5\,h^{-1}\,Mpc$) um das Haufenzentrum bei etwa 10% liegt und innerhalb desselben Radius auch bei einem rotationsellipsoidalen Galaxienhaufen vertretbar bleibt ($10\% - 25\%$).

Contents

Contents

iv

List of Figures

List of Tables

Introduction and motivation

Over the course of millennia, any model of the cosmos, seen as an entity comprising Heavens, Earth, natural phenomena, time and humanity, has mostly been rooted in religion. If one restricts oneself to an analysis of western history, it is already possible to identify two main approaches to the Ancient Greek depiction of the Universe: the one appealing to a divine order[1], such as in Homer and Hesiod, and the one anchoring the discourse on the nature, formation and composition of the world to the logical reading of natural reality, such as in Anaxagoras, Empedocles, Democritus and Aristotle. These two distinct views proceed along intertwining paths across history. Attempts to disentangle the rational description of the Universe from its religious and metaphysical aspects have met with intrinsic difficulties: the broad scope of the topic encompasses cosmogony, questions on the origins and purpose of life and human consciousness, the debate on the ultimate fate of the Universe and of mankind and, finally, knowledge arising from the collection of empirical data via careful observation of the firmament and scrutiny of the skies by laymen and mathematicians, astronomers and philosophers.

Even with the birth of the scientific method and the development of modern science, Cosmology was for a long time relegated to the rank of a largely speculative branch of knowledge and it was not until the past century that it evolved into a rigorous scientific discipline identifying the Universe as a whole as its main domain of study.

Despite its fast pace of development, though, many of the original questions about the Universe remain unanswered and many more new questions arose.

One of the most profound problems that troubles the astronomers since the last century regards the actual composition of the Universe. The latest results from the Planck mission [136] report 68.3% of dark energy, 26.8% of dark matter and 4.9% of ordinary, baryonic matter for the energy-matter budget of the cosmos. The idea of an invisible substance permeating the Universe is not new and the first account of a "dark matter" can be traced back to a paper by Fritz Zwicky in 1933. In 1970, Vera Rubin conducted what can be considered one of the first deductions of dark matter from observations. Starting from an analysis of the spectra of spiral galaxies and the study of their rotation

---

[1]The same word $\kappa o \sigma \mu o \varsigma$ in Greek stands for *order*.

curves, she noticed a discrepancy between the theoretical expectation about those curves and the actual observations. A way to resolve this conflict would have been questioning the validity of Newton's theory at large scales, another possible solution lay in admitting that another kind of non-visible matter was present in the galaxies themselves and that the actual mass of galaxies exceeded in good part the one predicted by the sole analysis of their luminous content. In 2000, Yannick Mellier and his team analysed images from the Canada-France-Hawaii Telescope's high-resolution wide-field imaging camera and published a cartography of the dark-matter distribution in a two-square-degree section of sky containing around 200,000 galaxies. This first publication led the way to a mapping of the dark-matter distribution in the local Universe. Today we know that the dark matter in galaxies is at least ten times more than the visible matter. The ratio in galaxy clusters is even more extreme: the dark matter content exceeds by thirty times that of the luminous matter.

The success of the cosmological standard model implies that massive, gravitationally bound cosmic objects such as galaxy clusters should be dominated by dark matter and characterised by its properties. Numerical simulations routinely find that the dark-matter distribution in galaxy clusters is expected to exhibit universal properties, for example its radial density profile and its degree of substructure. For our understanding of the nature of dark matter, it is important to test whether the mass distribution in real clusters confirms the expectations from simulations.

Galaxy clusters are much less affected by baryonic physics than galaxies since the baryonic cooling time exceeds their lifetime except in their innermost cores. Thus, they represent an important probe for the nature of dark matter and play a key role in testing our current understanding of cosmic structure formation.

A growing number of increasingly wide surveys in a broad range of wavebands provide or will soon provide precise information on large galaxy-cluster samples. For instance, one of the goals of the Cluster Lensing And Supernova survey with Hubble (CLASH, [138]) is the mapping of dark matter in clusters based on strong and weak gravitational lensing. The Dark Energy Survey (DES, [4]), started in September 2013, will combine several probes of dark energy, and ESA's Euclid mission [89] will mainly focus on weak gravitational lensing measurements and galaxy clustering, but will also provide data on galaxy clusters and the integrated Sachs-Wolfe effect. The Kilo Degree Survey (KiDS) aims at mapping the matter distribution in the Universe by means of weak gravitational lensing and photometric redshift measurements [46].

Strong and weak gravitational lensing are widely used as an effective tool for reconstructing the projected mass or gravitational-potential distributions in galaxy clusters [18, 33, 37, 43, 105, 106, 109]. Lensing effects are due to light deflection alone and thus (largely) insensitive to equilibrium and stability assumptions. They can be completely characterised by the scaled and projected Newtonian gravitational potential of the lensing matter distributions and thus most directly constrain the projected, two-dimensional
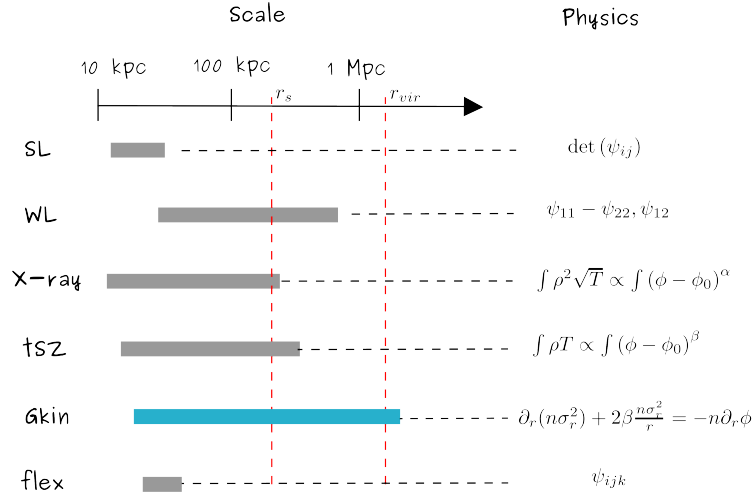
Figure 1.1: A quick look at the physics shows that all of these quantities constrain the projected gravitational potential in a different way: strong lensing constrains the determinant of the Hessian matrix of the lensing potential, ψ, i.e. the matrix of the second-order partial derivatives of ψ; weak lensing constrains combinations of the second derivatives of ψ; X-rays and the thermal Sunyaev-Zel'dovich effect provide the relation reported in the figure; galaxy kinematics constrain the gradient of the gravitational potential; gravitational flexion constrains the third-order derivatives of ψ. The relation between galaxy kinematics and lensing is the main topic of this work and will be investigated further in Chapters 7 and 8.

gravitational potential. Non-parametric, adaptive methods have been developed and are now routinely being applied to recover cluster potentials. However, clusters provide a multitude of other observables through X-ray emission, the thermal Sunyaev-Zel'dovich effect and galaxy kinematics which can be used to investigate their internal structure.

X-ray emission and the thermal Sunyaev-Zel'dovich effect constrain respectively the temperature, the density and the pressure of the intracluster gas, galaxy kinematics constrain the gradient of the gravitational potential and gravitational lensing constrains the curvature of the potential (i.e. the gravitational tidal field). The essential implication of these considerations is that each of these quantities provides information on the projected gravitational potential at different scales, therefore allowing us to cover a broad range of radii (from few kpc to over 1 Mpc) and thus to construct a much more comprehensive picture of galaxy clusters, as sketched in Fig. 1.1.

Some of these observables have already been combined in joint methods to constrain the projected gravitational potential (strong and weak gravitational lensing, X-ray emission and thermal Sunyaev-Zel'dovich effect, for instance) but what is missing is

a consistent method to jointly constrain the projected gravitational potential of galaxy clusters with as little prejudice as possible by making use of all these observables at once. This is certainly an enticing prospect and represents the overarching theme of this thesis. In particular, we will aim at devising an algorithm for the reconstruction of the projected gravitational potential starting from some of the available observables listed in Fig. 1.1.

As mentioned above, combining all observables has the substantial advantage that all available information is bundled in single models, and that a range of linear scales covering approximately two orders of magnitude can faithfully be bridged. We will start by introducing the derivation of the projected, gravitational potential of a cluster from its surface brightness using X-ray data as an input and, in a second moment, we will sketch the steps needed to derive it from the observed relative changes in the intensity of the CMB photons through the thermal SZ effect using SZ data. Subsequently, we will focus on the relation between galaxy kinematics and gravitational lensing and present in detail the development and implementation of an algorithm for the reconstruction of the projected, gravitational potential of a galaxy cluster from the line-of-sight projections of the velocity dispersions of its members with the goal of inserting this work into a broader, joint method accounting for information from all available cluster observables in the future. We will also argue that, despite the physics describing these three separate phenomena is profoundly different, it is possible to exploit their formal analogy to develop one single reconstruction method.

A roadmap of the content of the following chapters can be sketched in this way. The theoretical and physical framework for research on galaxy clusters is described in Chapter 2, which is meant to offer a broad, panoramic view on cosmology. Chapter 3 discusses the main issues in introducing a basic model of structure formation and defining a density profile and a mass function for galaxy clusters, quantities that are central in any attempt to describe them in a comprehensive way. The chapter ends with a brief account of the observational properties of galaxy clusters that will be used in the course of this work. The dynamical structure of clusters of galaxies is reviewed in Chapter 4. The key idea which our reconstruction algorithm is based on is introduced in Section 5.1 and the method for the reconstruction of the projected gravitational potential of galaxy clusters from the X-ray emission of thermal gas or its interaction with CMB photons is outlined in the second part of Chapter 5. Sect. 5.3 presents the results for X-ray data and section 5.4 delineates the steps necessary to implement the algorithm in the case of the thermal SZ effect. Chapter 6 briefly presents the Richardson-Lucy deprojection method, which will be used to retrieve three-dimensional quantities from projected ones in order to insert them in the reconstruction algorithm. In Chapters 7 and 8, the problem of reconstructing the projected gravitational potential starting from the projected velocity dispersions of the cluster galaxies along the line of sight is discussed. Chapter 7 presents the formulation of the reconstruction algorithm for a spherical galaxy cluster,

while the assumption of spherical symmetry is relaxed in Chapter 8 in favour of triaxiality. The main results of this thesis are summarised in the Conclusions.

Part of the content and of the ideas presented in this thesis has appeared already, or will soon appear, in the following publications:

- D. Stock, S. Meyer, E. Sarli, M. Bartelmann, I. Balestra, C. Grillo, A. Koekemoer, A. Mercurio, M. Nonino, P. Rosati. *The projected gravitational potential of the galaxy cluster MACS J1206 derived from galaxy kinematics.*, submitted to A&A, 2015

- C. Tchernin, C. L. Majer, S. Meyer, E. Sarli, D. Eckert, M. Bartelmann. *Reconstructing the projected gravitational potential of Abell 1689 from X-ray measurements.*, A&A, 574, id.A 122, 7 pp., 2015

- E. Sarli, S. Meyer, M. Meneghetti, S. Konrad, C. L. Majer, M. Bartelmann. *Reconstructing the projected gravitational potential of galaxy clusters from galaxy kinematics.*, A&A, 570, id.A 9, 9 pp., 2014

- C. L. Majer, S. Meyer, S. Konrad, E. Sarli, M. Bartelmann. *Reconstruction the mass distribution of galaxy clusters from the inversion of the thermal Sunyaev-Zel'dovich effect.*, in prep.

- S. Konrad, C. L. Majer, S. Meyer, E. Sarli, M. Bartelmann. *Joint reconstruction of galaxy clusters from gravitational lensing and thermal gas. I. Outline of a non-parametric method.*, A&A, 570, id.A 118, 7 pp., 2013

*He who does not know what the world is, does
not know where he is. And he who does not
know for what purpose the world exists, does
not know who he is, nor what the world is.*

Marcus Aurelius

Foundations of cosmology and cosmic structure formation

A debate on the origins and structure of the Universe is present in every civilisation and has been declined in various ways throughout all human history. For millennia, though, religious beliefs and scientific understanding of the world have been blended together in a discipline that combined observations with faith. Modern cosmology, in its interpretation as the branch of astrophysics devoted to the study of the Universe as a whole, is a very young science and took its actual form only over the past century. The purpose of this chapter is to give an idea of the central concepts and discoveries at the base of modern Cosmology. Section 2.1 provides a very broad historical overview on the milestones that shaped the evolution of our current understanding of the Universe. Section 2.2 deals with the theoretical framework (Sect. 2.2.1 to 2.2.5), the definitions of distances (Sect. 2.2.7) and the parameters (Sect. 2.2.6) describing a homogeneous Universe and presents the latest constraints obtained on them. Sect. 2.3 is meant to introduce the basic theory illustrating the formation of cosmic structures: we start from motivating the necessity of introducing inhomogeneities in our picture of the evolution of the Universe and we proceed with an outline of the main tools at our disposal to describe the growth of perturbations in Sect. 2.3.1. We discuss their statistical properties in Sect. 2.3.2.

2.1   An expanding Universe

The birth of modern Cosmology is traditionally associated with the formulation of Einstein's general theory of relativity in 1915 [59].

It is arguable whether pinpointing a given time in History in order to identify a turning point in a specific discipline would not result in a pure intellectual exercise, given the intrinsic non-linearity that characterises the development of physical sciences in general. In the particular case of Cosmology, though, it is interesting to notice how such an arbitrary and debateable choice rests on the grounds of the conceptual pitfalls

hidden in the *principle of inertia*, one of the cornerstones of Newtonian dynamics.

Newton's theory postulated the existence of preferred motions in space, defined as inertial reference frames. The simultaneous presence of both preferred reference frames and a relativity principle in the theory led to an insoluble contradiction and codified the distinction between inertial and non-inertial motions. In the latter case, the laws of dynamics need the introduction of absolute space as a privileged reference frame with respect to which definitions like the one of uniform and rectilinear motion could hold. Newton labeled the absolute space *sensorium dei* [144], God's sensory organ, with respect to which bodies could be declared truly moving or truly at rest.

Since the publication of Isaac Newton's work, *Philosophiæ Naturalis Principia Mathematica* [122], in 1687, the concepts of absolute space, time and motion (including rotations and accelerations) became pillars of the broadly accepted dynamical description of the world until the end of the 19th century and were hardly challenged, with the notable exceptions of Gottfried Wilhelms Leibniz [41], George Berkeley [20] and Carl Neumann [120]. In the *General Scholium* appended to the *Principia* in 1713, Newton described the famous rotating bucket argument, designed to support his position in favour of absolute motion. The experiment is prepared by hanging a bucket filled with water to a very long cord attached to the ceiling and turning the cord around until it is strongly twisted. When the water is at rest with the bucket, the cord is left unwinding and the bucket starts rotating in the opposite direction because of the torsion of the cord. Newton observed four distinct stages of this process. In the very first one, the bucket is standing still, the cord is tightly twisted and the water surface is flat. At this initial stage, there is no deformation and no relative motion between the bucket and the water. In the second moment, the cord is permitted to unwind and the bucket starts rotating. Since the motion of the bucket is not yet communicated to the water, there is no deformation of the surface of the water but there is a relative motion between the bucket and the water. In the third phase, the water starts rotating and slightly ascending the walls of the bucket. In the fourth and last phase, the increased rotation will impress a concave shape to the surface of the water, deformation that will remain even when the water and the bucket will have the same angular velocity and therefore no relative motion.

From this experiment Newton concluded the impossibility to identify a correlation between the deformation of the water surface and the relative motion because one can observe no deformation both when there is and when there is not a relative motion between water and bucket. This observation led him to postulate the existence of absolute space as a reference frame for the centrifugal forces.

For more than a century, inertia was seen as an absolute property of nature. This principle remained, as well, in the attempt of a mechanical interpretation of the electromagnetic phenomena and in the aether's theory.

Mach's principle. In the decades following the publication of the *Principia*, several criticisms to Newton's argument were expressed. All of them, though, proved

inconclusive. The very first cogent objection to the dominating idea of absolute space was articulated by Ernst Mach. In a treatise published in 1872, *History and Root of the Principle of the Conservation of Energy* [100], he manifested his conviction that the law of inertia had been wrongly interpreted:

If we think of the Earth at rest and the other celestial bodies revolving around it, there is no flattening of the Earth ... at least according to our usual conception of the law of inertia. Now one can solve the difficulty in two ways; either all motion is absolute, or our law of inertia is wrongly expressed ... I [prefer] the second.

In 1893 [99] he directly addressed the bucket argument and asserted that:

Newton's experiment with the rotating vessel of water simply informs us, that the relative rotation of the water with respect to the sides of the vessel produces no noticeable centrifugal forces, but that such forces are produced by its relative rotation with respect to the mass of the earth and the other celestial bodies. No one is competent to say how the experiment would turn out if the sides of the vessel increased in thickness and mass till they were ultimately several leagues thick. The one experiment only lies before us, and our business is, to bring it into accord with other facts known to us, and not with the arbitrary fictions of our imagination.

In other words, Mach identified the origin of centrifugal forces as gravitational and referred them to the action of the mass of celestial objects on other masses.

The notion that the distribution and motion of the matter in the Universe determines the inertial reference frames was later designated by Albert Einstein as *Mach's principle* [62, 128].

General Theory of Relativity. With the formulation of the special theory of relativity [58], it became clearer that the fundamental question triggered by Newton's interpretation of the concept of inertia ("with respect to what reference frames are the laws of dynamics valid?") was wrongly posed. Newton's theory of dynamics could hold without absolute space as its axiomatic basis and offered a method to construct an infinite class of equivalent inertial frames. Despite offering profound modifications to the "theory of space and time", special relativity was not immune to the same "epistemological defect" [60]: in a similar fashion to their predecessor, absolute space, inertial frames singled out a preferred state of motion and were not an "observable fact of experience". In Einstein's words, "it conflicts with one's scientific understanding to conceive of a thing which acts but cannot be acted upon".

This realisation accompanied Einstein in his work for more than a decade, during which two major moments can be identified. The first achievement is the formulation of the principle of equivalence as described in a letter to Sommerfeld written

on 5th November 1908. A vital assumption is the equivalence of gravitational (*schwere*) and inertial (*träge*) masses (letter to Wien, 10 July 1912 [63]). The second breakthrough is the final presentation of his new theory of gravity in a series of lectures to the Prussian Academy of Sciences, the first of which was given on the 25th of November 1915 [59] and introduced the field equations describing the dynamics of the gravitational field. He published them in 1916 in the Annalen der Physik in an article titled "Die Grundlage der allgemeinen Relativitätstheorie"[1][60]. There he noted that a definite answer to the lingering problem of inertia could be offered by a theory that would focus on observable facts alone, relative motions. Instead of limiting the validity of physical laws to the class of inertial frames, of which it would be impossible to say whether they exist independently of the rest of the Universe, the relativity principle should be extended and the new theory should embrace the postulate of *general covariance*:

> *the laws of nature must be fully independent of the*
> *choice of any coordinate system or reference frame.*

This assumption implies that the physical laws must be covariant for all possible transformations and substitutes the inertial frames with a class of freely-falling, non-rotating reference frames, that are locally inertial.

The concept of local inertial frames is a direct consequence of the second pillar on which Einstein's theory of gravity was built, the principle of equivalence:

> *an accelerated, non-rotating laboratory in the absence of gravitational effects*
> *and a non-accelerated laboratory endowed with a gravitational field are*
> *equivalent.*

The combination of general covariance and principle of equivalence is the backbone of this new worldview. On one hand, general covariance marks the exquisitely geometric character of general relativity, whose geometric arena is differential geometry. On the other hand, the equivalence principle prescribes that a locally constant and linear (i.e. non-rotating) acceleration field is locally indistinguishable from the gravitational field.

The role of the masses and of energy is now to curve the space-time, i.e. a pseudo-Riemannian manifold whose metric tensor is treated as a dynamical field, in their surroundings and the law of gravitation turns into the structure condition of a curved and extremely flexible environment.

---

[1]The Foundation of the General Theory of Relativity

Einstein-de Sitter. The years between 1915 and 1930 saw the publication of some of the most relevant and influential theoretical works in the history of relativistic Cosmology. The formulation of the field equations paved the way to the application of general relativity to construct cosmological models. Driven by the persuasion that a Universe obeying Mach's principle was epistemologically preferable, Einstein [61] ensured that his field equations would not have an acceptable solution in the absence of matter by including the term $-\lambda g_{\mu\nu}$ in the left-hand side, where the coefficient λ was a "temporarily unknown universal constant"[2], today known as *cosmological constant* and denoted with the Greek capital letter Λ. The effectively repulsive cosmological term was supposed to counterbalance the effects of gravity and enforce a static and closed cylindrical Universe, in which Einstein believed Mach's principle would hold [21], without destroying the general covariance. The importance of Mach's principle in the development of general relativity and of Einstein's cosmological model is still matter of debate. [3] The essential point is that Mach managed to turn the attention from the motion of a body with respect to another body to the study of the Universe as a whole, effectively initiating the sequence of considerations and analyses that led to the birth of modern Cosmology.

Less than seven weeks after the paper by Einstein was published, the Dutch astronomer Willem de Sitter [48, 49], with whom Einstein had frequently corresponded in the previous months, presented an exact solution of the generalised field equations[4] that proposed a non-Machian cosmological model based on a high degree of space-time symmetry. De Sitter's spherical solution offered the possibility of a Universe in which the presence of matter was not required and that stood in intense anthitesis with Einstein's world view.

Friedmann-Lemaître-Robertson-Walker. In 1922 the Russian Alexander Friedmann[5] sent to Paul Ehrenfest a manuscript accompanied by a letter in which he asked him to publish his paper about the curvature of space. An excerpt of this letter[6] reads:

I'm sending you a brief note regarding the question about the possible shape of the universe more general than the cylindrical world of Einstein, and the spherical

---

[2]Einstein [61] introduced λ first in the Poisson equation, i.e. into Newtonian theory, and subsequently in the field equations.

[3]Einstein noted later that Mach's principle played a purely heuristic role in the development of general relativity, for instance. For a very interesting account of the debates that accompanied the birth of modern cosmology, the reader is referred to [21].

[4]Therefore including the cosmological term.

[5]The presence of multiple spellings of his surname is in part due to the confusion made from the editors of *Die Zeitschrift für Physik* who typed Friedmann in 1922 and Friedman in 1924. The modern transliteration into English of his last name is Fridman but we will adopt the original one of 1922 as it is still the most commonly used.

[6]https://www.lorentz.leidenuniv.nl/history/Friedmann_archive/

world of De Sitter; aside from these two cases there appears also a world, the space of which possesses a curvature radius varying with time; it seemed to me that a question of this sort may interest you or De Sitter. In the near future I will send you a German translation of this note, if you find the question considered in it interesting, then please be so kind to have it placed in some journal.

The paper was published in the German journal *Die Zeitschrift für Physik* [72] and showed that Einstein's emphasis on the necessity of a static Universe was misplaced. If the spatial curvature of the Universe was taken to be time-dependent, the field equations allowed for non-static cosmologies with positive or negative curvature. Friedmann's analysis included Einstein and de Sitter's world models as special cases in the assumption of a time-independent curvature and continued to a generalisation that led to explicitly evolving cosmological models. As in Einstein and de Sitter's solutions, the Universe is self-contained and unfolds into nothing. A remarkable point of this consideration is set, in Friedmann's first paper, by the definition of the growth time of the curvature radius from 0 to a certain value R_0 as *die Zeit seit die Erschaffung der Welt*, the time since the creation of the world. This definition contains *in nuce* the idea of the *Big Bang*. The fundamental contributions of Friedmann are not limited to the construction of a general model that could incorporate the apparently conflicting cosmological applications elaborated by Einstein and de Sitter. In the 1922 paper, he formulated the two basic assumptions which, together with the general theory of relativity, represent the foundations of the cosmological standard model: the principles of isotropy and homogeneity of the Universe. In a second paper [73], published in 1924, he provided the solution for a Universe with negative spatial curvature definitely proving that a static solution would not be stable.

The notion that the Universe originates from nothing was later formalised by George Lemaître who, in the English translation of his article from 1927, speculated about a "primeval atom" [90, 91, 98], an initial point from which the Universe expanded. The relevance of Lemaître's work, acknowledged only after the publication in 1931 of his article in the Monthly Notices of the Royal Astronomical Society upon Eddington's recommendation, is not restricted to the idea of the Big Bang. In his 1927 paper, *Un Univers homogène de masse constante et de rayon croissant rendant compte de la vitesse radiale des nébuleuses extragalactiques*, he managed to mark the causal connection (as attested by its title) between the cosmic expansion deriving from the non-static solutions of Einstein's field equations and the recent observations of the recession velocities of extragalactic nebulæ. Lemaître derived differential equations for the curvature and the density identical to those found by Friedmann by following a rather different approach. For the first time in a generally relativistic cosmological model, he introduced a concept borrowed from thermodynamics, the conservation of energy,
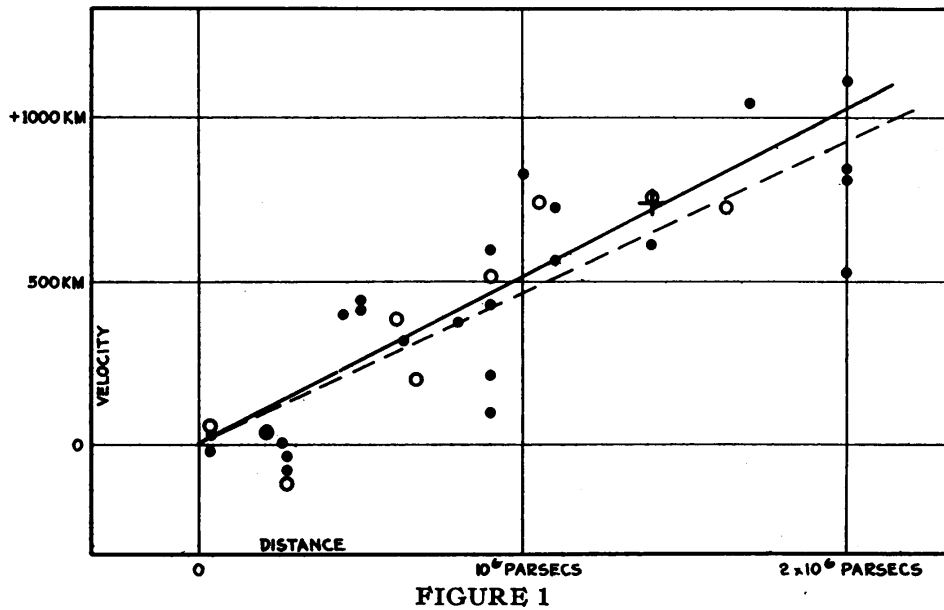
Figure 2.1: Velocity-distance relation among extragalactic nebulæ [82].

and included both the radiation pressure and the matter density in the energy-momentum tensor while assuming that the matter density contribution would be negligible. These equations were the starting point from which he could derive the relation of proportionality between the recession velocities and the distances that is now known as *Hubble's law* and, by accounting for observations made by Strömberg with the Mount Wilson telescope, give an explicit expression to the proportionality constant, today known as the *Hubble constant*.

The most general form of homogeneous and isotropic models within the framework of general relativity was formalised by Robertson [145] and Walker [176] in landmark papers during the second half of the 1930s and the metric of space-time derived by these four scientists is today called Friedmann-Lemaître-Robertson-Walker metric.

Hubble's law. Lemaître's discovery, published in French in an obscure Belgian journal, was overlooked. It was not until 1929 that the interpretation of cosmological redshift as a consequence of cosmic expansion was formalised by Edwin Hubble [82]. Hubble used a sample of 24 extragalactic nebulæ for which distances and velocities were available at Mount Wilson Observatory and found a "roughly linear relation between velocities and distances among nebulæ" that will later take the form:

13

$$v = H_0 d, \qquad\qquad (2.1)$$

and is now known as Hubble's law. Hubble's law quickly became the strongest observational evidence supporting the hypothesis of an expanding Universe. Distances and velocities were not measured directly. Hubble estimated the galaxy distances from luminosities of "Cepheid variables, novæ and blue stars involved in emission nebulosity" and the velocities from the redshift measurements by Vesto Slipher [160] and Milton Humason, Hubble's assistant at Mount Wilson. Due to the large errors in the calibration of the distances and the fact that at that time it was not known that different subcategories of Cepheids exist and have different properties, the value obtained by Hubble for his eponymous constant was around 500 km/s/Mpc, notably higher than the one accepted today.[7] The most recent Planck results point in fact toward a value of 67.4 ± 1.4 km/s/Mpc [136].

Figure 2.1 shows the original plot of the relation between "radial velocities and distances among extragalactic nebulæ" that is now called Hubble diagram.

Dark Matter. Since 1844 and the discovery of Sirius B by Friedrich Bessel [22], astronomers used an observational strategy that relies on the gravitational effects that "hidden" matter exerts on visible matter in order to detect new astronomical objects. The same strategy was applied to the case of the anomalous motions of the planet Uranus and led to Leverrier's discovery of Neptune in 1846 [74]. The generalisation of this method came in the course of the 1930's with the works of Oort, Zwicky and Babcock. In 1932, Jan Oort [123] identified the motion perpendicular to the galactic plane [8] of the nearby stars as an indicator of the presence of dark matter in the neighbourhood of the Sun and observed that "it might be a quite considerable quantity", comparable with the quantity of the luminous matter. A year later, Fritz Zwicky extended this method to the study of clusters of galaxies [186]. The significancy of his contribution was due to the idea of applying for the very first time the virial theorem to the Coma cluster. In this way he obtained evidence of unseen mass, which he referred to as *dunkle Materie*, that totally dominated the cluster and accounted for the missing mass necessary for the cluster to be held together by gravity. Similar evidence of a very high mass-to-light ratio was found in 1936 by Sinclair Smith [161] for the Virgo cluster. One of the earliest indications of dark matter in galaxies is contained in Horace Babcock's PhD dissertation [9]. In his work he studied the rotation curve of the Andromeda

---

[7]The estimate by Lemaître was 575 km/s/Mpc. Observing on the dimensions of the errors, he noted: *Tout ce que l'imprécision des observations permet de faire est de supposer v proportionell à r et d'essayer d'éviter une erreur systématique dans la détermination du rapport v/r* [90].

[8]i.e. the vertical motion

galaxy and his measurements revealed a radial growth of the mass-luminosity ratio which he did not attribute to dark matter but either to absortion "in the outer portions of the spirals" or to further unspecified vnew dynamical considerations, which will permit of a smaller relative mass in the outer parts".

Dark matter soared to the rank of a scientifically interesting problem only in the 1970's [57, 124], from the observational side, when its presence was systematically noticed both in spiral and dwarf galaxies[9] and in galaxy clusters and, from the theoretical side, when its existence was incorporated in models of structure formation. Today, despite the absence of a general consensus[10], dark matter is considered by most to be the responsible factor for the discrepancy between the predicted and observed rotation curve of spiral galaxies and has become one of the fastest growing fields of research in astrophysics.

The necessity to explain rotation curves of galaxies and mass-to-light ratios of galaxy clusters are only two of the main arguments that led to postulate the existence of dark matter. Other two crucial reasons in support of its introduction are to be found in the Big Bang Nucleosynthesis and in the Cosmic Microwave Background theories.

Big Bang Nucleosynthesis. In the 1940's, physicists and astronomers who supported the Big Bang model had at their disposal a coherent mathematical and physical framework based on the FLRW metric, the cosmological principle and the idea of an expanding Universe. Many questions, though, remained unanswered. One of these pressing problems regarded the origin of the light element abundances. George Gamow had pointed out that several nuclear species must have originated "as a consequence of a continuous building-up process arrested by a rapid expansion and cooling of the primordial matter" [5, 75]. In order to find a quantitative agreement between the predicted and observed primordial composition of the Universe, it was necessary to assume that the high temperatures of the early Universe would trigger processes of nuclear fusion able to produce the required proportions of ^{3}He, ^{4}He, ^{7}Li and ^{2}H. A first publication pointing in this direction was the letter sent on April 1, 1948 to the Physical Review by Ralph Alpher, Hans Bethe and George Gamow. In their paper, later known as $\alpha\beta\gamma$ paper from the surnames of its authors, they successfully managed to provide a correct account of the relative abundances of the hydrogen and helium isotopes. Even though they wrongly claimed the formation of heavier atoms via the successive capture of neutrons by the newly formed nuclei, this letter marked the beginning of a new theory: the Big Bang Nucleosynthesis (BBN), also called primordial nucleosyn-

---

[9]Later studies of the velocity dispersions in elliptical galaxies led to the same conclusions.s

[10]There exist models suggesting alternative explanations, such as the MoND (Modified Newtonian Dynamics).

thesis. A further step towards an explanation of the heavy element abundances was taken by Margaret Burbidge, Geoffrey Burbidge, William Fowler, and Fred Hoyle who, in 1957, formulated the hypothesis that only hydrogen, helium and deuterium are of cosmological origin, while heavier atoms are created in stars [36]. Their report on the "Synthesis of the elements in stars" is today credited as the birth of the stellar nucleosynthesis model.

The statement that the light elements form in the early Universe is a decisive implication of the Big Bang theory and the observational evidence found in its support represent one of the theory's most striking triumphs. The primordial nucleosynthesis and the use of scaling arguments also allow an estimation of the cosmic baryon density from the proton and neutron densities. The quantity obtained in this way, already in the 1970's, appeared to be too low and in contrast with the estimate deriving from calculations of the expansion rate of the Universe. Also in this case a solution to the missing matter problem was prompted by the introduction of dark matter into the theory.

Cosmic Microwave Background. Another fundamental prediction of Big Bang Cosmology is the existence of the Cosmic Microwave Background (CMB) radiation, the relic thermal radiation of photons that started freely propagating when the matter became neutral after the recombination of electrons and protons. The recombination occurred when the age of the Universe was 3×10^5 years[11] and its temperature had lowered to 3×10^3 K: photons were no longer prisoners of Thomson scattering and could decouple from matter. This event had three relevant consequences:

1. The thermodynamical equilibrium reached by photons and electrons before decoupling imprinted the photons of the last scattering surface with a blackbody spectrum at a temperature of 2.72548 ± 0.00057 K [69].

2. The black-body spectrum was preserved by the cosmic expansion, whose only effect is a systematic increase in the wavelengths.

3. The CMB appears, on large scales, isotropic and homogeneous to all fundamental observers, further endorsing the Cosmological Principle.

The first prediction of a cosmic radiation background was connected with the requirement of the BBN theory to have a hot beginning. In 1948 Alpher and Herman forecasted a temperature of around 5 K for the relic radiation [6]. Publications with different methods and values for the temperature of the CMB were issued and discussed for more than a decade before a direct detection was made. Finally, in 1964, Robert Dicke, who was setting up with his group at Princeton

---

[11]At a redshift $z = 1100$.

University a radiometer to try to measure it, received a phone call from Arno Penzias and Robert Woodrow Wilson, two physicists working at the Bell Telephone Laboratories in a nearby town. The two Bell employees were working on a new type of antenna and had found a higher noise temperature than expected. This excess temperature of approximately 3.5 ± 1.0 K was described as "isotropic, unpolarized, and free from seasonal variations" [132]. The interpretation of it as the signature of a hot Big Bang came from the Princeton group, whom they had scooped, Robert Dicke, P. J. E. Peebles, P. G. Roll and D. T. Wilkinson [54].

The discovery of radiation from the "primeval fireball" offered new insights into the origin of galaxies. Firstly, it set a time when bound structures like galaxies could start to form and, secondly, it could be regarded as the sought-after mean to imprint onto the power spectrum of initial density fluctuations some characteristic features, such as lengths and masses, that could serve as observational probes for a confirmation of the theory. The prediction of structures in the CMB was independently formulated in 1970 by Peebles and Yu [130] and Sunyaev and Zel'dovich [167, 168]. In their works, the two groups derived what is today called baryon acoustic oscillations in the galaxy power spectrum and suggested that their relative amplitude should be of the order of 10^{-4}. Subsequent attempts to measure these fluctuations failed and in 1982 Peebles [126] proposed a model assuming that "the mass of the Universe is dominated by a gas of particles that interact weakly, if at all, with baryonic matter and radiation. These dark matter particles have negligible primeval velocities, hence the eventual name, cold dark matter, and the model name, CDM" [129]. The CDM model rested on the assumption of general relativity as the correct theory of gravity at cosmological scales and was based on a FLRW metric and the cosmological principle. It described the geometry of the observable Universe on the basis of the ratio between the actual matter density and the critical density for which the Universe is spatially flat, a quantity that can be derived from Friedmann's equations by assuming that the cosmological constant is zero.

Inflation. A solid motivation for supporting a model based on the concept of a critical density was provided by the theory of cosmic inflation. Friedmann cosmology in the 1970's was far from being a complete theory. In particular, two major problems had been discovered which needed a careful explanation: the flatness problem and the horizon problem.

The flatness problem is a question concerning the fine-tuning of the density of matter and energy in the universe and was originally identified by Robert Dicke in 1969. A key prediction of Friedmann's world model, deriving from the combination of general relativity and the cosmological principle, is that three types of universe can be possible, as sketched in Figure 2.2. If there is sufficient mat-
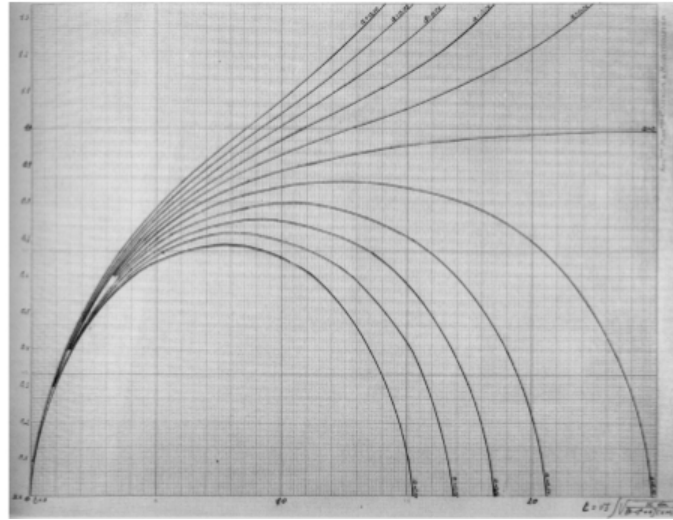
Figure 2.2: Handwritten plot by Lemaître illustrating the time evolution of the radius of the universe with the cosmological constant (labelled a), for a space with positive curvature. All the models start with a singularity in $(x = 0, t = 0)$. For a sufficiently large cosmological constant, the universe becomes open. The most recent cosmological data are compatible with a Lemaître's solution with positive curvature and accelerated expansion (top curve) [98].

ter density for gravity to triumph over expansion, the universe will be spatially closed; if the matter density is not high enough, it will be spatially open and if gravity balances expansion, the Universe will be spatially flat or, in other words, Euclidean. Dicke noted that even the tiniest departure from the critical density in the early Universe would have been enormously magnified during the expansion, leading either to a closed or an open universe. In either case, no structure formation in the way observed today would have been possible.

The horizon problem is an issue regarding the finiteness of the speed of light on one hand and the homogeneity of the CMB spectrum on the other. It was pointed out by Charles Misner that patches of the sky that are not in causal contact with each other should exhibit different physical properties and yet the cosmic background radiation appears isotropic and homogeneous everywhere in the sky.

These two problems, among others (such as the absence of magnetic mono-poles), could be solved in 1981 by Alan Guth [78], who postulated a very early phase of inflationary expansion in the evolution of the Universe (at some time between 10^{-36} s and 10^{-33} s after the Big Bang) which reconciled theory with observations. In the same year Mukhanov and Chibisov [113] noticed that inflated quantum fluctuations could lead to the formation of cosmic structures. In the following

years, numerous variants of the inflation theory were proposed and some of the detailed predictions on the initial conditions of the Universe provided by inflationary theories could be experimentally verified only in recent years. The existence of fluctuations in the CMB has been proven by missions like COBE, WMAP and Planck. The detection of quantum fluctuations in the gravitational field, known as gravitational waves, was announced by the BICEP2 collaboration in March 2014 but their extraordinary claims, if not completely dismissed, were proven to be premature by the Planck collaboration [135].

ΛCDM. Right after its debut in 1982, the physical implications of the Cold Dark Matter model were explored by many groups and several candidates were soon proposed [1, 29, 32, 139]. The idea that cold dark matter would not interact with radiation, while baryons were still coupled to the CMB, would provide an explanation of two apparently contrasting observations: the clumpy distribution of matter in the Universe on one side and the simultaneous presence of tiny anisotropies in the CMB on the other. In 1984 Peebles [127] suggested a further modification to the CDM model: by introducing a cosmological constant it would be possible to go to lower mass density while permitting spatial flatness and meeting the requirements of the inflationary scenario. The same strategy was suggested by Kofman and Starobinskii [86] a year later and the modified framework they proposed took the name of Lambda-CDM (ΛCDM).

In 1987 numerical simulations carried out by Bond and Efstathiou [31] and by White, Davis, Efstathiou and Frenk [180] contributed to the promotion of ΛCDM as a promising model for structure formation analyses.

In 1992 reports of the findings of the COsmic Background Explorer (COBE) mission launched a few years earlier were announced. COBE had provided evidence that the CMB has a nearly perfect black-body spectrum and that very faint anisotropies could be detected in it. These findings scored a crucial point in favour of the Big Bang theory by fulfilling its predictions. In the course of the years, two major follow-up missions were launched: the Wilkinson Microwave Anisotropy Probe (WMAP) and Planck satellites.

For nearly ten years (February 2003 - December 2012) WMAP data releases, containing a full-sky map of the CMB, helped refining the measurements of the temperature fluctuations in it and provided further constraints on cosmological parameters and other model values, such as the age of the Universe and the Hubble constant. In the abstract of the 9-Year release paper [19], the authors conclude: "With no significant anomalies and an adequate goodness-of-fit, the inflationary flat ΛCDM model and its precise and accurate parameters rooted in WMAP data stands as the standard model of cosmology."

The last mission devoted to studying the CMB anisotropies in order of time is
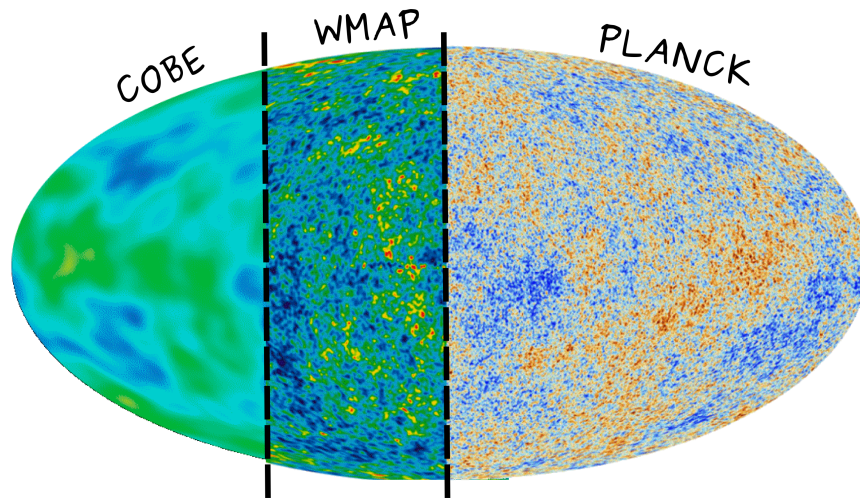
Figure 2.3: Visual comparison between the full-sky maps provided by COBE, WMAP and Planck. The three satellites provided solid observational evidence in support of the idea of cosmic microwave background by identifying the predicted small temperature fluctuations arising from early weak fluctuations in the matter distribution.

the European Planck cosmology probe. The three-year results were released in February 2015 and the Planck all-sky map is to date the most detailed image of the early Universe. For an overview of the Planck estimates of the main cosmological parameters, see Table 2.1.

The published results provide both striking support to the notion of inflation and show remarkable agreement with the ΛCDM model. The confirmation that the Universe is spatially flat, together with the recent developments on inflation and the discovery of the accelerated expansion of the Universe complete the cosmological standard model.

Accelerated expansion. A method to gain information on the geometry of the universe was inaugurated by Hubble and is based on the observation of the standard candles, a class of objects of which either the absolute magnitude, or luminosity, is known or the relation between their luminosity change and redshift is well-understood. The same method has been used in recent years on Type-Ia Supernovæ. The most stunning result of this application was published nearly simulta-
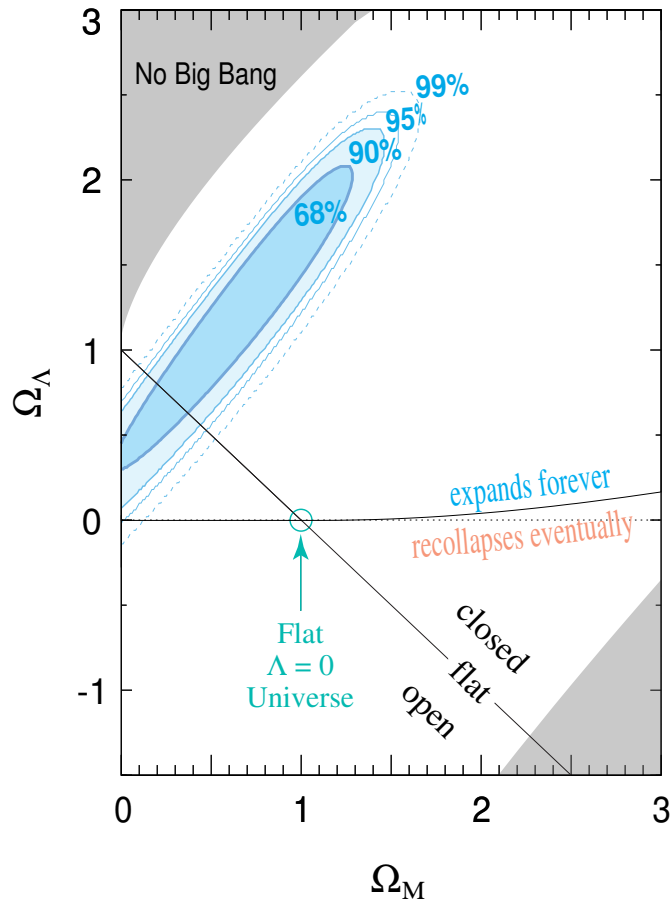
Figure 2.4: Best-fit confidence regions in the $\Omega_M - \Omega_\Lambda$ plane. The $68\%, 90\%, 95\%$ and 99% statistical confidence regions are shown. Note that the spatial curvature of the universe -open, flat, or closed - is not determinative of the future of the universe's expansion, indicated by the near-horizontal solid line. In cosmologies above this near-horizontal line the universe will expand forever, while below this line the expansion of the universe will eventually come to a halt and recollapse. This line is not quite horizontal, because at very high mass density there is a region where the mass density can bring the expansion to a halt before the scale of the universe is big enough that the mass density is dilute with respect to the cosmological constant energy density. The upper-left shaded region, labeled "no Big Bang", represents "bouncing universe" cosmologies with no Big Bang in the past. The lower right shaded region corresponds to a universe that is younger than the oldest heavy elements for any value of $H_0 > 50 \text{kms}^{-1}\text{Mpc}^{-1}$. [133].

neously by two competing groups in 1998 and 1999, the Supernova Cosmology Project led by Saul Perlmutter [133] and the High-Z Supernova Search Team led by Brian Schmidt and Adam Riess [143]. The main goal of their work was a systematical study of high-redshift supernovæ and, in the course of the data analysis, the two teams found observational evidence that, contrary to any expectation, the Universe is undergoing a phase of accelerated expansion. In Perlmutter et al. [133], while discussing the meaning of Figure 2.4, the authors note that "the data are strongly inconsistent with the $\Lambda = 0$, flat universe model (indicated with a circle) that has been the theoretically favored cosmology. If the simplest inflationary theories are correct and the universe is spatially flat, then the supernova data imply that there is a significant, positive cosmological constant. Thus the universe may be flat *or* there may be little or no cosmological constant [12], but the data are not consistent with both possibilities simultaneously. This is the most unambiguous result of the current data set".

In Figure 2.5 we show the results of the other collaboration.

The history of the cosmological constant is dramatic. From the day of its first introduction by Einstein in 1917, it has been postulated, forgotten, removed from the theory and resurrected several times whenever a new inexplicable problem in cosmology arose. The publication of the results of Perlmutter, Riess and Schmidt opened a completely new perspective on the evolution of the Universe and several models were proposed to explain their unexpected findings. A possible solution would be modified gravity models, which would not require the presence of a cosmological constant, and another one would exactly be the reintroduction into the theory of the idea of a vacuum energy dominating the expansion, which could be either dependent on time or constant. In the latter and simpler case, this vacuum energy could be identified with the cosmological constant originally postulated by Einstein. The acceleration of today's cosmic expansion is generally considered as a manifestation of an unknown, uniformly- distributed form of energy, labeled *dark energy*, to which a negative pressure is associated and that is viewed as the liable factor for this kind of repulsive gravity.

Currently, a flat FLRW Universe with a non-zero cosmological constant including cold dark matter represents the broadly-accepted standard model of cosmology.

---

[12]and a more sophisticated inflationary scenario or even something completely different, we could add.
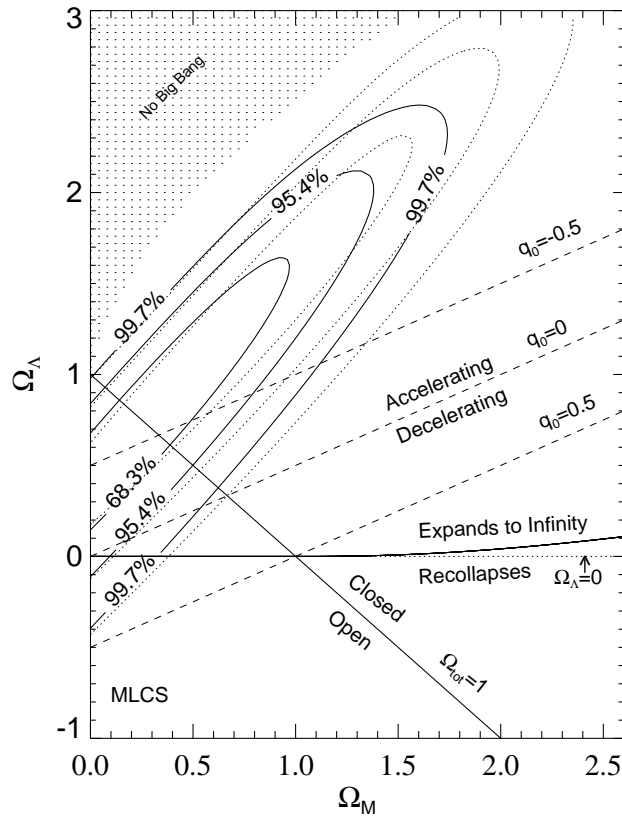
Figure 2.5: Joint confidence intervals for $(\Omega_M, \Omega_\Lambda)$ from SNe Ia. Regions representing specific cosmological scenarios are illustrated. Contours are closed by their intersection with the line $\Omega_M = 0$ [143].

2.2 The homogeneous Universe

2.2.1 The cosmological principle

As mentioned in Section 2.1, three main assumptions are used in Friedmann cosmology in order to describe an expanding Universe. The first one is that general relativity is the correct theory of gravity, the second and the third ones are that the Universe is spatially homogeneous and isotropic. These last two hypotheses go under the common name of *cosmological principle*.

The cosmological principle combines local isotropy with a Copernican principle:
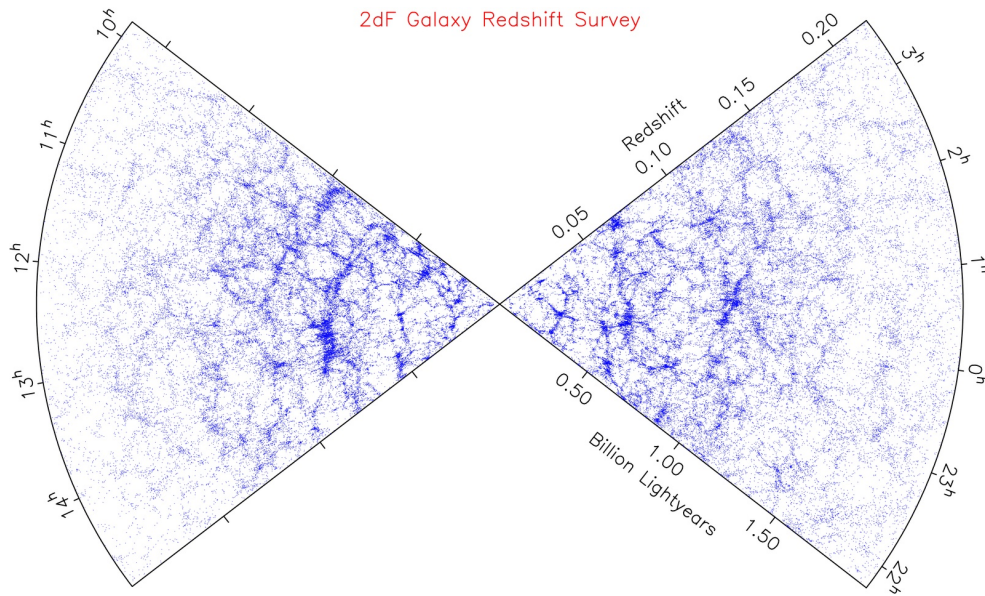
Figure 2.6: The projected distribution of galaxies shown in this cone diagram is evidently anisotropic. Image taken from http://www2.aao.gov.au/ TDFgg/

- Local isotropy states that, on large scales, a freely-falling (i.e. fundamental) observer experiences the observables of the Universe (CMB, Hubble flow, galaxy distribution) as statistically *isotropic*, i.e. the same in all directions.

- The Copernican principle posits that man is in no way a favoured observer and that Earth is neither in a central nor in a privileged position in the Universe.

A Universe that appears isotropic to all its fundamental observers is necessarily homogeneous. An interesting effect descending naturally from the homogeneity principle is the synchronisation of cosmological time, t, with the proper time of observers moving with the mean motion of the Universe.

The cosmological principle was originally formulated by Friedmann in 1922 as a foundation of his solution to Einstein's field equations and has been retained as a working hypothesis until now. Its two main assumptions, though, are quite vigorous ones and need to be justified in some way. The idea of a completely isotropic and homogeneous universe, in fact, contrasts with the indisputable existence of structures. The question that arises from these considerations regards the level of homogeneity and isotropy required for the cosmological principle to hold and is still an open issue [42].

On one hand, while offering a glimpse of the Universe in its early days, data collected by the COBE, WMAP and Planck collaborations in the past twenty years reveal the extraordinary degree of isotropy of the cosmic microwave background, which corroborates the symmetry hypothesis.

On the other hand, the distribution of the nearby galaxies up to a redshift of $z = 0.3$ that emerged from the Two Degree Field Galaxy Redshift Survey (2dF survey, [44]) is unmistakably anisotropic. A reconciliation of these two apparently contradictory remarks can be achieved by recalling that the only requirement of the cosmological principle is that the Universe exhibits a homogeneous character when its properties are averaged on sufficiently large scales. Despite its manifest inhomogeneities (voids, filaments and walls can be seen everywhere in Figure 2.6), a rather uniform pattern in the large-scale structure (LSS) of the Universe can be identified.

2.2.2 Robertson-Walker geometry

The line element

The structure of spacetime in general relativity is described via the line element:

$$\mathrm{d}s^2 = g_{\mu\nu}\mathrm{d}x^\mu\mathrm{d}x^\nu, \tag{2.2}$$

and the dynamics of the metric tensor $g_{\mu\nu}$ is governed by Einstein's field equations which couple matter and energy to curvature and, in their generalised version, read:

$$G_{\mu\nu} = \frac{8\pi G}{c^2}T_{\mu\nu} - \Lambda g_{\mu\nu}, \tag{2.3}$$

where $G_{\mu\nu}$ is the Einstein tensor, G is the gravitational constant, c is the speed of light, $T_{\mu\nu}$ is the energy-momentum tensor and Λ is the cosmological constant.

The adoption of the cosmological principle allows a simplification of the form of the metric through the definition of a global coordinate, the cosmological time, according to which spacetime can be described as a unique foliation of 3-spaces at constant time. Isotropy allows to find spatial coordinates such that $g_{0i} = 0$. As we mentioned in Section 2.2.1, global isotropy implies uniform density. The existence of a global time t and the synchronisation of clocks leads to $g_{00} = -c^2$ and to the definition of fundamental observers for whom $\mathrm{d}x^i = 0$ and whose proper time coincides with the coordinate time. This ansatz reduces the line element to:

$$\mathrm{d}s^2 = -c^2\mathrm{d}t^2 + g_{ij}\mathrm{d}x^i\mathrm{d}x^j. \tag{2.4}$$

Denoting the line element of the so-defined spatial hypersurfaces with $\mathrm{d}l$ and rescaling it with a time-dependent function $a(t)$ permits to write the line element of the spacetime as:

$$\mathrm{d}s^2 = -c^2\mathrm{d}t^2 + a(t)^2\mathrm{d}l^2. \tag{2.5}$$

The function $a(t)$ is termed *scale factor* and measures the expansion rate of the universe. By convention, it is normalised such that $a(t_0) = a_0 = 1$, where t_0 is the present time.

A further consequence of the cosmological principle is that the possible 3-space geometries allowed are restricted to cases with constant curvature K. As seen in Section 2.1, the possibilities are:

- $\mathbf{K > 0}$: 3-sphere with positive curvature everywhere, spatially closed, finite volume, bounded;

- $\mathbf{K < 0}$: 3-saddle with negative curvature everywhere, spatially open, infinite volume, unbounded;

- $\mathbf{K = 0}$: Flat Euclidean 3-space, spatially open, infinite volume, unbounded.

The isotropy assertion imposes spherical symmetry and the line element that describes spatial shells of constant curvature, k, can be cast into the form:

$$\mathrm{d}l^2 = \frac{\mathrm{d}r^2}{1 - kr^2} + r^2 \mathrm{d}\Omega^2, \tag{2.6}$$

where $\mathrm{d}\Omega^2$ is the solid-angle element:

$$\mathrm{d}\Omega^2 = \mathrm{d}\theta^2 + \sin^2\theta \mathrm{d}\phi^2. \tag{2.7}$$

In spherical coordinates, therefore, the line element becomes:

$$\mathrm{d}s^2 = -c^2\mathrm{d}t^2 + a(t)^2 \left[\frac{\mathrm{d}r^2}{1 - kr^2} + r^2 \mathrm{d}\Omega^2 \right]. \tag{2.8}$$

This is known as the *Friedmann-Lemaître-Robertson-Walker metric*.
For the sake of convenience, a new radial coordinate is usually introduced:

$$\mathrm{d}w^2 = \frac{\mathrm{d}r^2}{1 - kr^2}. \tag{2.9}$$

In this way we can recast the FLRM metric as:

$$\mathrm{d}s^2 = -c^2\mathrm{d}t^2 + a(t)^2 \left[\mathrm{d}w^2 + f_k^2(w)\mathrm{d}\Omega^2 \right], \tag{2.10}$$

where $f_k(w)$ parametrises the possible 3-space geometries in the following way:

$$f_k(w) = \begin{cases} \frac{1}{\sqrt{k}} \sin\left(\sqrt{k}w\right), & \text{if } k > 0, \\ w, & \text{if } k = 0, \\ \frac{1}{\sqrt{|k|}} \sinh\left(\sqrt{|k|}w\right), & \text{if } k < 0. \end{cases} \tag{2.11}$$

2.2.3 Redshift

In this framework, the scale factor, $a(t)$, is the only degree of freedom left in the system and the dynamics of the metric is reduced to the dynamics of the scale factor. In particular, a central concept in cosmology can be derived from the study of the light propagation in an expanding universe. If one considers a radial light ray, its trajectory will follow a null geodesic: $d\Omega = 0$ and $ds = 0$. If we assume that the worldlines of the photons we observe today were emitted at certain times t_e, from Equation (2.10) we have:

$$w = \int_{t_e}^{t_0} \frac{c \, dt'}{a(t')}.$$
(2.12)

The coordinate distance w between emitter and observer must be constant and its first derivative must vanish, which allows us to write:

$$w = \int_{t_e + \Delta t_e}^{t_0 + \Delta t_0} \frac{c \, dt'}{a(t')},$$
(2.13)

and

$$\frac{c\Delta t_0}{c\Delta t_e} = \frac{\nu_e}{\nu_0} = \frac{\lambda_0}{\lambda_e} = \frac{a(t_0)}{a(t_e)} = 1 + \frac{\lambda_0 - \lambda_e}{\lambda_e} = 1 + z,$$
(2.14)

assuming that the cycle time of a light wave corresponds to the inverse of its frequency. This expression can be interpreted by noticing that wavelengths are also stretched by expansion: if the Universe shrinks, they are blue-shifted; if it expands, they are red-shifted. This is the reason why the factor z is called cosmological *redshift*. Since, by convention, $a(t_0)$ is set to unity, we can retrieve the relation between the scale factor and the redshift:

$$1 + z = \frac{1}{a}.$$
(2.15)

2.2.4 Dynamical properties of the metric

The assumption of the cosmological principle and of the FLRW metric (Eq. (2.10)) represents the basis of the exact solution of Einstein's Field Equations that goes under the name of *Friedmann's equations*.

The next step is to take an ideal fluid as a source of the gravitational field. By definition, an ideal fluid is isotropic in its rest frame [178], has neither viscosity nor heat conduction [156] and is completely characterised by its energy density ρc^2 and by the pressure p. If we choose the density and the pressure to be functions only of time, we can write the energy-momentum tensor in Equation 2.3 to be:

$$T_{\mu\nu} = (\rho c^2 + p)\tilde{u}_\mu \tilde{u}_\nu + p g_{\mu\nu}, \tag{2.16}$$

where $\tilde{u}_\mu$ is the 4-velocity of an element of the fluid.

These preliminary remarks allow us to finally write the Friedmann equations that govern the dynamics of the scale factor:

$$\left(\frac{\dot{a}}{a}\right)^2 = \frac{8\pi G}{3}\rho - \frac{kc^2}{a^2} + \frac{\Lambda}{3}, \tag{2.17}$$

$$\left(\frac{\ddot{a}}{a}\right) = \frac{4\pi G}{3}\left(\rho + \frac{3p}{c^2}\right) + \frac{\Lambda}{3}. \tag{2.18}$$

These two equations can be combined to give the adiabatic equation:

$$\frac{\mathrm{d}}{\mathrm{d}t}\left[a^3(t)\rho(t)c^2\right] + p(t)\frac{\mathrm{d}a^3(t)}{\mathrm{d}t} = 0, \tag{2.19}$$

which is the cosmological version of the first law of thermodynamics.[13]

2.2.5   Matter models

A fundamental hypothesis in the ΛCDM Cosmology is that the Universe, seen as a fluid, is in thermodynamical equilibrium and its equation of state reads $p = w\rho c^2$ with constant[14] w. If we remember that a particle can be labeled as *non-relativistic* if $v \ll c$ and *relativistic* in the opposite condition, we can call a gas (at a given temperature T) *non-relativistic* if it satisfies the condition $k_B T \ll mc^2$ and *relativistic* if, viceversa, $k_B T \gg mc^2$, where m is the average mass of its particles. Following this definition, we can broadly identify two different types of matter constituting the cosmic fluid: non-relativistic matter, also called *ordinary* or *baryonic* matter and a relativistic component, called *radiation*. A third constituent is the *dark energy*, associated to the cosmological constant Λ. Accordingly, the equation of state parameter assumes the values:

$$w = \begin{cases} 0, & \text{matter,} \\ 1/3, & \text{radiation,} \\ -1, & \text{cosmological constant.} \end{cases} \tag{2.20}$$

---

[13]For a thourough derivation, please see `http://www.ita.uni-heidelberg.de/research/` `bartelmann/Lectures/cosmology/cosmology.pdf`.

[14]w is not constant in dark energy models, for instance.

2.2.6 Cosmological parameters

In cosmology it is common to encounter a number of parameters and functions and we will define them briefly in this paragraph.

Hubble function: From Equation (2.2.4), it is possible to define the Hubble function as the logarithmic change in the expansion rate:

$$\left(\frac{\dot{a}}{a}\right) = H(t). \tag{2.21}$$

Hubble constant: At present time the Hubble function becomes:

$$H(a(t_0)) = H(1) = H_0, \tag{2.22}$$

and has the unit of an inverse time: $H_0 \approx 3.2 \times 10^{-18} h \, \text{s}^{-1}$, where h is called *Hubble parameter*, parametrises our lack of knowledge on the value of H_0 and is given by $H_0/(100 \text{ km/s/Mpc})$.

Hubble time: The inverse of the Hubble constant is:

$$t_H = \frac{1}{H_0}, \tag{2.23}$$

and would represent the age of the Universe if its expansion rate was constant throughout its evolution.

Critical density: Assuming $k = 0 = \Lambda$, the critical density for the Universe to be spatially flat is:

$$\rho_{cr} = \frac{3H^2}{8\pi G}, \tag{2.24}$$

and its value today is

$$\rho_{cr,0} = \frac{3H_0^2}{8\pi G} = 1.86 \times 10^{-29} h^2 \, \text{g cm}^{-3}. \tag{2.25}$$

Density parameter: The dimensionless ratio between the actual matter density and the critical density provides a convenient way to specify the geometry of the Universe:

$$\Omega(t) = \frac{\rho(t)}{\rho_{cr}(t)}. \tag{2.26}$$

The individual contributions of the different components of the Universe can also be illustrated via density parameters, such as the contribution due to the presence of luminous matter, Ω_*, or the contribution due to the matter estimated to be contained in galaxies, Ω_G. The most useful and recurring definitions are the matter density parameter, the radiation density parameter and the cosmological constant density parameter.

Matter density parameter: It is the contribution of both the baryonic and dark matter to the critical density of the Universe:

$$\Omega_m(t) = \frac{\rho_m(t)}{\rho_{cr}(t)}, \tag{2.27}$$

and it is often split into the fraction of baryonic matter, Ω_b, and the one due to dark matter, Ω_{CDM}.

Radiation density parameter: The evolution of the Universe depends also on electromagnetic energy, relativistic particles and neutrinos. In particular, the radiation density is dominated by the energy density of the CMB:

$$\Omega_r(t) = \frac{\rho_r(t)}{\rho_{cr}(t)}. \tag{2.28}$$

Cosmological constant density parameter: Even though the nature of dark energy is still an enigma, observations are able to determine its input to the cosmic density:

$$\Omega_\Lambda(t) = \frac{\Lambda}{3H^2}. \tag{2.29}$$

Curvature density parameter: A similar definition can be given for the curvature as well:

$$\Omega_k(t) = -\frac{kc^2}{a^2 H^2}. \tag{2.30}$$

The introduction of these parameters permits to reformulate Friedmann's equation as:

$$H^2(a) = H_0^2 E^2(a) = H_0^2 \left[\Omega_{r,0} a^{-4} + \Omega_{m,0} a^{-3} + \Omega_{\Lambda,0} + \Omega_{K,0} a^{-2} \right], \tag{2.31}$$

which tells us how the Universe changes as it expands or shrinks in relation to today and at present time (a = 1) provides us with the identity:

$$\Omega_{r,0} + \Omega_{m,0} + \Omega_{\Lambda,0} + \Omega_{K,0} = 1. \tag{2.32}$$

In Table 2.1 [137] we report the values of these parameters found by the Planck collaboration. The density parameter attributed to the cosmological constant nowadays is around 70%, which leads us to view dark energy as the dominant influence on the current phase of expansion of the Universe. The previous two phases in the history from the Big Bang to today are considered to be first radiation dominated and subsequently matter dominated. The relative importance of the various density parameters over time can be easily seen by inspecting the square brackets of Equation 2.31: it is immediately obvious that they scale with different powers of the scale factor, a.

Table 2.1: Constraints on Ω_{m0} (matter density parameter), $\Omega_{\Lambda0}$ (dark energy density parameter), Ω_{b0} (baryonic matter density parameter), H_0 (Hubble constant), n_S (spectral index of the primordial power spectrum), σ_8 (power spectrum normalisation), z_{eq} (equality redshift) and the age of the Universe estimated by [137]. The column labeled "Planck" gives results for the Planck temperature power spectrum data alone. The column labeled "Planck + lensing" combines the Planck temperature data with Planck lensing. The column labeled "Planck + WMAP pol." includes WMAP polarization at low multipoles. The results presented in [137] are the best fit parameters (i.e. the parameters that maximise the overall likelihood for each data combination) as well as the 68% confidence limits for the constrained parameters.

Parameter	Planck	Planck + lensing	Planck + WMAP pol.
Ω_{m0}	0.314 ± 0.020	0.307 ± 0.019	$0.315^{+0.016}_{-0.018}$
$\Omega_{\Lambda0}$	0.686 ± 0.020	0.693 ± 0.019	$0.685^{+0.016}_{-0.018}$
$\Omega_{b0}h^2$	0.02207 ± 0.00033	0.02217 ± 0.00033	0.02205 ± 0.00028
H_0	67.4 ± 1.4	67.9 ± 1.5	67.3 ± 1.2
n_S	0.9616 ± 0.0094	0.9635 ± 0.0094	0.9603 ± 0.0073
σ_8	0.834 ± 0.027	0.823 ± 0.018	0.829 ± 0.012
$z_{e}q$	3386 ± 69	3362 ± 69	3391 ± 60
$Age[Gyr]$	13.813 ± 0.058	13.796 ± 0.058	13.817 ± 0.048

2.2.7 Cosmological distances

In cosmology and general relativity, the concept of distance is no longer unambiguous because of the relative character of simultaneity and the finiteness of the speed of light. Since the measurement of a distance is taken along the past light cone and the Universe expands, it is not surprising that, in a cosmological framework, distances change in time.

A number of definitions are available and, even though they converge to each other in the limit of a Minkowski spacetime, they considerably differ from one another in an expanding spacetime.

Proper distance: It is possible to define the proper distance as the distance that light travels between a source at redshift z_2 and an observer at redshift $z_1 < z_2$:

$$D_{prop}(z_1, z_2) = \int_{t_1}^{t_2} c\,\mathrm{d}t = \int_{a(z_1)}^{a(z_2)} \frac{c\,\mathrm{d}a}{\dot{a}} = \frac{c}{H_0} \int_{a(z_1)}^{a(z_2)} \frac{\mathrm{d}a}{aE(a)}. \qquad (2.33)$$

Comoving distance: This is the distance scale that expands with the Universe and is defined as the spatial distance between the intersections of the worldline of two comoving sources at redshifts $z_1 < z_2$ with the spatial hypersurface $t = t_0$ [152].

In GR light propagates along null geodesics and from the FRLW metric 2.10 we can write [15] $c\,dt = -a\,dw$ and remembering that $dt = \frac{da}{\dot{a}}$:

$$D_{com}(z_1, z_2) = w(z_1, z_2) = c \int_{a(z_2)}^{a(z_1)} \frac{da}{\dot{a}a} = w(z_2) - w(z_1). \tag{2.34}$$

$$D_{ang} = \frac{a(z_2)}{a(z_1)} f_K[w(z_1, z_2)], \tag{2.35}$$

Luminosity distance: The distance between a source and an observer can be also defined as:

$$D_L = \left(\frac{L}{4\pi F}\right)^2, \tag{2.36}$$

where L is the intrinsic luminosity of the source and F is the flux measured from an observer and both these quantities are bolometric, therefore integrated over all frequencies. In the Euclidean limit, the definitions of luminosity and angular diameter distance would be equivalent. In a more general context, they are connected via the *Etherington* relation [64]:

$$D_L = (1 + z)^2 D_{ang}, \tag{2.37}$$

which implies that, in an expanding Universe, the luminosity distance is larger than the angular diameter one.

2.3 The formation of structures in the Universe: introducing inhomogeneities

2.3.1 The growth of perturbations

As mentioned in Sect. 2.2.1, the cosmological principle is valid when averaging on very large scales. Nonetheless, it is also necessary to account for inhomogeneities such as the galaxies (around $10\,\mathrm{kpc}\,h^{-1}$), galaxy clusters and superclusters (around 1 to $10\,\mathrm{Mpc}\,h^{-1}$) , filaments and voids (around $50\,\mathrm{Mpc}\,h^{-1}$) and all the other structures one can observe when looking at the Universe on smaller scales. Even though the primordial distribution and the mechanism that triggered the formation of such inhomogeneities is not yet completely clarified, many studies point toward a period of accelerated expansion that goes under the name of inflation as a good candidate to explain the known features of such perturbations.

---

[15]Assuming we are in the position $w = 0$. The choice of the minus sign is due to the fact that light emitted from a source at redshift $z_2 > z_1$ will have $dt > 0$ and $dw < 0$.

Given the small scale of these inhomogeneities with respect to the Hubble radius, i.e. the typical scale of the Universe, and typical velocities being much smaller than the speed of light, Newtonian dynamics is in general considered a reasonable approximation to use and provides us with a solid theory for describing them in the context of a non-relativistic cosmic fluid.

The very first tool we can borrow from fluid mechanics is the continuity equation:

$$\frac{\partial \rho(t, \vec{x})}{\partial t} + \vec{\nabla} \cdot (\rho \vec{v}(t, \vec{x})) = 0, \tag{2.38}$$

which codifies the conservation of mass and the dependence of density and velocity on time and position in an inhomogeneous Universe.

The conservation of momentum is prescribed by the Euler equation:

$$\frac{\partial \vec{v}}{\partial t} + (\vec{v} \cdot \vec{\nabla})\vec{v} = -\frac{\vec{\nabla}p}{\rho} - \vec{\nabla}\phi, \tag{2.39}$$

where the terms on the RHS contain the pressure gradient and the gravitational forces and the Newtonian potential ϕ is related to the density field via the Poisson equation:

$$\nabla^2 \phi = 4\pi G \rho. \tag{2.40}$$

The density perturbations are described by the dimensionless density contrast δ:

$$\delta(t, \vec{x}) = \frac{\rho(t, \vec{x}) - \bar{\rho}(t)}{\bar{\rho}(t)}, \tag{2.41}$$

which represents the difference between the density at a given coordinate and the mean density normalised by the mean density.

The evolution of the perturbations can be studied in two different regimes: the linear and the non-linear regime.

The use of Eqs. (2.38) to (2.40) and linear perturbation theory permit to derive the time evolution equation for the density contrast:

$$\ddot{\delta}(t, \vec{x}) + 2H\dot{\delta}(t, \vec{x}) - \frac{c_s^2}{a^2}\nabla^2 \delta(t, \vec{x}) - 4\pi G \delta(t, \vec{x}) = 0, \tag{2.42}$$

where the over-dots identify partial time derivatives and a transformation from physical to comoving coordinates $\vec{r} = a\vec{x}$ is performed. Decomposing δ into plane waves:

$$\delta(t, \vec{x}) = \int \frac{d^3 k}{(2\pi)^3} \hat{\delta}(t, \vec{k}) e^{-i\vec{k}\cdot\vec{x}}, \qquad \hat{\delta}(t, \vec{k}) = \int d^3 x \, \delta(t, \vec{x}) e^{i\vec{k}\cdot\vec{x}}, \tag{2.43}$$

with $\hat{\delta}$ the Fourier transform of δ, yields its equivalent form in Fourier space:

$$\ddot{\delta}(t,\vec{k}) + 2H\dot{\delta}(t,\vec{k}) + \delta(t,\vec{k})\left(\frac{c_s^2}{a^2}k^2 - 4\pi G\rho_0\right) = 0, \tag{2.44}$$

with ρ_0 the background value of the density field. The sound speed c_s is the proportionality factor relating pressure and density fluctuations in the equation of state: $\delta p = c_s^2 \delta\rho = c_s^2\rho_0\delta$. The definition of the Jeans length, λ_J, naturally follows from Eqs.(2.44) and (2.43):

$$\lambda_J = \frac{2\pi}{k_J} = c_s\sqrt{\frac{\pi}{G\rho_0}}. \tag{2.45}$$

This scale is the threshold where attraction and pressure balance each other: perturbations smaller than the Jeans length (therefore with $k > k_J$) oscillate, those larger either decay or grow.

If we restrict ourselves to the case of perturbations much larger than the Jeans length, we can observe how the growth rate of perturbations varies with the species dominating the energy density of the Universe. It can be shown that $\delta \propto a^2$ in the radiation-dominated era and afterwards $\delta \propto a$ in the matter-dominated one.

The linear evolution of the density contrast obeys:

$$\delta(a) = \delta_0 D_+(a), \tag{2.46}$$

and the linear growth factor $D_+(a)$, which describes the evolution of the density contrast with respect to the scale factor, in ΛCDM cosmologies is well approximated by the fitting formula [39]:

$$D_+(a) = \frac{5a}{2}\Omega_m\left[\Omega_m^{4/7} - \Omega_\Lambda + \left(1 + \frac{1}{2}\Omega_m\right)\left(1 + \frac{1}{70}\Omega_\Lambda\right)\right]^{-1}. \tag{2.47}$$

For a $\delta \gtrsim 1$, the assumption of small fluctuations of the background density and velocity fields is no longer valid and the perturbations become non-linear. An analytic treatment of these equations for a mildly non-linear regime requires different approximations such as the spherical collapse model, for instance, that will be mentioned in Sect. 3.2.1. For treating perturbations at later times it is common to use numerical simulations such as the Millenium simulation.[16]

2.3.2 The power spectrum

As we already discussed in the previous section, a central requirement of the current standard cosmological theory is the ability to reconcile the high degree of uniformity

---

[16]For details about the Millenium simulation see http://www.mpa-garching.mpg.de/millennium/ and refences therein.

seen at large scales and the incredible isotropy observed in the CMB that are pre-scribed by the cosmological principle with the structures that are unmistakably present at smaller scales.

The density contrast δ is a random field and because of the cosmological principle it can be assumed to be homogeneous and isotropic, which implies that its statistical prop-erties need to be invariant under rotations and translations. The idea that the statistical properties of a field describing inhomogeneities should be homogeneous sounds less paradoxical when one assumes the existence of an ensemble of Universes and sees our Universe as a statistical realisation of this random field. An issue that can be brought up against this argument is that we find ourselves in the condition to observe only one reali-sation of this ensemble. This is usually overcome by resorting to the ergodic hypothesis which states the equivalence between ensemble averages, i.e. taken on several different realisations of the distribution, and sample averages, i.e. averages taken on uncorrelated samples within the same realisation.

Adler (1981) [3] proved that a random field is ergodic if it can be described by Gaus-sian statistics and if its power spectrum is continuous. In linear perturbation theory, each Fourier mode evolves independently. Thus, the density field in real space is a combina-tion of independent random variables $\delta(k)$ drawn from the same distribution. According to the central limit theorem, this distribution has to be Gaussian and a Gaussian field is completely specified by two statistical properties: the mean and the variance.

The mean of the density contrast vanishes by definition:

$$\langle \delta \rangle = \langle \frac{\rho - \rho_0}{\rho_0} \rangle = \frac{\langle \rho \rangle}{\rho_0} - 1 = 0. \tag{2.48}$$

The second important property to study is the variance of δ, which measures on average the departure of the density field from its mean: the more inhomogeneous the density field is, the larger the variance. In Fourier space (see Eq.(2.43)) the variance is expressed by:

$$\langle \hat{\delta}(\vec{k})\hat{\delta}^*(\vec{k'}) \rangle = (2\pi)^3 P(k)\delta_D(\vec{k} - \vec{k'}), \tag{2.49}$$

which contains the definition of power spectrum, $P(k)$, and where δ_D is the Dirac's delta distribution which ensures homogeneity by prescribing that different modes are uncorrelated in Fourier space. The isotropy argument of the cosmological principle garantees that $P(k)$ is independent of the direction of the wave vector. [17]

In real space the variance is related to the autocorrelation function or *2-point corre-lation function*, $\xi(y)$:

$$\xi(y) = \langle \delta(\vec{x})\delta(\vec{x} + \vec{y}) \rangle, \tag{2.50}$$

where the average $\langle \cdot \rangle$ extends over all positions $\vec{x}$ and orientations of $\vec{y}$ and the correla-tion function depends only on the magnitude y. The variance σ^2 of the density contrast

---

[17]From this relation we can observe that the dimensions of the power spectrum are $[L]^3$ or, equivalently, k^{-3}. In general, one plots the dimensionless function of k: $\Delta^2(k) = k^3 P(k)/(2\pi)^3$.

is then the correlation function at $\vec{y} = 0$:

$$\sigma^2 = \langle \delta^2(\vec{x}) \rangle, \tag{2.51}$$

which makes sense if we observe that the mean is null.

Thanks to Eq. (2.49), it is possible to find an expression relating the variance to the power spectrum:

$$\sigma_R^2 = 4\pi \int \frac{k^2 \mathrm{d}k}{(2\pi)^3} P(k) W_R(k), \tag{2.52}$$

which shows how the density field can be completely described by its first two moments (i.e. mean and variance). $W_R(k)$ is a window function restricting the variance to density fluctuations of spatial scale R. We note that the 2-point correlation function specifies a Gaussian random field completely. If the field was non-Gaussian, the use of higher-order moments (skewness, kurtosis, up to N-point correlation functions) would be necessary.

3

Galaxy Clusters

Galaxy clusters constitute the largest gravitational potential wells in the Universe. Their extraordinary richness in observable properties makes them a valuable tool both for astrophysics and for cosmology. On the one hand, they are the perfect laboratory in which models of galaxy formation and evolution can be tested and the intergalactic medium be studied. On the other hand, they are inevitably imprinted by the underlying cosmology and can be exploited as magnifying lenses to gain information on objects that would otherwise not be in reach of telescopes.

In this chapter, we review the main aspects of galaxy clusters that will be central concepts for the scope of this work. Section 3.1 presents a brief overview of clusters in general and of their relevance to observational astronomy and cosmology. Section 3.2 begins with the introduction of the spherical collapse model of structure formation, proceeds in reviewing several possible models describing the density profile of galaxy clusters and ends with a section dedicated to the mass function. The observational properties of clusters that will be used in the upcoming chapters are examined in Section 3.3.

3.1 Galaxy clusters: a brief overview

Clusters of galaxies are the largest and most massive, gravitationally bound structures in the Universe. A tendency of galaxies (then called "nebulæ") to cluster had already been noticed in the eighteenth century by Charles Messier and William Herschel. From that moment on several catalogues of collections of galaxies started to be compiled and their relevance as objects of astronomical study increased after the discovery that our Universe is not limited to the Milky Way and the extragalactic origin of galaxies was confirmed (See Section 2.1 and references therein for a more extensive treatment of the topic).

As described in Chapter 2, the energy content in the Universe is mostly dark. Galaxies are embedded into dark matter haloes and the main constituent of a galaxy cluster is dark matter, followed by a hot, X-ray luminous intracluster medium (ICM), which

accounts for most of the luminous baryonic matter, and by the optical galaxies. More precisely, the mass content of a galaxy cluster of $10^{14} - 10^{15}$ solar masses can be identified to be composed of $85 - 90\%$ of dark matter and $10 - 15\%$ of baryons [104], with 10% of the baryonic component to be ascribed to unbound, intracluster galaxies [184].

The depth of their potential wells makes clusters an ideal approximation of isolated systems in which the physics of the intracluster medium (effects of major mergers, energy feedback from supernovæ and active galactic nuclei, outbursts from supermassive black holes...) can be investigated and models of galaxy formation can be tested.

Furthermore, clusters are an excellent environment to test cosmological models. Their dynamical timescales are very large (of the order of Gyrs) and this implies that, on one side, we can study their evolution even at low redshifts because cluster formation is an ongoing process and, on the other, that we can use them to constrain cosmological parameters (such as the matter density parameter, Ω_m, (Eq. 2.27) and the equation of state for dark energy, w (Eq. (2.20)).

Another great service paid to cosmology is that, via gravitational lensing, clusters can be used as natural cosmic telescopes to explore regions of space that would otherwise be unaccessible. This also explains why astronomers are so interested in the mass of galaxy clusters, a precise determination of which would be beneficial both in the study of objects at high redshift and in probing the validity of competing cosmological scenarios. As we will see in Section 3.2.3, though, a rigorous and exact definition of the concepts of cluster mass and mass function is as elusive as it is of fundamental importance. We will therefore argue for the necessity of adopting the concept of the cluster lensing potential as the cardinal quantity to use instead of the mass in our reconstruction method.

3.2 Formation and abundance

One of the primary problems in cosmology concerns the formation of dark matter haloes in the ΛCDM picture of a hierarchical build-up of structures from smaller to larger scales via a sequence of mergers and accretion. Given the complexity of the equations describing this scenario, several numerical techniques have been developed in order to account for gravitational interactions, collisions among gas particles and pressure forces. In addition, it is possible to construct analytical models that illustrate the basic processes that lead to halo formation. One of these analytical models, and probably the most widely used, is the spherical collapse model, which becomes useful when the linear theory described in Section 2.3.1 breaks down. As a rule-of-thumb, one assumes that this occurs when the density contrast is no longer small compared to unity. In the case of galaxy clusters, $\delta \approx 10^3$, we can see therefore why a non-linear approach is required to treat them.

3.2.1 Spherical collapse model

A dark matter halo can be assumed to be a self-gravitating, quasi-equilibrium system of dark matter particles which formed by gravitational collapse [181]. Considering an Einstein-de Sitter (spatially flat and matter dominated) universe with critical density, ρ_{cr}, the spherical collapse (or *top-hat*) model studies the evolution of a homogeneous overdense sphere of density $\rho_{cr} + \delta\rho$ in an expanding background. This density perturbation evolves like a closed universe with a matter density parameter $\Omega_m = 1 + \delta$ and grows until it reaches a maximum radius $r = r_{max}$ (*turn-around*) at a time $t = t_{max}$ and then collapses in a finite time. This implies that its scale factor reaches a maximum as well. The evolution equation for the scale factor of such a perturbation is the first of Friedmann equations (Eq. (2.2.4)) with a positive curvature term. The Newtonian equation of motion for the radius of the perturbation is:

$$\ddot{r} = -\frac{GM}{r^2}, \tag{3.1}$$

where $M = \frac{4\pi\rho r^3}{3}$ for a homogeneous sphere, and the integral of motion which corresponds to the conservation of energy reads:

$$\frac{1}{2}\dot{r}^2 - \frac{GM}{r} = E, \tag{3.2}$$

where E is the total energy per unit mass of the system. A criterion for collapse can be found in the above relation for $E < 0$. A parametric solution for Eq. (3.1) is given in [125] in the special case of an Einstein-de Sitter universe[1] and the relation between the radius of the sphere and the time is:

$$r(\theta) = A(1 - \cos\theta), \tag{3.3}$$
$$t(\theta) = B(\theta - \sin\theta), \tag{3.4}$$

where θ denotes the development angle and is a scaled form of the conformal time. The relation between the constants A and B is given by $A^3 = GMB^2$. From the first functional form in Eq. (3.3) it is possible to determine the maximal size that the density fluctuation will reach by setting:

$$\frac{dr}{d\theta} = A\sin\theta = 0, \tag{3.5}$$

for which three solutions are available: $\theta = 0, \pi, 2\pi$. $\theta = 0$ corresponds to $t = 0$, $\theta = \pi$ corresponds to the maximum expansion radius at turn-around time, $t_{max} = t_a$ and $\theta = 2\pi$ indicates the time in which the sphere is fully collapsed to a singularity. This happens

---

[1]For a derivation, please see `http://www.ita.uni-heidelberg.de/research/bartelmann/Lectures/cosmology/cosmology.pdf`.

because the model only accounts for gravitational interactions. A more realistic treatment would consider the scattering of the particles and, by including it, it is possible to define a virialisation condition imposing that the spherical blob stops its collapse before reaching an infinite density and enters virial equilibrium. A hypothesis to explain the stability of the observed haloes is that they virialize, i.e. form a spherical system which satisfies the scalar virial theorem:

$$E_k = -\frac{1}{2}E_{pot}, \tag{3.6}$$

where E_k, E_{pot} are the kinetic and potential energies respectively. The virial radius is reached when the system has collapsed to approximately half its maximum radius and the density contrast[2] is $\delta \approx 200$.

3.2.2 The density profile of galaxy clusters

One of the central quantities in any comprehensive description of a galaxy cluster is its density profile. Unfortunately, providing a realistic treatment of all the DM and baryonic physics playing a role in clusters is not a challenge easy to face. If we restrict ourselves to a DM-only scenario where gravity is the sole actor in a CDM Universe, we can see from numerical simulations [116, 164] that the density profile of the DM halo, ρ_{DM}, exhibits a central density cusp and scales with r^{-1} in the inner part and with r^{-3} at larger radii. In more recent years, N-body simulations have specified even more the shape of this functional behaviour [76, 118].

Once we add baryons to the picture, things complicate further: cooling cores and a higher concentration for the dark matter are phenomena that have to be investigated [163], among many other effects.

Although it may appear to be a daunting task, being able to determine the density profile of galaxy clusters and to decompose it in the profile describing the baryonic and the dark matter components of the cluster is of immense importance in shaping a better understanding of the nature, structure and formation mechanisms of clusters of galaxies and on the nature of the dark matter.

In a later section, we will discuss the wealth in observational properties of galaxy clusters. An accurate model for their density profile is in general deemed necessary for studying the mass distributions at a wide range of radii [121].

In chapters 5 and 7, we will present a method that avoids putting too strongly constraining assumptions on the density profile. We will see, though, in Chapter 4 that this choice, as any other legitimately different one, has a price in terms of the other assumptions that one has to impose on the model.

---

[2]To be more precise, $\Delta_v \approx 178$ where $\Delta_v - 1 \approx \delta$.

The Hernquist profile

In 1990 Lars Hernquist [80] introduced the profile that later became known under his name. Starting from a spherical gravitational potential ϕ:

$$\phi(r) = -\frac{GM}{r+a},$$ (3.7)

in which he assumed the presence of a scale length, a, Hernquist derived a simple analytic form for the density profile, ρ:

$$\rho(r) = \frac{M}{2\pi} \frac{a}{r} \frac{1}{(a+r)^3},$$ (3.8)

which mimics the r^{-4} behaviour empirically determined for the observed luminosity distribution of elliptical galaxies and bulges and described by the de Vaucoulers' law [50].

By inserting it in the Poisson equation and fixing the integration constant such that the gravitational force vanishes at the centre (i.e., $\partial_r \phi = 0$ for $r = 0$), it is possible to retrieve the form (Eq. (3.7)) of the potential.

The Navarro, Frenk and White profile

In a series of papers published between 1995 and 1997 [115, 116, 117], Julio Navarro, Carlos Frenk and Simon White reported analyses of numerical simulations from which it emerged that a functional form that fits well the density profile of spherically averaged dark matter haloes is:

$$\frac{\rho(r)}{\rho_{cr}} = \frac{\delta_c}{x(1+x)^2} \quad \text{with} \quad x = \frac{r}{r_s},$$ (3.9)

where ρ_{cr} is the critical density for closure, r_s is the scale radius and δ_c is a dimensionless density contrast defined as:

$$\delta_c = \frac{200}{3} \frac{c^3}{\ln(1+c) - c/(1+c)}.$$ (3.10)

This profile differs from Hernquist's profile in its asymptotic behaviour for $r > r_s$: we can in fact notice that it tends to r^{-3} instead of r^{-4}.

The scale radius is defined as $r_s = r_{200}/c$, with r_{200} taken as the fiducial virial radius, the radius of a sphere whose mean density is 200 times the critical density, ρ_{cr}, and c is a factor called *concentration*, the only parameter on which the model depends for a given mass.

In the 1997 paper, Navarro, Frenk and White proposed that the density profile (that today carries their name and is often referred to as NFW profile) could be *universal*.

ΛCDM
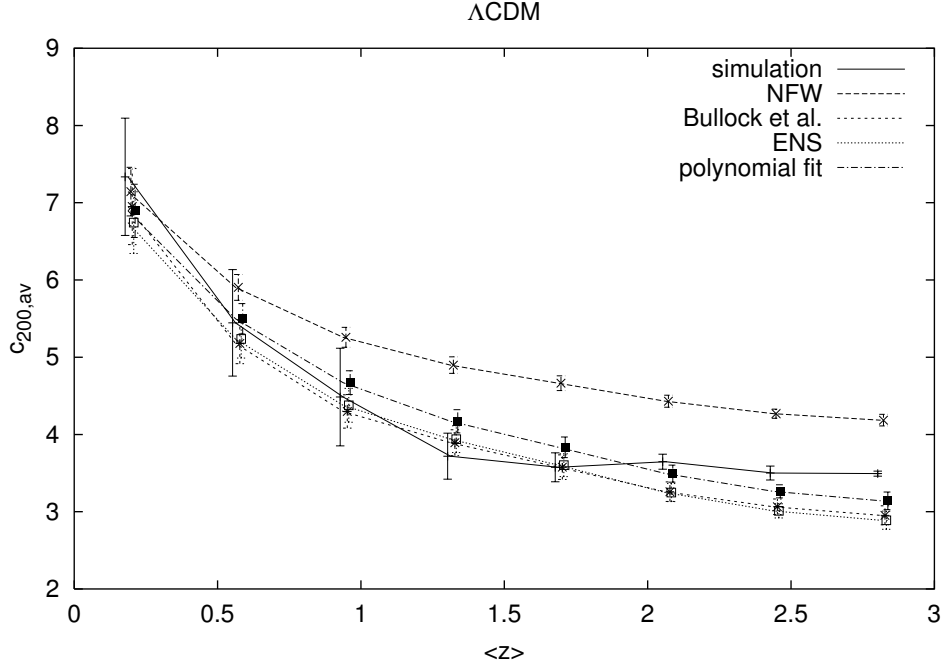
Figure 3.1: Concentration parameter as a function of redshift [55]. Galaxy clusters with the same mass show a higher concentration at higher redshifts.

All simulated and observed clusters of galaxies, in fact, exhibited the same shape of the profile, despite different halo masses, redshift, initial fluctuation spectrum and cosmological parameters that characterised them.

The Einasto profile

More recent simulations suggest the presence of a flattening central density profile that is better described by the Einasto profile [56]:

$$\rho_E(r/r_s) = \rho_s \exp\{-(2/\alpha_E)[(r/r_s)^{\alpha_E} - 1]\}, \tag{3.11}$$

where α_E is a structural parameter describing the degree of curvature of the profile, ρ_s is the density at the radius r_s that defines a volume containing half the total mass. At $r = r_s$ the double-logarithmic slope:

$$\alpha = \frac{d\ln\rho}{d\ln r} = -2(r/r_s)^{\alpha_E} \tag{3.12}$$

of the density profile has a value $\alpha = -2$, which coincides with the value of the NFW profile at r_s.

The Einasto profile with $\alpha_E = 1/5$ [107] was found to be a good fit for the density profile of numerically simulated dark matter haloes. While the NFW profile exhibits a central density cusp, the Einasto profile does not. If dark matter particles decay or annihilate, the annihilation rates depend on the squared particle density [15]. A profile with a finite-density core, as the Einasto profile is, would therefore lead to sensibly lower predictions of the annihilation rates than the NFW and to different levels of substructuring.

3.2.3 The mass functions and the quest for a definition of the mass of galaxy clusters

In the current paradigm of structure formation, clusters of galaxies, which can be viewed as rare peaks in the density field, are thought to be the last objects to collapse under the pull of gravity. While the struggle to identify a density profile that fits them in an accurate way is relevant in order to understand their internal structure, the attempt to predict the abundance of haloes is important in order to have information on their statistical distribution and to characterise the objects we observe based on their mass. The crucial quantity to do so is the *mass function* defined as:

$$\mathrm{d}N = n(M, z)\mathrm{d}M, \tag{3.13}$$

where $\mathrm{d}N$ is the number density of haloes per unit comoving volume with mass within M and $M + \mathrm{d}M$ as a function of redshift. Clusters of galaxies form the massive end of the halo mass function. An analytic expression for it was given by William H. Press and Paul Schechter in a paper they published in 1974. Their model is known as *Press & Schechter formalism* [140].

Their derivation relies on the assumption that the mass in all volumes in which the threshold of the critical density contrast δ_c is exceeded belongs to collapsed haloes and that the density fluctuation field, filtered by a top-hat window function, has a Gaussian probability distribution. The critical density contrast, δ_c, corresponding to virialised structures, is predicted by the spherical collapse model to have an approximate value of 1.69. The halo mass function, therefore, takes the shape:

$$n(M, z)\mathrm{d}M = \sqrt{\frac{2}{\pi}} \frac{\rho_0}{M} \frac{\mathrm{d}\nu}{\mathrm{d}M} \exp\left(-\frac{\nu^2}{2}\right) \quad \text{with} \quad \nu = \frac{\delta_c}{\sigma_R(M)D_+(z)}, \tag{3.14}$$

where ρ_0 is the average matter density of the Universe today, $D_+(z)$ is the growth factor from Eq. (2.47) and $\sigma_R(M)$ is the standard deviation of the mass fluctuations computed on the scale R. The exponential cutoff above a mass M_* defined by $\sigma_R(M_*) = \delta_c$ allows one to constrain the cosmological parameters, in particular σ_8 and Ω_m.

The Press & Schechter formalism, though, is not devoid of complications. Chiefly, it ignores the *cloud-in-cloud problem*: by assuming that only originally overdense regions

can be included in collapsed objects, it neglects the finite probability that overdense regions, enclosed within overdense regions, can enter the haloes as well. This problem was well known to the scientific community, since it represented a reason against the peak formalism proposed by Bardeen, Bond, Kaiser and Szalay [13], and it was solved by Press and Schechter by artificially introducing a factor of 2 in their expression to account for the missing matter. An alternative and more rigorous derivation of the mass function, which offered a way out of this *ad hoc* introduction, was devised by Bond, Cole, Efstathiou and Kaiser in 1991 [30]. They suggested the excursion set formalism, also known as *extended Press & Schechter* (EPS) formalism, making use of the statistics of random walks to infer the halo mass function.

Over the years, many shortcomings of the theory have been observed and modifications have been formulated. In particular, the EPS formalism is built upon the spherical collapse model, whilst nowadays the collapse is believed to be ellipsoidal. Another problem resides in the fact that it uses results from linear theory in order to predict structures that form in a non-linear density field.

The EPS theory was further extended with fitting functions by Ravi Sheth and Giuseppe Tormen to account for an ellipsoidal collapse in 1999 [158] and later by Jenkins et al. in 2001 [83]. Comparisons with numerical simulations, notably the Millenium Simulation [164], showed a remarkable agreement with the predictions of the modified versions of the EPS model.

The main point that we intend to make with this brief review is that the concept of mass is not uniquely defined despite it is crucial for cosmological studies. In particular, a galaxy cluster does not have a well-defined boundary, nor a well-defined centre and sphericity is a poor assumption for its geometry. In the following section we will introduce a quantity that one can resort to in order to bypass these problems, the projected potential.

3.3 Obervational properties of galaxy clusters

As we mentioned at the beginning of this chapter, galaxy clusters are very rich in observational properties. In this section we will limit ourselves to a brief overview of the observational features relevant for this work: gravitational lensing, X-ray emission, thermal Sunyaev-Zel'dovich effect and dynamics of member galaxies.

3.3.1 Gravitational lensing in clusters

When light rays propagate through a gravitational field, they are deflected. Despite this effect had already been speculated about by Isaac Newton, John Mitchell (1784), Pierre Simon de Laplace (1797) and Johann von Soldner (1804) [88, 162], to name some, it was not until the formulation of Einstein's general theory of relativity that a

Figure 3.2: Abell 1689. Galaxy clusters are the largest gravitationally bound objects in the Universe. Courtesy of NASA.

quantitative description of this phenomenon became available to the astronomical and physical community. The term used to describe the deflection of light by massive bodies and the phenomena stemming from it is gravitational lensing. Several reviews provide an extensive treatment of the topic and its applications [16, 17, 114, 153].

Galaxy clusters, with their huge masses, are perfect to identify the observational signatures of the strong and weak regimes of gravitational lensing: giant arcs in the case of strong lensing and arclets in the case of weak lensing. An example is shown in Fig. 3.2.

Gravitational lensing is a versatile instrument and serves both as a probe to study the physics of galaxy clusters and as a magnifying glass to explore objects that are further away from the reach of telescopes [111, 185]. It is sensitive both to luminous and dark matter. In fact, the gravitational field through which light propagates is related to the mass density of the lens via Poisson's equation, which implies that, on the one hand, lensing cannot discriminate between luminous and dark matter and that, on the other, light deflection is not affected by the nature of the matter nor by its equilibrium state [152].

A well-known combination of differential geometry and electrodynamics requires
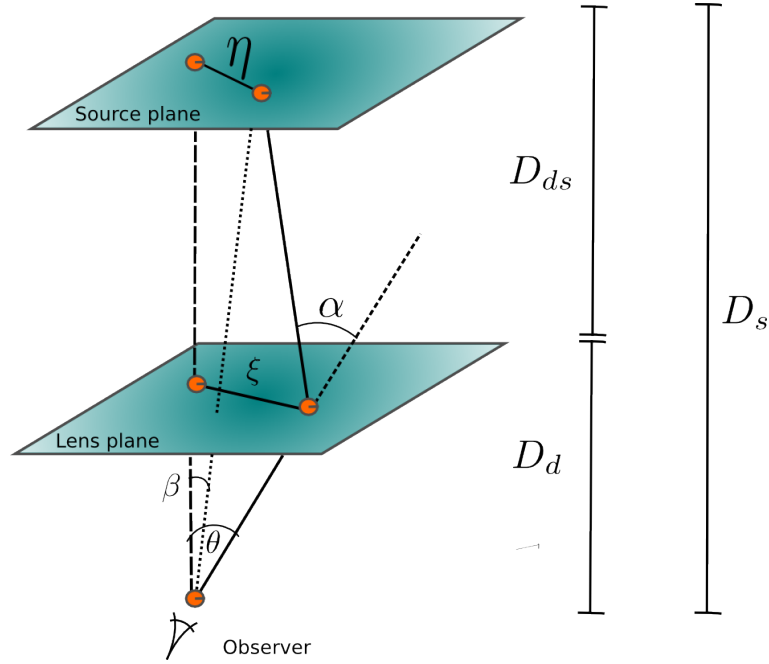
Figure 3.3: Lensing geometry in the thin screen approximation [114]. The thickness of the lens is negligible in comparison with the extent of the light path and the mass distribution of the lens can be substituted by a thin mass sheet orthogonal to the line of sight, the lens plane. The measurement of distances relies on the underlying cosmology, as described in Chapter 2, and allows to pass from physical to angular scales.

light propagation to occur along the null geodesics of the space-time metric. However, a typical lensing system is a localised matter distribution and can be fairly described by resorting to the thin lens approximation sketched in Fig. 3.3. The thin lens approximation can be invoked when the thickness of the lens is negligible in comparison to the extent of the path undertaken by light to reach the observer. This requirement is frequently met: a galaxy cluster has a typical size of a few Mpc, while the distances between the source, the lens and the observer are usually of the order of fractions of the Hubble length $cH_0^{-1} = 3h^{-1} \times 10^3$ Mpc.

In the cartoon (Fig. 3.3), D_s is the distance between the observer and the source, D_d represents the distance between the observer and the lens and D_ds indicates the distance between the lens and the source, α is the deflection angle, θ is the observed angular position and β is the unlensed angular position of the source. The unlensed position of the source and its images are related via the lens equation, or *ray-tracing* equation:

$$\vec{\beta} = \vec{\theta} - \vec{\alpha}(\vec{\theta}). \tag{3.15}$$

The lens equation is non-linear in the general case, which implies that multiple images at positions $\vec{\theta}_i$ can correspond to the same source position $\vec{\beta}$.

The main quantity we are interested in here is the lensing (or *deflection*) potential, ψ, defined as a scaled projection[3] along the line of sight of the Newtonian gravitational potential of the lens, ϕ:

$$\psi(\theta) = \frac{2}{c^2} \frac{D_{\mathrm{ds}}}{D_{\mathrm{d}} D_{\mathrm{s}}} \int \phi(D_{\mathrm{d}}\theta, z) \mathrm{d}z. \tag{3.16}$$

The deflection angle $\vec{\alpha}$ is related to the lensing potential ψ by:

$$\vec{\alpha} = \vec{\nabla}_\theta \psi. \tag{3.17}$$

The Laplacian of the lensing potential describes the convergence $\kappa(\vec{\theta})$, i.e. the surface mass density of the lens plane scaled to its critical value:

$$\kappa(\vec{\theta}) = -\frac{1}{2} \vec{\nabla}_\theta^2 \psi. \tag{3.18}$$

These two relations make the lensing potential a more straightforward and less error-prone quantity to address than the mass of a galaxy cluster, which, as we have seen, relies on a more cumbersome definition.

As mentioned in the Introduction, in fact, even though traditionally the mass of galaxy clusters is constrained making use of gravitational lensing, X-ray emission, the thermal SZ effect and galaxy kinematics, none of these observables measures cluster mass. On the other hand, all of them constrain in a way or another the projected gravitational potential. In particular, gravitational lensing constrains the curvature of the gravitational potential (i.e. the gravitational tidal field). X-ray emission and the thermal Sunyaev-Zel'dovich effect constrain respectively the temperature and the pressure of the intracluster gas, which can be related to the lensing potential, as we will see in Chap. 5. Galaxy kinematics constrain the gradient of the gravitational potential. Another negative aspect of the definition of cluster mass is that it is a global quantity requiring integration over second derivatives of the gravitational potential [8]. This operation is difficult to unequivocally perform on objects with irregular shapes and lacking precisely identifiable boundaries, as in the case of galaxy clusters.

If a source is much smaller than the scale on which the properties of the lens change, the lens mapping $\vec{\theta} \mapsto \vec{\beta}$ is always locally linear and the distortion of images is encoded in the Jacobian matrix:

$$\mathcal{A}(\vec{\theta}) = \frac{\partial(\vec{\beta})}{\partial(\vec{\theta})} = \begin{pmatrix} 1 - \kappa - \gamma_1 & -\gamma_2 \\ -\gamma_2 & 1 - \kappa + \gamma_1 \end{pmatrix} \tag{3.19}$$

---

[3]We will later reconstruct a projection of the gravitational potential along the line of sight, a quantity that is proportional to the lensing potential defined in Eq. (3.16).

which is written in terms of the lensing potential ψ, convergence κ and shear $\gamma = \gamma_1 + i\gamma_2$. The shear is the quantity that describes the shape distortion due to the gravitational tidal field and is related to the lensing potential by:

$$\gamma(\vec{\theta}) = \frac{1}{2}\psi_{,11} - \psi_{,22} + i\psi_{,12}. \tag{3.20}$$

The inverse of the Jacobian matrix, $\mathcal{A}(\vec{\theta})$, is called magnification matrix $M(\vec{\theta}) = \mathcal{A}^{-1}(\vec{\theta})$ and its determinant is called magnification, μ:

$$\mu = \det M = \frac{1}{\det \mathcal{A}} = \frac{1}{(1-\kappa)^2 - |\gamma|^2}. \tag{3.21}$$

A galaxy cluster acts therefore as a lens and distorts the shape, size and position of the background sources. Since lenses magnify background sources, clusters can be used as natural telescopes. Surface brightness has been shown to be conserved [125]. In this way, this magnification effect makes the background sources appear brighter than they would otherwise be and provides a larger angular resolution for the sources, allowing in many cases a detection that would not be possible without the presence of the cluster.

3.3.2 X-ray emission

Observations of clusters of galaxies show that they are some of the brightest X-ray emitters (with luminousities around $10^{43} - 10^{45}$ erg/s) in the Universe, second only to quasars. The main emission mechanism of diffuse X-rays has been identified to be the thermal bremsstrahlung by a hot ($T \sim 10^8$ K), low-density ($10^{-2} - 10^{-3}$ atoms/cm^3) plasma. The X-ray spectra of clusters also show line emission from ionised iron (Fe^{26+}) and other metals, which have been ejected from the galaxies in the intracluster gas [148].

If we consider a spherical cluster as a first approximation, and we assume that the ionised gas is in hydrostatic equilibrium, the mass profile of the cluster within the radius r can be described by [66]:

$$M(< r) = -\frac{k_B T}{Gm}\left(\frac{\mathrm{d}\ln\rho}{\mathrm{d}\ln r} + \frac{\mathrm{d}\ln T}{\mathrm{d}\ln r}\right)r, \tag{3.22}$$

where $\rho(r)$ and $T(r)$ are the density and temperature profiles of the ionised gas and m is the average mass of the gas constituents. The density profile $\rho(r)$ can be observationally determined by studying the surface brightness, S_X:

$$S_X(r) = 2\int_r^\infty \mathrm{d}r' \frac{r'}{\sqrt{r'^2 - r^2}} j_X(r'), \tag{3.23}$$

where $j_X(r) \propto n_e^2 \sqrt{T}$ is the luminosity density or emissivity and n_e is the electron number density [87]. In Chapter 5 we will show how to obtain information on the projected gravitational potential of the cluster from the surface brightness map.
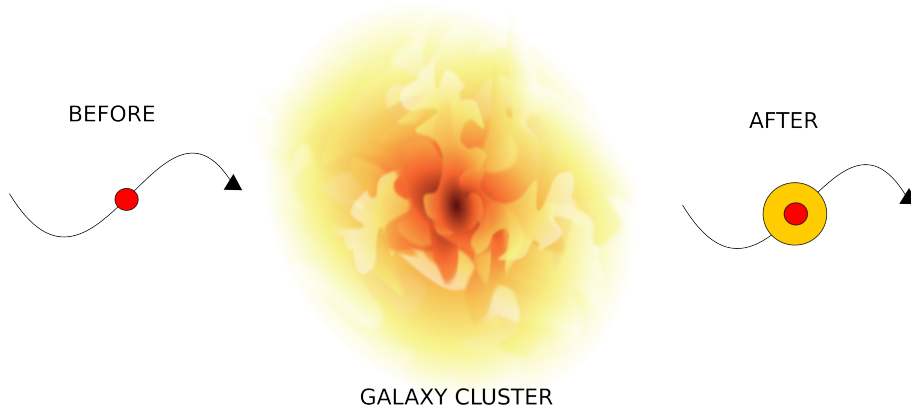
Figure 3.4: Thermal Sunyaev-Zel'dovich effect: some low-energy CMB photons receive an energy boost during the collision with the electrons of the hot ($T \sim 10^8 K$) intracluster medium. Image of cluster courtesy of J.C. Waizmann.

3.3.3 Thermal SZ effect

The thermal Sunyaev-Zel'dovich (or tSZ) effect [166] originates from the interaction between some of the CMB photons and high-energy electrons via inverse Compton scattering: by colliding with the electrons of the hot gas in clusters, the CMB photons scatter off and become more energetic. As a result, the initially perfect black-body spectrum of the cosmic microwave background radiation is distorted by the clusters of galaxies in its foreground. The observational signature of this effect is a transfer of photons from the low-energy (Rayleigh-Jeans) portion to the high-energy (Wien) section of the spectrum. This observable distortion from the original Planck spectrum is a valuable tool to probe both the properties of the cluster and the gas clustering as well as the cosmology. In particular, it is possible to use it to determine the value of H_0: since the Compton-y parameter is inversely proportional to the squared angular diameter distance, D_{ang}^2, and D_{ang}^2 is inversely proportional to H_0^2, it follows that the Compton-y parameter is directly proportional to H_0^2.

The thermal SZ effect depends on the integrated product of the number density of the electrons and the temperature and is encoded in the thermal Compton-y parameter, an integral of the electron pressure along the line-of-sight [141]:

$$y(\vec{s}) = \frac{k_B}{m_e c^2} \sigma_T \int \mathrm{d}z T(\vec{s}, z) n_e(\vec{s}, z), \qquad (3.24)$$

in which the thermal energy ($k_B T$) of the electrons is divided by the rest mass energy ($m_e c^2$), multiplied by the Thomson cross section, σ_T, and the electron number density,

n_e. The Compton-y parameter permits to quantify the intensity change, I_{SZ}, of the CMB radiation seen through a galaxy cluster with respect to the black-body spectrum $B_\omega(T)$ of the CMB:

$$\frac{\Delta I_{SZ}}{B_\omega(T)} = g(x)y(\vec{s}),$$ (3.25)

where x denotes the energy of the photon in units of the mean thermal energy, i.e. the dimensionless frequency:

$$x = \frac{\hbar\omega}{k_B T},$$ (3.26)

and the spectral function $g(x)$ is described by:

$$g(x) = \frac{x^4 e^x}{(e^x - 1)^2}\left[\frac{x(e^x + 1)}{e^x - 1} - 4\right].$$ (3.27)

It is negative for $x < 3.83$ and positive for larger values. This implies that the tSZ effect causes a positive signal for frequencies above 217 GHz, frequency corresponding to $x = 3.83$, and at the same time a negative one below. This signal represents a unique spectral signature for SZ studies. It is necessary to notice that the distortion in the CMB spectrum is tiny: the relative change in temperature of a CMB photon is of order 10^{-4} along a line of sight that crosses the centre of a rich cluster.

3.3.4 Galactic dynamics

Clusters are bound systems of galaxies and gas and are mainly dominated by their dark matter content. This statement alone explains why studying their dynamical and statistical properties, such as the velocity dispersions of their member galaxies, and their relation to the mass distribution is a powerful diagnostics to add relevant information to the picture that we have of them. Since a major part of this work deals with galactic dynamics, we chose to dedicate a separate chapter (Chapter 4) to it.

4

The dynamical structure of galaxy clusters

Given the breadth of the topic, writing a complete and comprehensive review of galactic dynamics would certainly be a complex task and exceed the scopes of this thesis. Several excellent reviews of galactic dynamics are available and were used for the extension of this chapter, in particular [25, 146]. The following chapter outlines the main theoretical foundations that will represent the starting point for the formulation and implementation of the method for the reconstruction of the lensing potential of galaxy clusters that we will detail in Chapters 7 and 8. Section 4.1 discusses the Vlasov (or collisionless Boltzmann) equation. In section 4.2, moments of the Vlasov equation are taken to obtain the Jeans equations. A specification in spherical coordinates is provided. Sections 4.3 and 4.4 introduce the concepts of mass-sheet degeneracy and mass-anisotropy degeneracy.

4.1 The Vlasov equation

A galaxy can be pictured as a self-gravitating system of stars and dark matter particles in a six-dimensional phase space and described via a particle distribution function or phase-space density $f(\mathbf{x}, \mathbf{v}, t)$.

We plan to use the study of the motion of the cluster member galaxies to infer the shape of the gravitational potential within which they move. Throughout this thesis we will assume that the cluster potential is solely sourced by the dark-matter distribution and that the baryonic effects can be neglected to leading order. Since dark matter constitutes roughly 90% of the energy density of a galaxy cluster, this assumption seems physically meaningful, at least as a first-order approximation. Hence, we will treat galaxies as test particles in an external gravitational potential, a situation that is *a priori* different from the case of a self-gravitating system typical for stellar kinematics studies. However, methods from stellar kinematics can be adapted to galaxy kinematics in clusters because the gravitational potential ϕ contained in the equations is generally not

restricted to the self-gravity of the system and can therefore be treated as an external quantity that may be sourced by a different matter distribution than the test particles. In contrast to hydrodynamics or plasma physics, which are dominated by short-ranged interactions, gravitational forces are long ranged and cannot be shielded. Therefore, no nearest-neighbour approximation is possible and the motion of a point-like test particle is affected by gravitational interactions with other particles in the full test volume. Given a test particle with mass m' moving in a volume filled by roughly equally distributed particles of mass m and particle number density n, the combined force of a surrounding spherical shell with radius r and thickness dr is given by

$$dF = 4\pi r^2 \frac{Gmm'}{r^2} n dr. \tag{4.1}$$

Assuming a constant particle number density, this relation can be integrated and yields:

$$F = \int_0^r 4\pi r'^2 \frac{Gmm'}{r'^2} n dr' = 4\pi Gmm'r, \tag{4.2}$$

which diverges linearly for $r \to \infty$. This consideration shows that long-range forces have ample influence on the motion of the test particle and that the density distribution of particles in the full test volume has to be taken into account. Long-ranged interactions play therefore an important role and are strongly dominating over short-ranged ones.

This argument is supported by considering the typical relaxation time scales due to the long-range interactions in galaxy clusters. For a generic astrophysical system, the relaxation time describes the timescale for a test particle to substantially change the direction of its motion due to gravitational interaction. For a stellar motion with initial velocity v in a disk-like configuration of radius R that is composed of N particles, this timescale can be estimated to be [14]:

$$t_{\text{relax}} = \frac{R}{v} \frac{N}{8 \ln N}. \tag{4.3}$$

This equation just constitutes an order-of-magnitude estimation and the fact that galaxy clusters are obviously not disk-like objects will be ignored for the sake of this example. For a typical cluster, masses are given by 10^{14} solar masses which can be split into a system of approximately $N = 1000$ objects of galaxy mass. We assume a virial radius of 1 Mpc and estimated galaxy velocities of 1000 km/s. Inserting these numbers into Eq. (4.1) yields a relaxation time of about $t_{\text{relax}} \approx 5 \cdot 10^{11}$ years, which exceeds the age of the Universe and therefore of the cluster lifetime by almost one order of magnitude.

Thus, one can safely assume that the test galaxy moves without being influenced by small-scale encounters with local dark-matter distributions or by collisions with other particles. Hence, the galaxy distribution in the cluster can be well approximated as a collisionless system moving under the influence of an external gravitational potential.

At a time t, the number dN of particles located in the volume element d^3x centred in $\mathbf{x}$ and velocity in the d^3v centred in $\mathbf{v}$ is:

$$dN = f(\mathbf{x}, \mathbf{v}, t)d^3x\,d^3v, \tag{4.4}$$

and the number density of the system is:

$$n(\mathbf{x}) = \int d^3v\, f(\mathbf{x}, \mathbf{v}, t). \tag{4.5}$$

A statistical description of the system can be achieved by assuming that the distribution function $f(\mathbf{x}, \mathbf{v}, t)$ satisfies Vlasov's equation, also known as the collisionless Boltzmann equation:

$$\frac{\partial f}{\partial t} + \sum_{i=1}^{6}\left(v_i\frac{\partial f}{\partial x_i} - \frac{\partial \phi}{\partial x_i}\frac{\partial f}{\partial v_i}\right) = 0, \tag{4.6}$$

where ϕ is the smooth potential under whose influence the particles in the system are moving. In vector notation,

$$\frac{\partial f}{\partial t} + \left(\mathbf{v}\cdot\nabla f - \nabla\phi\frac{\partial f}{\partial \mathbf{v}}\right) = 0. \tag{4.7}$$

This is the fundamental equation of stellar dynamics, a special case of Liouville's theorem, and states that the flow of stellar phase points through phase space is incompressible [25]. In other words, the phase-space density is conserved along flow-lines. If one makes use of the Lagrangian derivative:

$$\frac{df}{dt} \equiv \frac{\partial f}{\partial t} + \sum_{\alpha=1}^{6}\dot{w}_\alpha\frac{\partial f}{\partial w_\alpha}, \tag{4.8}$$

where $(\vec{x}, \vec{v}) = \vec{w} = (w_1, ..., w_6)$ are the phase-space coordinates, then the Vlasov equation can be expressed as:

$$\frac{df}{dt} = 0. \tag{4.9}$$

When analysing spherical or axially symmetric cluster configurations, it is convenient to transform the Vlasov equation to coordinates that reflect the symmetry properties of the system. If we assume, for instance, the galaxy cluster to obey spherical symmetry, choosing spherical polar coordinates allows to study the galaxy motion in a centrally symmetric potential $\phi(r)$.

In spherical polar coordinates (r, θ, φ), Vlasov's equation reads:

$$\frac{\partial}{\partial t}f + \dot{r}\frac{\partial}{\partial r}f + \dot{\theta}\frac{\partial}{\partial \theta}f + \dot{\varphi}\frac{\partial}{\partial \varphi} + \dot{v}_r\frac{\partial}{\partial v_r}f + \dot{v}_\theta\frac{\partial}{\partial v_\theta}f + \dot{v}_\varphi\frac{\partial}{\partial v_\varphi}f = 0, \tag{4.10}$$

where the time derivatives of the coordinates can be written in terms of the velocity components:

$$\dot{r} = v_r \tag{4.11}$$

$$\dot{\theta} = \frac{v_\theta}{r} \tag{4.12}$$

$$\dot{\varphi} = \frac{v_\varphi}{r\sin\theta}. \tag{4.13}$$

and the components of the acceleration can be derived from the Euler-Lagrange equations:

$$\dot{v}_r = \frac{v_\theta^2 - v_\varphi^2}{r} - \frac{\partial}{\partial r}\phi, \tag{4.14}$$

$$\dot{v}_\theta = \frac{v_\varphi^2 \cot\theta - v_r v_\theta}{r} - \frac{\partial}{\partial v_\theta}\phi, \tag{4.15}$$

$$\dot{v}_\varphi = \frac{-v_\varphi v_r - v_\varphi v_\theta \cot\theta}{r} - \frac{1}{r\sin\theta}\frac{\partial}{\partial\varphi}\phi. \tag{4.16}$$

4.2 The Jeans equations

Vlasov's equation (Eq. (4.6)) is a partial differential equation governing the time evolution of a phase-space density, which in general is a function in six dimensions, all parametrised by time. A complete solution is therefore not straightforward and is often impossible to achieve. In general, two strategies are available: either one simplifies the problem by taking appropriate assumptions on the system or takes moments of the equation by projecting out dimensions. This second strategy leads to a set of equations that we will extensively use in the course of this work: the Jeans equations.

The zeroth moment of Eq. (4.6) is simply obtained by integrating Eq. (4.6) over all possible velocities:

$$\int \frac{\partial f}{\partial t}\mathrm{d}^3v + \int v_i \frac{\partial f}{\partial x_i}\mathrm{d}^3v - \frac{\partial\phi}{\partial x_i}\int \frac{\partial f}{\partial v_i}\mathrm{d}^3v = 0. \tag{4.17}$$

For each velocity component, the mean velocity is defined by:

$$\bar{v}_i = \frac{1}{n(\mathbf{x})}\int \mathrm{d}^3v\, f v_i. \tag{4.18}$$

Rearranging its first two terms and taking Eq. (4.5), Eq. (4.18) and the divergence theorem into account, it is possible to rewrite Eq. (4.17) as:

$$\frac{\partial n}{\partial t} + \frac{\partial(n\bar{v}_i)}{\partial x_i} = 0, \tag{4.19}$$

a continuity equation for the spatial stellar density.

In order to get the next three equations, one can multiply Eq. (4.17) by v_j and integrate over all velocities:

$$\frac{\partial}{\partial t} \int f v_j \mathrm{d}^3 v + \int v_i v_j \frac{\partial f}{\partial x_i} \mathrm{d}^3 v - \frac{\partial \phi}{\partial x_i} \int v_j \frac{\partial f}{\partial v_i} \mathrm{d}^3 v = 0. \tag{4.20}$$

Following the same strategy as before, the result is:

$$\frac{\partial (n \bar{v}_j)}{\partial t} + \frac{\partial (n \overline{v_i v_j})}{\partial x_i} + n \frac{\partial \phi}{\partial x_j} = 0, \tag{4.21}$$

where

$$\overline{v_i v_j} = \frac{1}{n} \int v_i v_j f \mathrm{d}^3 v, \tag{4.22}$$

which can be written as the sum of the contribution of the streaming motion, $\bar{v}_i \bar{v}$, and the velocity dispersion tensor accounting for the distribution of stellar velocities with respect to the mean at each point, σ_{ij}^2:

$$\sigma_{ij}^2 = \overline{(v_i - \bar{v}_i)(v_j - \bar{v}_j)} = \overline{v_i v_j} - \bar{v}_i \bar{v}_j. \tag{4.23}$$

The velocity dispersion tensor described by Eq. (4.23) is manifestly symmetric ($\sigma_{ij} = \sigma_{ji}$) and, at any given point **x**, defines a velocity ellipsoid: an ellipsoid whose principal axes are determined by the orthogonal eigenvectors of the dispersion tensor and whose lengths of the semi-axes are defined by the square roots of its eigenvalues.

By subtracting v_j times the continuity equation (Eq. (4.19)) from Eq. (4.21) and making use of Eq. (4.23), one obtains a set of three equations known as Jeans equation for a collisionless fluid:

$$n \frac{\partial \bar{v}_j}{\partial t} + n \bar{v}_i \frac{\partial \bar{v}_j}{\partial x_i} = -n \frac{\partial \phi}{\partial x_j} - \frac{\partial (n \sigma_{ij}^2)}{\partial x_i}, \tag{4.24}$$

which is the equivalent of Euler's equation for fluid dynamics, a comparison which suggests to interpret the last term on the right-hand side as an anisotropic pressure. It is nevertheless crucial to notice how in this case an equation of state is missing that relates the pressure to the density.

In the case of fluid dynamics, there are five unknowns (three streaming motions, the density and the pressure) and there are the continuity equation, three components of the Euler equation and one equation of state to close the system. In the case of stellar dynamics, there are ten unknowns (three streaming motions, the density and six independent components of the dispersion tensor) and three components of Jeans equation and the continuity equation, leaving us with an underdetermined set of equations. We will further analyse this point in Chapters 7 and 8.

Another necessary remark to make is that, although any real distribution function obeys the Jeans equation, not every solution of the Jeans equation is a physical distribution function. In order to be as such, it should be everywhere non-negative. We will see in Chapter 6 that this requirement allows us to successfully apply the Lucy-Richardson deprojection algorithm to the problem of identifying the lensing potential of spherical and triaxial galaxy clusters.

4.2.1 The Jeans equation in spherical coordinates

We start from Vlasov's equation in spherical coordinates, (r, θ, φ), Eq. (4.10). If we substitute Eqs. (4.11) to (4.16) and integrate over the velocities to obtain the moment equations, we get the Jeans equation for each component of the gradient of the potential. The radial Jeans equation reads[1]:

$$
n \partial_t \bar{v}_r + n \left(\bar{v}_r \partial_r \bar{v}_r + \frac{\bar{v}_\theta}{r} \partial_\theta \bar{v}_r + \frac{\bar{v}_\varphi}{r \sin\theta} \partial_\varphi \bar{v}_r \right)
$$
$$
+ \partial_r (n\sigma_{rr}^2) + \frac{1}{r} \partial_\theta (n\sigma_{r\theta}^2) + \frac{1}{r \sin\theta} \partial_\varphi (n\sigma_{r\varphi}^2) \qquad (4.25)
$$
$$
+ \frac{n}{r} [2\sigma_{rr}^2 - (\sigma_{\theta\theta}^2 + \sigma_{\varphi\varphi}^2 + \bar{v}_\theta^2 + \bar{v}_\varphi^2) + \sigma_{r\theta}^2 \cot\theta] = -n \partial_r \phi,
$$

where $\partial_{x_i} = \frac{\partial}{\partial x_i}$. Several assumptions can be taken to simplify this equation. The first of which is to demand a stationary stellar-dynamical equilibrium, which sets the time derivative to zero and excludes any explicit time dependence from the galaxy number density and the mean radial velocity. Imposing spherical symmetry on the gravitational potential makes it physically meaningful to assume that the mean velocities in the tangential and polar directions vanish. Additionally, the velocity components can be considered to be statistically independent of each other. The tangential and polar velocity dispersions can be assumed to be equal since no preferred angular direction exists in a centrally symmetric configuration. One can therefore write:

$$
\bar{v}_\theta = \bar{v}_\varphi = 0, \qquad (4.26)
$$
$$
\sigma_{r\theta}^2 = \sigma_{r\varphi}^2 = \sigma_{\theta\varphi}^2 = 0, \qquad (4.27)
$$
$$
\sigma_{\theta\theta}^2 = \sigma_{\varphi\varphi}^2. \qquad (4.28)
$$

The Jeans equation is at this point a linear, first-order inhomogeneous differential equation for $n\sigma_r^2$:

$$
\partial_r (n\sigma_r^2) + 2\beta \frac{n\sigma_r^2}{r} = -n \partial_r \phi, \qquad (4.29)
$$

---

[1]There exists two additional equations constraining the tangential and polar mean velocity components respectively. Since they are of similar complexity and will be trivial for our further investigations once we assume Eqs. (4.26), we decided to omit reporting them here.

where we have introduced the anisotropy parameter, β, measuring the departure from isotropy of the velocity dispersion tensor:

$$\beta = 1 - \frac{\sigma_{\theta\theta}^2}{\sigma_{rr}^2}.$$
(4.30)

The anisotropy parameter takes values in the range $-\infty < \beta < 1$, where the extremes correspond to the cases of purely circular and purely radial orbits respectively. If $\beta = 0$, the velocity space is completely isotropic. A glance at Eq. (4.30) makes it evident how difficult it proves to determine the anisotropy parameter, $\beta(r)$, from observations. In fact, observations do not provide information on the radial or tangential velocity dispersions, σ_{rr}^2 or $\sigma_{\theta\theta}^2$, but only on the ones projected along the line-of-sight, σ_{los}^2, which are observed, among other quantities, in the Doppler distortion of the spectra: the width of a line that experiences Doppler broadening is directly related to the velocity dispersion averaged along the line of sight.

Furthermore, the observed spectral line is the result of the superposition of spectral lines of many galaxies along the line of sight and hence it incorporates information about the galaxy distribution as well. More precisely, brighter regions along the line of sight contribute more strongly than fainter ones. Assuming that the distribution of light along the line of sight is related to the galaxy density by some constant factor, we do not infer the projected velocity dispersion alone, but rather its density-weighted average. This is a most welcome property since, after appropriate deprojection, the results can straightforwardly be inserted into the Jeans equation.

We will make use of this last consideration and of Eq. (4.29) in Chap. 7 to formulate an algorithm able to recover the lensing potential of a galaxy cluster from the projection along the line of sight of the velocity dispersions of its member galaxies.

A general formulation of the Jeans equation in spherical coordinates and its solution:

$$n\sigma_r^2 = -\int_\infty^r n(r')\partial_r\phi(r')\exp\left\{2\int_r^{r'}\frac{\beta(r'')}{r''}dr''\right\}dr'.$$
(4.31)

can be found in [10].

4.3 Why gravitational lensing alone is not enough

As we discussed in Chapter 3, gravitational lensing is sensitive to the mass along the line of sight. Ideally, one would have one, well-defined lens but, especially in clusters of galaxies, this is often not the case. Additional shear and convergence from nearby objects and mass along the line of sight can be present. [177] studied, for example, the case of secondary matter planes producing strong lensing effects due to chance alignments along the line of sight and found, among other things, that these gravitational contaminations cause small but systematic effects leading to overestimation of the masses

of individual clusters by gravitational lensing techniques as compared with the results obtained with the velocity dispersions of the cluster members and/or the X-ray temperature.

The convergence of the lens is often degenerate with the morphology of the sources and this phenomenon, known as *mass-sheet degeneracy* [67, 154], makes it strictly impossible to disentangle the convergence of the lens from the other contributions when relying only on lensing with a single lens. Assuming that all the mass is concentrated in the lens will therefore result in a bias either in the estimate of the mass of the galaxy cluster or in the estimates of the cosmological parameters.

Over the years, several techniques have been devised to limit the effects of this degeneracy. [35] proposed to lift the degeneracy by resorting to the magnification effect: the local number counts of background sources is directly related to the magnification of the lens, which allows an estimate of the convergence [71, 169].[2] Another method proposed by [34] relies on the use of distortion and redshift information of background sources. Depending on the goal one has, a multi-wavelength/multi-probe approach can be effective in increasing the information one can extract from the data, while limiting the problem of dealing with the mass-sheet degeneracy. The same argument can be made for dynamics.

4.4   Why dynamics alone is not enough

The exploitation of dynamics is of profound relevance because it provides information on the mass of the clusters at large radii and gives additional constraints on quantities that can be studied through several other techniques, as we will see in the next chapters. Moreover, data come with different uncertainties and the dynamical and lensing masses are affected by projection in different ways. However, it has to be said that dynamics rely on an equilibrium assumption, while lensing does not, and that any attempt to determine the mass of a galaxy or a cluster is not a trivial operation.

Depending on what kind of information is required, the density profile, the mass-to-light ratio or the velocity anisotropy need to be modeled, sometimes assumptions on all these quantities have to be taken at once. The anisotropy profile is inevitably and directly correlated with the three-dimensional shape of the galaxy distribution via the tensor virial theorem and this implies that assumptions about the shape or viewing angle of the galaxy distribution are necessary, or that, alternatively, a deprojection algorithm has to be used. Other methods [38] require the phase-space distribution function to determine the anisotropy profile.

A degeneracy that all the dynamical studies need to take into consideration is the *mass-anisotropy degeneracy*: different assumptions regarding the anisotropy profile $\beta(r)$

---

[2] From Eq. (3.3.1) one can see that to first order the magnification is related to $1 + 2\kappa$, where κ is the convergence of the lens.

(Eq. (4.30)) lead to significantly different predictions for the mass distribution $M(r)$ of the cluster. Several methods have been presented to break or partially break this degeneracy. Examples are a joint analysis of the observed profiles of velocity dispersion and constraints from the fourth velocity moments (*kurtosis*) [93] or the use of flexible B-spline functions for the representation of the radial velocity dispersion in the spherically symmetric Jeans equation assuming a given functional form of the mass density [52, 53].

In dynamics, there exists a vast arsenal of techniques for the determination of galaxy and cluster masses, spanning from the Schwarzschild superposition of orbits [45] in the case of stellar kinematics and the Jeans analysis [25] to the caustic method [51], the use of analytical distribution functions, N-body simulations [47] and maximum-likelihood fits of the distribution of observed tracers in the projected phase space [101]. All these techniques have strengths and weaknesses and are successfully applied to a broad range of data. The choice of a specific method is customarily tied to the kind of information one wants to extract from the data and the kind of assumptions one is ready to make.

Our approach is based on the use of the Jeans equation and, in the spherical case, does not require assumptions on the shape of the density profile. As we have seen in the previous sections, the components of the Jeans equation do not constitute a closed set. In the case of spherically symmetric clusters, presented in Chapter 7, an additional constraint relating the density-weighted velocity dispersions, which we will call an effective galaxy pressure, to the density itself via a polytropic equation of state will be taken. By adopting this polytropic relation, we will be able to invert the radial component of the Jeans equation relating the effective galaxy pressure to the dark matter potential gradient.

In the case of a triaxial ellipsoid, a suitable form of a polytropic equation of state for the effective pressure is so far not available. It has though been feasible to approach the problem with perturbative techniques. Our results will be detailed in Chapter 8.

5

Introduction to the reconstruction method and application to the potential reconstruction from thermal gas emission

Galaxy clusters are characterised at different scales by a wealth of observational properties. As we discussed in the Introduction and in Chapter 3, these properties can turn into powerful diagnostics to obtain further insight on the physical nature of clusters. Over the years, several methods combining two or more of them have become available but none of these methods exploits the full spectrum of available cluster observables. Starting from the consideration that it is possible to relate all of these observables to the lensing potential, the essential goal of our approach is to construct a broad, joint method for its reconstruction that combines the information encoded in all of them in order to build a more comprehensive picture of galaxy clusters.

Section 5.1 introduces the key idea upon which we based the implementation of the reconstruction method and discusses the overarching theme of this thesis.

The second part of this chapter is dedicated to the application of the method to the reconstruction of the lensing potential from the observed surface brightness profile of X-ray emission in clusters.

Approximately 15% of the mass of a cluster of galaxies is composed of a hot, diffuse plasma that fills the cluster's potential well, as we mentioned in Chapter 3. A load-bearing assumption of the standard model of galaxy clusters posits that the galaxies and the gas in a cluster are in an approximate hydrostatic equilibrium with the gravitational potential of the cluster and that they approximately trace each other in the cluster [11, 65, 70, 148].

Section 5.2 presents the general calculation for the density in the case of a galaxy cluster in hydrostatic equilibrium and whose member galaxies form a polytropic gas and have isotropic velocities. Section 5.3 summarises a method to reconstruct the lensing potential of galaxy clusters from the observed X-ray surface brightness profile of galaxy clusters, described in detail in [87] and [170]. We start with the key points for its implementation and present the results of its application to a simulated cluster. In
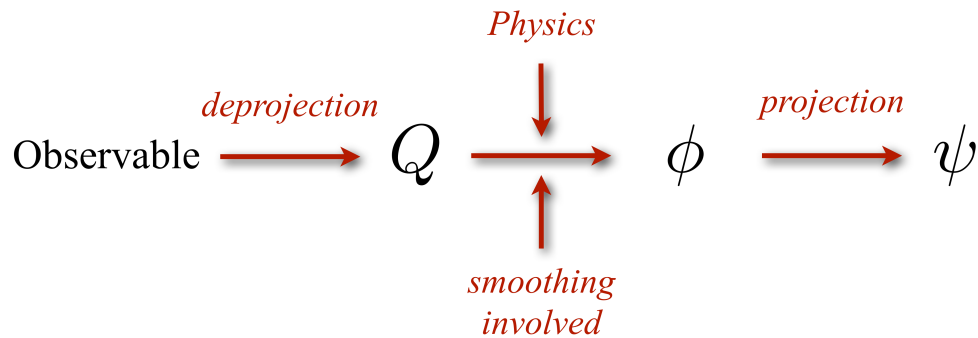
Figure 5.1: Key idea: Different phenomena can be described by a formally similar algorithm.

the following, we proceed with the results of its application to observational data in the case of Abell 1689. Section 5.4 reports on a method for recovering the projected gravitational potential from the observed relative changes in the intensity of the CMB photons through the thermal SZ effect, that will be published in Majer et al. 2015 (in prep.).

5.1 The key idea

As mentioned in the Introduction, this work is part of a more general effort aiming at the formulation of a unique, joint method for the reconstruction of the lensing potential of galaxy clusters that incorporates information from all the available cluster observables.

The key idea on which we base our method is sketched in the cartoon shown in Fig. 5.1. The input to the algorithm comes from a cluster observable (in turn, the observed X-ray surface brightness profile of galaxy clusters, the relative changes in the intensity of the CMB photons through the thermal SZ effect and the projected velocity dispersions of the cluster galaxies along the line of sight). This cluster observable is a projected quantity and we deproject it by means of the Richardson-Lucy deprojection method that we will discuss in Chapter 6. This method requires a shape to be assumed. For the purposes of the deprojection, it turns out to be sufficient to assume a spherical galaxy cluster, as it will be shown in Chapters 7 and 8. We have then a deprojected quantity Q, which we want to relate to the three-dimensional gravitational potential ϕ of the cluster. This is the step in which the physics describing the different phenomena (X-ray emission due to thermal bremsstrahlung, thermal SZ effect and galaxy kinematics) plays a major role. At this point, we have a relation connecting the deprojected observable to the gravitational potential. We can then invert it to obtain an expression for the gravitational potential and subsequently project it along the line of sight to recover the

quantity of interest, the projected potential.

A model-free, maximum-likelihood reconstruction method combining strong- and weak-lensing information was developed by [18, 37, 109] and is called SaW-Lens, an acronym standing for *Strong And Weak Lensing*.

The input to SaWLens is a catalogue containing the positions of the sources in an arbitrary coordinate frame and the two corresponding components of the ellipticity. Information regarding the strong-lensing constraints can be provided by giving as an input a catalogue containing the positions of multiple images and of estimates of critical-point coordinates.

A two-component χ^2-function is then defined as:

$$\chi^2(\psi) = \chi_W^2(\psi) + \chi_S^2(\psi),$$

(5.1)

where the individual terms depend on the lensing potential ψ and account for the information provided by the strong- ($\chi_S^2(\psi)$) and weak-lensing ($\chi_W^2(\psi)$) constraints, such as multiple images, critical curves, ellipticity and, as an additional option, flexion measurements. Since the individual χ^2-functions are statistically independent, they can be combined. The overall χ^2-function is then minimised with respect to ψ in every pixel:

$$\frac{\partial \chi^2(\psi)}{\partial \psi_l}! = 0, \;\; l \in [0, N_{\text{pixels}}],$$

(5.2)

where l indicates the grid position and N_{pixels} the number of pixels.

The result of this minimisation is the lensing potential that reproduces the multiple input constraints best. For a more detailed presentation of SaWLens, we refer the reader to [108].

This maximum-likelihood approach can be extended to incorporate in the reconstruction of the lensing potential the information contained in all the cluster observables at once, covering in this way a wide range of scales:

$$\chi^2(\psi) = \chi_W^2(\psi) + \chi_S^2(\psi) + \chi_X^2(\psi) + \chi_{SZ}^2(\psi) + \chi_{\text{kin}}^2(\psi) + ...$$

(5.3)

where $\chi_X^2(\psi)$ is the term accounting for the information provided by the X-ray emission, $\chi_{SZ}^2(\psi)$ includes the reconstruction from the relative changes in the intensity of the CMB photons through the thermal SZ effect and $\chi_{\text{kin}}^2(\psi)$ includes the reconstruction from the line-of-sight projected velocity dispersions of the cluster galaxies.

For clarity, in the next sections we will briefly review the method for deriving the lensing potential from the X-ray surface brightness profile of galaxy clusters and anticipate the method for the potential reconstruction from the relative changes in the intensity of the CMB photons through the thermal SZ effect. Chapter 7 and Chapter 8 are instead dedicated to the detailed description of the algorithm for the reconstruction of the lensing potential from kinematics, which is the main topic of this thesis.

5.2 General calculation for the isotropic case

In or near hydrostatic equilibrium and independently of the cluster shape, the hydrostatic equation reads:

$$\frac{\vec{\nabla} p}{\rho_{\text{gas}}} = -\vec{\nabla}\phi, \tag{5.4}$$

where p and ρ_{gas} are the gas pressure and density, respectively. The gravitational potential ϕ of the cluster is dominantly sourced by the dark matter distribution.

We assume a polytropic stratification for the gas:

$$p = p_0 \left(\frac{\rho_{\text{gas}}}{\rho_0}\right)^\gamma, \tag{5.5}$$

where γ is the polytropic index and the quantities with a subscript 0 refer to an arbitrary fiducial radius r_0 that could, for example, be set to the virial radius.

Inserting this relation in Eq. (5.4) yields:

$$\vec{\nabla}\left[p_0 \left(\frac{\rho_{\text{gas}}}{\rho_0}\right)^\gamma\right] = -\rho_{\text{gas}}\vec{\nabla}\phi, \tag{5.6}$$

Since we know that:

$$\vec{\nabla}\left[\left(\frac{\rho_{\text{gas}}}{\rho_0}\right)^{\gamma-1}\right] = (\gamma - 1)\left(\frac{\rho_{\text{gas}}}{\rho_0}\right)^{\gamma-1}\vec{\nabla}\left(\frac{\rho_{\text{gas}}}{\rho_0}\right), \tag{5.7}$$

if we integrate both sides and rearrange the terms, we obtain:

$$\rho_{\text{gas}} = \rho_0 \left[\frac{\rho_0}{p_0}\frac{(\gamma-1)}{\gamma}(\phi_{\text{cutoff}} - \phi)\right]^{\frac{1}{(\gamma-1)}}, \tag{5.8}$$

where we introduced a cutoff radius $r_{\text{cutoff}} > r_0$ and fixed the gravitational potential such that $\phi_{\text{cutoff}} = \phi(r_{\text{cutoff}})$.

5.3 Implementation of the method and application to simulated X-ray data

As we introduced in Chapter 3, the main emission mechanism of diffuse X-rays has been identified to be the thermal bremsstrahlung by a hot ($T \sim 10^8$K), low-density ($10^{-2} - 10^{-3}$ atoms/cm^3) plasma. With the term *bremsstrahlung*, we designate the electromagnetic radiation produced by the acceleration of a charge (e.g., in a plasma, an electron) in the Coulomb field of another charge (e.g. an ionised nucleus). A classical

treatment of this problem shows that an unbound electron coming from infinity and scattering off an ion with charge Ze, where Z is the atomic number and e is the elementary charge, follows a hyperbolic orbit, where the distance of closest approach is referred to as *impact parameter*, b. A Fourier transform of this orbit allows us to retrieve the spectrum (i.e., the distribution of the energy over frequency) for a single electron. At this point we can account for the fact that we do not deal with a single process but with a superposition of such interactions.

Introducing the number density of ions and electrons n_i and n_e and integrating over all impact parameters, we obtain the mean bremsstrahlung spectrum assuming that all the electrons have the same velocity v_∞ at infinite distance. Of course, this is not a realistic description of the phenomenon. We therefore want to generalise these results to a population of electrons with a given velocity distribution. The case in which we are interested is a thermal population, namely an electron population with a locally uniform temperature T. Then, the velocity distribution of the particles is Maxwellian. Such a process occurring in a plasma in thermal equilibrium is called *thermal bremsstrahlung*.

In [14] we can find an expression for the spectra described above and for the frequency-dependent emissivity due to non-relativistic, thermal bremsstrahlung that one can obtain after integrating the mean bremsstrahlung spectrum over a thermal electron population:

$$j_X(\omega) = \frac{16\pi^2}{3\sqrt{3}} \frac{Z^2 e^6 n_i n_e}{m_e^2 c^3} \bar{g}(\omega) \sqrt{\frac{2m}{\pi \kappa_B T}} \exp\left(-\frac{\hbar\omega}{k_B T}\right), \tag{5.9}$$

where ω is the frequency, $\hbar$ is the reduced Planck constant, k_B is Boltzmann's constant and m_e is the mass of the electron. This spectrum is flat up to a cutoff at $\frac{\hbar\omega}{k_B T}$ and falls off exponentially at higher frequencies. The velocity-averaged Gaunt factor $\bar{g}(\omega)$ encapsulates the quantum-mechanical correction to the classical formulae and can be approximated by unity in many astrophysical situations.

If we substitute the electron and ion number densities with the gas density ρ and integrate over all frequencies, we arrive at an expression for the frequency-integrated emissivity due to bremsstrahlung:

$$j_X = \frac{16\pi^2}{3\sqrt{3}} \frac{Z^2 e^6}{\bar{m} m_e^2 c^3 \hbar} \sqrt{\frac{2m}{\pi}} \rho^2 \sqrt{k_B T} = C\rho^2 T^{1/2}, \tag{5.10}$$

where C is the bremsstrahlung constant and $\bar{m}$ is the mean gas-particle mass.

In [87] we develop a method for recovering the projected gravitational potential from the observed X-ray surface brightness profile of galaxy clusters. We start by assuming hydrostatic equilibrium. In this case, the density ρ and the temperature T of the gas are fully characterised by the Newtonian potential ϕ. We can follow the logic exposed in section 5.2 and, according to Eq. (5.8), we find for the density an expression:

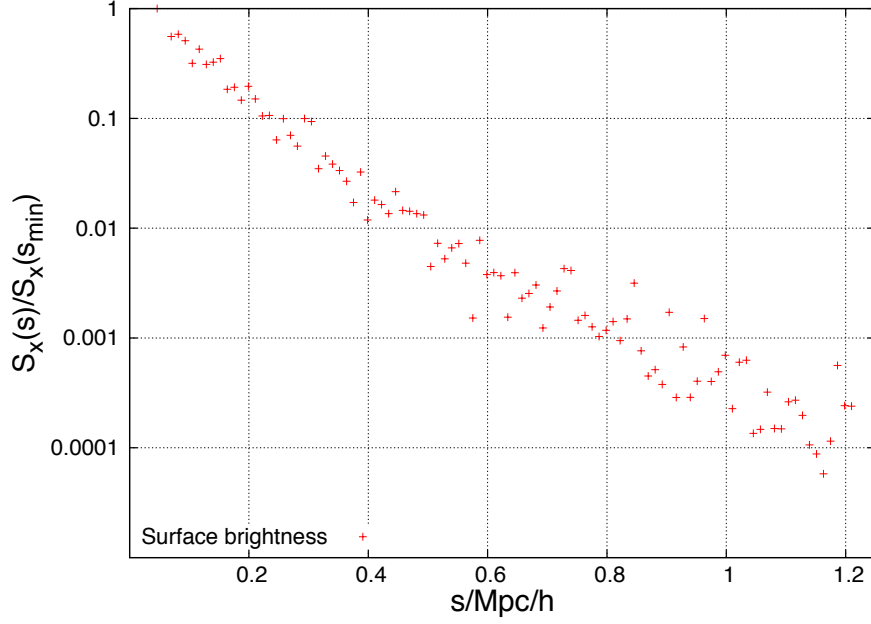$$\rho_{\text{gas}} = \rho_0 \varphi^{\frac{1}{(\gamma-1)}}, \tag{5.11}$$

Figure 5.2: Azimuthally averaged and normalised surface brightness profile of a simulated galaxy cluster with a mass of $5 \times 10^{14} \, h^{-1} M_\odot$ and a redshift of 0.2 as a function of the projected radius s [87].

where we have introduced the dimensionless potential:

$$\varphi = \frac{\rho_0}{p_0} \frac{(\gamma - 1)}{\gamma} (\phi_{\text{cutoff}} - \phi), \tag{5.12}$$

and where the quantity:

$$\gamma \frac{p_0}{\rho_0} = c_{s,0}^2 \tag{5.13}$$

is the squared sound speed at the cutoff radius.

The temperature of an ideal gas in thermal equilibrium with the potential φ is:

$$T = \frac{\bar{m}}{k_B} \frac{P}{\rho} = \frac{\bar{m}}{k_B} \frac{P_0}{\rho_0} \varphi = T_0 \varphi, \tag{5.14}$$

where T_0 is the temperature at the fiducial radius.

If we combine Eq. (5.14) with Eq. (5.10), we can find the following relation:

$$j_X = C \rho_0^2 T_0^{1/2} \varphi^\eta, \quad \eta := \frac{3 + \gamma}{2(\gamma - 1)}. \tag{5.15}$$
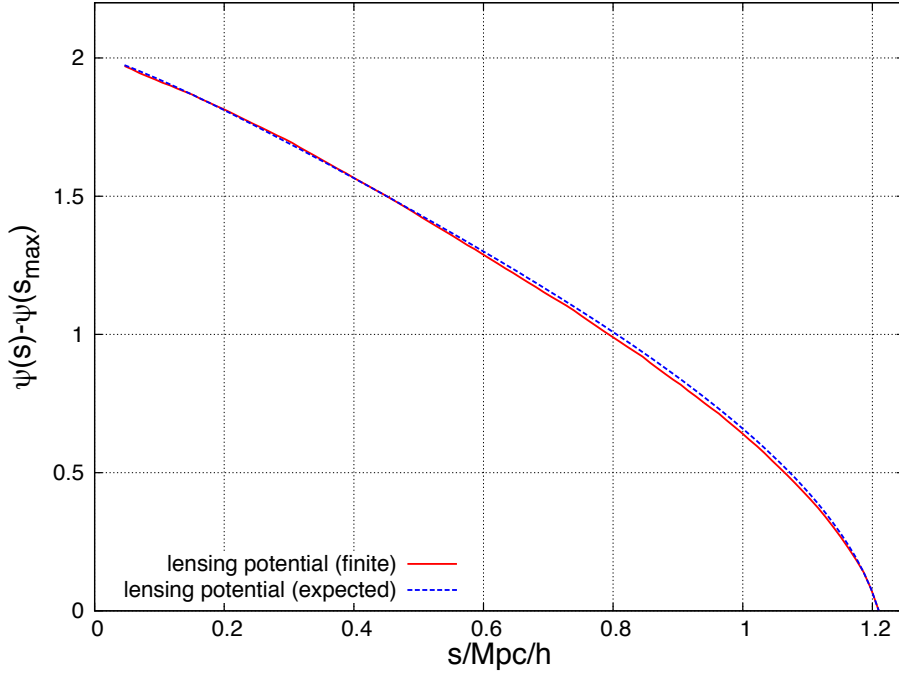
Figure 5.3: Reconstructed and normalised projected potential of the simulated galaxy cluster whose surface brightness profile is shown in Fig.5.2 as a function of the projected radius s. The potential was reconstructed assuming $\alpha = 0.4$ (Eq. (6.10)) and $L = 0.3\,h^{-1}$Mpc in the Richardson-Lucy deprojection [87].

Assuming a polytropic relation between the temperature profiles and the integrated emissivity profiles yields adiabatic indices that lie in the range $1.1 \lesssim \gamma \lesssim 1.2$ [68].

If we look again at the idea sketched in Fig. 5.1, we can see that we obtained an expression of the three-dimensional Newtonian potential in terms of a deprojected quantity, the frequency-integrated emissivity due to bremsstrahlung, and that we are now able to obtain an estimate for the projected gravitational potential.

Our algorithm to constrain the projected potential from the projected X-ray surface brightness is composed of the following steps:

1. We deproject the projected X-ray surface brightness map, S_X, by resorting to the Richardson-Lucy method described in Chapt. 6 and find an estimate for the frequency-integrated emissivity, $\tilde{j}_X$;

2. We use Eq. (5.15) to derive an estimate for the three-dimensional Newtonian

potential[1]:

$$\tilde{\varphi} = \left(\frac{\tilde{j}_X}{C\rho_0^2 T_0^{1/2}} \right)^{1/\eta} ; \qquad (5.16)$$

3. We project $\tilde{\varphi}$ along the line of sight and obtain an estimate $\tilde{\psi}$ for the two-dimensional potential, which is proportional to the lensing potential and can therefore be combined with estimates of ψ derived from lensing and other reconstruction methods.

In order to test our algorithm, we simulate galaxy clusters in a spatially flat, standard ΛCDM Universe with $\Omega_m = 0.3$, $\Omega_b = 0.04$ and $\Omega_\Lambda = 0.7$. We assume that the density profile of the dark matter in the cluster potential well has the NFW form [117], described by Eq. (3.9) in Sect. 3.2.2. The gas-mass fraction is set to equal the universal baryon mass fraction $f_b = \Omega_b/\Omega_m$ and the gas is assumed to consist of 75% of hydrogen and 25% of helium, both completely ionised, with an effective adiabatic index $\gamma = 1.2$. The virial radius of the cluster is approximated by r_{200}.

We use Eqs. (5.12) and (5.14) to compute the gas density and temperature profiles. We set the cutoff radius for the gravitational potential to $100\,r_{200}$, which makes the temperature profile drop to zero at a large radius.

For a detailed description of the properties of the simulated CCD image and of further tests of our algorithm, please refer to [87]. The normalised surface brightness profile for one realisation of a galaxy cluster with a mass $5 \times 10^{14} h^{-1} M_\odot$ and a redshift of 0.2, which represents the input to our algorithm[2], is shown in Fig.5.2.

The output of our algorithm, namely the reconstructed and normalised projected potential, is shown in Fig. 5.3 and plotted against the expected result for reference. The expected projected gravitational potential is taken to be the solution of Poisson's equation assuming an NFW density profile with the addition of Poissonian noise [87].

5.3.1 Application to observational data

Our method has been applied to X-ray observations of the cluster Abell 1689 in [170]. The cluster is located at a redshift of 0.183 in the Virgo constellation and is a well-known strong-lensing cluster. Kinematics and X-ray studies ([94, 110, 112, 131, 157]) revealed a discrepancy between the hydrostatic mass and the mass estimated from gravitational lensing and offered several possible explanations, mostly agreeing on indicating a merger aligned with the line of sight ([7] and references therein).

To recover the cluster potential from X-ray measurements, we first deproject the X-ray data, then convert the X-ray three-dimensional profile into the three-dimensional

---

[1]It is probably worthwhile observing that the exponent η in Eq. (5.15) is a large number (its value lies in the range $10 \lesssim \eta \lesssim 20$) and that therefore the exponent $1/\eta$ in Eq.(5.16) is a small number, which helps smoothing $\tilde{\varphi}$ and thus damping errors.

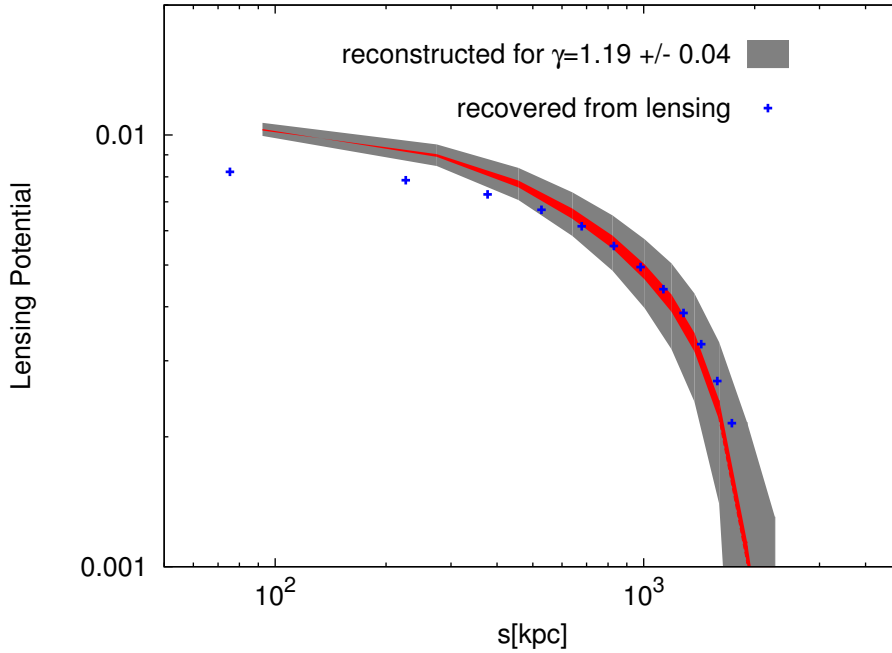[2]The concentration parameter (Eq. (3.10)) for the NFW profile has been set to $c = 5$.

Figure 5.4: Projected gravitational potential reconstructed using the method described in [87] compared to the potential recovered from weak gravitational lensing as a function of the projected radius *s*. The projected potential reconstructed from the X-ray emission has been obtained by assuming a polytropic index $\gamma = 1.19 \pm 0.04$. The choice of this value is based on a fit of the polytropic relation between the emissivity and the temperature profile [170]. The potential recovered by lensing is shown in blue; the mean projected potential obtained from X-ray observations with $\gamma = 1.19 \pm 0.04$ is shown in red, the uncertainties of the latter are shown in gray. The mean and errors have been obtained using a Monte Carlo method to randomize the algorithm described in Konrad et al 2013 [87]. The reconstructed lensing potential has been normalized to the lensing data within a circular shell region delimited by the radii in the range [92; 1734] kpc.

gravitational potential using equilibrium assumptions, and project it again to compare it with the two-dimensional gravitational potential obtained by gravitational lensing, following the algorithm described in Sect. 5.1 and in this section. The reconstructed, two-dimensional potential, assuming a polytropic index $\gamma = 1.19 \pm 0.04$, is shown in Fig. 5.4. This profile is compared with the lensing potential obtained from weak lensing.

At radii larger than 500 kpc our reconstructed potential profile agrees well with the reconstructed lensing potential within the error bars, even if the potential reconstructed from the X-ray emission appears to be slightly less curved. The discrepancy at small radii and the slight curvature change at larger radii may be caused by the lack of resolution in the weak-lensing measurement and by the other assumptions made (sphericity,

polytropic stratification, hydrostatic equilibrium, ideal-gas equation of state) and is expected to vanish if more potential observables are taken into account. For instance, a combined strong- and weak-lensing reconstruction is expected to yield a better match in the region close to the cluster centre because the strong lensing is sensitive to this region and has the resolution to resolve it.

For a complete discussion of the application of the reconstruction method to Abell 1689 and an analysis of the possible reasons for such a discrepancy at small radii ($R \lesssim 500$kpc), please refer to [170].

5.4 Application to the thermal SZ effect

The above-described reconstruction method can also be applied to recover the projected gravitational potential from the observed relative changes in the intensity of the CMB photons through the thermal SZ effect and is currently under study (Majer et al. 2015, in prep.). As mentioned in Sect. 3.3.3, the thermal SZ effect is a small distortion of the black-body CMB spectrum due to inverse Compton scattering of the CMB photons with the more energetic ICM electrons.

By assuming hydrostatic equilibrium and a polytropic stratification of the intra-cluster gas, it is possible to find a relation between the Compton-y parameter and the Newtonian gravitational potential. Given these assumptions, we can use Eq. (5.12) for the binding potential of the cluster and derive Eq. (5.14) for the temperature of a gas in thermal equilibrium from the ideal gas equation.

Combining Eqs. (5.11), (5.14) and (3.24) allows to rewrite the Compton-y parameter in terms of the gravitational potential as:

$$y(\vec{s}) = \frac{k_B}{m_e c^2} \sigma_T T_0 \rho_0 \int \mathrm{d}z \varphi^\zeta(\vec{s}, z), \tag{5.17}$$

with the exponent $\zeta = \gamma(\gamma - 1)^{-1}$.

From Eqs. (3.25) and (5.17) we can infer the relation

$$P(\vec{r}) = P_0 \varphi^\zeta(\vec{s}, z), \tag{5.18}$$

between an effective pressure $P(\vec{r}) = P_0 T(\vec{r}) n_e(\vec{r})$ and the dimensionless gravitational potential φ, where the amplitude:

$$P_0 = g(x) \frac{k_B}{m_e c^2} \sigma_T T_0 \rho_0 \tag{5.19}$$

was introduced, where $g(x)$ is the spectral function described in Eq. (3.27) and x is the dimensionless frequency in Eq. (3.26). We can at this point notice a formal analogy with Eq. (5.15).

We can therefore use Eq. (5.18) to implement a method analogous to the one presented in Sect. 5.3:

1. We deproject the measured, relative specific intensity change (Eq. (3.25)), $\Delta \bar{I}_{SZ} s(B_\omega(T))^{-1}$, by resorting to the Richardson-Lucy method described in Chapt. 6 and find an estimate for the three-dimensional effective pressure P;

2. We use Eq. (5.18) to derive an estimate for the three-dimensional Newtonian potential:

$$\tilde{\varphi} = \left(\frac{P(\vec{r})}{P_0} \right)^{1/\tilde{\zeta}} ; \qquad (5.20)$$

3. We project $\tilde{\varphi}$ along the line of sight and obtain an estimate $\tilde{\psi}$ for the two-dimensional potential, which is proportional to the lensing potential and can therefore be combined with other estimates of ψ derived from lensing.

6

Richardson-Lucy deprojection method

In Chapter 5 we introduced the working principles of our reconstruction method. The first step of the algorithm sketched in Fig. 5.1 requires a deprojection: from a quantity projected along the line of sight we want to retrieve a three-dimensional quantity to relate to the Newtonian, gravitational potential of the cluster, which we will then integrate along the line of sight to obtain an estimate for the two-dimensional gravitational potential of the lens.

In this chapter we present the implementation of the deprojection method that we use in the following chapters for the reconstruction of the two-dimensional gravitational potential starting from the projections of the velocity dispersions of cluster galaxies along the line of sight. Its contents partially reproduce the section on deprojection contained in the paper *Reconstructing the projected gravitational potential of galaxy clusters from galaxy kinematics* [Sarli et al. 2014] [149]. Similar implementations have been used for the reconstruction of the projected gravitational potential from the observed X-ray surface brightness profile of galaxy clusters and from the observed changes in the intensity of the CMB photons using SZ data and are detailed in Konrad et al. 2013 [87] and Majer et al. 2015 (in prep.).

6.1 Inverse problems in astronomy

In physics, and therefore in astronomy and astrophysics, methods to solve data-interpretation problems can be generally categorised in two ways: direct and inverse. The direct method approaches the problems by identifying and following a causal sequence: starting from the formulation of hypotheses, their possible implications are analysed and compared to simulations or available observed data. Although this forward procedure is the most commonly and successfully used one and has the most predictive power, problems arise in many branches of astronomy and astrophysics that require an inverse formulation. For an interesting overview of forward and inverse problems in astronomy, please see Lucy 1994 [96]. In this paper, Lucy specifies two criteria that designate the inverse character of a problem. The first one is the lack of possibility of *in situ* measure-

ments of the quantity of interest, which is often the case in astronomy, and the second one is the absence of a physical model on which the predictions can be based on due to a poor theoretical understanding of the phenomenon. The first criterion is straightforwardly met in the study of galaxy clusters and, as seen in Chapter 4, the latter criterion is met in the case of the anisotropy profile of cluster galaxies.

A large number of inverse problems in astronomy can be cast in the form of a Fredholm or a Volterra integral equation [2]. The main difference between the two is that a Fredholm integral equation has constants as integration limits, while the Volterra integral equations have the independent variable of the equation as integration boundary. In 1-D notation, the Volterra integral equation of the first kind takes the generic form of:

$$\phi(x) = \int_0^x \psi(\xi) P(x|\xi) \mathrm{d}\xi, \tag{6.1}$$

and the Volterra integral equation of the second kind reads:

$$\phi(x) = \psi(x) + \int_0^x \psi(\xi) P(x|\xi) \mathrm{d}\xi, \tag{6.2}$$

where ψ is the function of interest, ϕ is the function available to observation and P is the projection kernel. Lucy points out that for almost all of the inverse problems that can be reduced to this standard form, the functions ϕ, ψ and P are non-negative. As mentioned in Sect. 4.2, this is also the case for any solution of the Jeans equation that is at the same time a physical distribution function. The topic we want to address belongs to this class of problems.

We will see in Chapter 7 that a central role in the reconstruction of the projected gravitational potential of galaxy clusters from the line-of-sight projected velocity dispersions of the cluster members is played by the inversion of a Volterra integral equation of the second kind relating the density-weighted, three-dimensional velocity dispersions of the cluster galaxies to the three-dimensional gravitational potential of the cluster. Observations, though, only yield the line-of-sight projection of the galaxy velocity dispersions and in order to be able to formulate our problem in terms of an equation of the form of Eq. (6.2), we first need to perform a deprojection.

6.2 Implementation of the Richardson-Lucy algorithm

Different deprojection techniques by which it is possible to retrieve the three-dimensional velocity dispersions are available. An option briefly discussed in [102, 147] is the deprojection by a Fourier transform. If proper integration variables are chosen, projection can be considered as a convolution problem (see Eq. (6.4)). A Fourier transform of this convolution leads to a product in Fourier space which can be inverted easily. Transforming back to real space yields the deprojected function[1]. Another possibility is the

---

[1] See [84] for a more detailed discussion.

Abel inversion used by [28, 102, 183], which involves a differentiation of the data. This can be very problematic in presence of noisy input data. We adopted as a third possible method the Richardson-Lucy deconvolution [24, 95, 142]. A central requirement of this method, due to its analogy to conditional probabilities, is a normalisation of the data. A strength of this method is the presence of a regularisation that helps controlling the noise.

A first version of this iterative deconvolution approximation method is presented in Richardson 1972 [142]. There a probability technique to the restoration of noisy degraded images, another case of inverse problem, is applied. The main idea of the paper is the use of Bayes' theorem to retrieve the original image W starting from a degraded image H and a point-spread function S (PSF) treating them as discrete probability distribution functions. Bayes' theorem is formulated[2] as the conditional probability of an event W given an event H:

$$P(W|H) = \frac{P(W)P(H|W)}{P(H)}, \tag{6.3}$$

where $P(W)$ is the prior on the original image, $P(H)$ is the evidence and $P(H|W)$ is the likelihood which encapsulates the lack of knowledge about the PSF and its possible effects on the original image. Fig. 6.1 contains a schematic representation of the problem. Richardson concludes his paper by remarking that no proof of convergence has been devised but by observing that the process converged in all the cases he studied.

In [95, 96, 97] the same technique is further studied and developed by Lucy, hence the name *Richardson-Lucy* algorithm.

The ingredients required for the implementation of this method in the case of the reconstruction of the projected gravitational potential from galaxy kinematics are a line-of-sight projection $g(s)$, assumed to be related to a three-dimensional quantity $f(r)$ by

$$g(s) = \int dz\, f\left(\sqrt{s^2 + z^2}\right) = \int dr\, f(r) K(s|r) \tag{6.4}$$

with a projection kernel $K(s|r)$. As we will see in the next chapters, for $g(s)$ we will have the projected velocity dispersions along the line of sight and for $f(r)$ the three-dimensional density-weighted radial velocity dispersions. In the example reported above (see Eq. (6.3)), the projection $g(s)$ would be identified by H, $f(r)$ by W and the kernel $K(s|r)$ by the PSF.

In spherical symmetry and with the anisotropy parameter $\beta(r)$, the projection kernel for the velocity dispersion is

$$K(s|r) = \frac{2}{\pi} \frac{r}{\sqrt{r^2 - s^2}} \Theta(r^2 - s^2) \left(1 - \beta(r)\frac{s^2}{r^2}\right), \tag{6.5}$$

---

[2]We decided to use the nomenclature chosen by Richardson, even if it can be misleading. When presenting Bayes' theorem, H is often used to denote the hypothesis or the model and D is taken to identify the data. In our case the data are denoted with H and the true image with W.
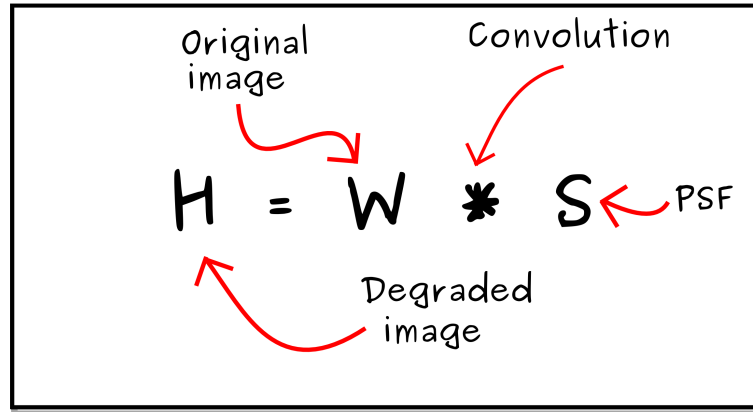
Figure 6.1: Sketch of the problem described in Richardson 1972 [142]. The paper reports about the application of probability methods to the restoration of degraded images. H is the degraded image, W is the original image, S is the point-spread function and the symbol $*$ denotes the operation of convolution.

where Θ is the Heavyside step function. For isotropic velocity dispersions or an isotropic gas pressure, the final factor in parentheses in Eq. (6.5) is unity. The kernel in Eq. (6.5) can be easily derived from Fig. 7.1 as shown by [26].

Provided that the integrals of $g(s)$, $f(r)$ and $K(s|r)$ are normalised to unity[3], the following iterative scheme ensues from Bayes' theorem (see [87, 95]):

$$\tilde{f}_{i+1}(r) = \tilde{f}_i(r) \int \mathrm{d}s \, \frac{g(s)}{\tilde{g}_i(s)} K(s|r) , \qquad (6.6)$$

where

$$\tilde{g}_i(s) = \int \mathrm{d}r \, K(s|r) \tilde{f}_i(r) . \qquad (6.7)$$

Thus, starting from a suitably guessed, normalised function $\tilde{f}_0(r)$, the scheme given by Eqs. (6.6) and (6.7) allows the recovery of the three-dimensional function $f(r)$ from its two-dimensional projection $g(s)$, assuming the spherical symmetry incorporated into the projection kernel $K(s|r)$. Experience shows that even for guess functions $\tilde{f}_0(r)$ that are wildly different from the true $f(r)$, the method converges surprisingly quickly within a few iteration steps.

The deprojection algorithm can be interpreted as the result of a maximum-likelihood problem obtained by variation,

$$\tilde{f}_{i+1}(r) = \tilde{f}_i(r) + \tilde{f}_i(r) \left[\frac{\delta H[\tilde{f}_i]}{\delta \tilde{f}_i(r)} - \int \mathrm{d}r \, \tilde{f}_i(r) \frac{\delta H[\tilde{f}_i]}{\delta \tilde{f}_i(r)} \right] , \qquad (6.8)$$

---

[3]The kernel $K(s|r)$ is normalised integrating over s.

where the functional derivatives of the functional $H[\tilde{f}]$

$$H[\tilde{f}] = \int \mathrm{d}s\, g(s) \ln \tilde{g}(s) \tag{6.9}$$

occur, where $\tilde{g}(s)$ is a functional of $\tilde{f}$ described by Eq. (6.7).

Both Richardson and Lucy observe that convergence is reached within few iterations. In order to apply this approach to realistic observational data containing small scale fluctuations due to background or instrumental noise, though, a regularisation term should be introduced as discussed in [97].

Following [97, 134, 174, 175], we introduce, therefore, a penalty functional $S[\tilde{f}]$ decreasing as $\tilde{f}$ increases in complexity and weighted with a non-negative regularisation parameter α:

$$H[\tilde{f}] \to Q[\tilde{f}] = H[\tilde{f}] + \alpha S[\tilde{f}] , \tag{6.10}$$

where α adjusts the relevance that we attribute to a simple model (large S) with respect to the goodness of our fit of the data (large H).

The penalty functional $S[\tilde{f}]$ can have the entropic form[4]:

$$S[\tilde{f}] = -\int \mathrm{d}r\, \tilde{f}(r) \ln \frac{\tilde{f}(r)}{\chi(r)} . \tag{6.11}$$

Here, $\chi(r)$ is a smooth prior function, or default solution (i.e. the solution in absence of data or in the limit $\alpha \to \infty$), chosen to suppress small-scale fluctuations. As a suitable prior, we may take the smoothed version of the deprojection result from the previous iteration step. This choice is known as floating default (see [81, 97]) and is defined by

$$\chi(r) = \int \mathrm{d}r'\, P(r|r') \tilde{f}(r') , \tag{6.12}$$

with a normalised, usually sharply peaked convolution kernel $P(r|r')$ symmetric in $r - r'$. We use a properly normalised Gaussian with a smoothing scale L,

$$P(r|r') \propto \exp\left(-\frac{(r-r')^2}{L^2}\right) . \tag{6.13}$$

It is crucial to remember that the adoption of a penalty functional and of a default solution introduces a bias in one's estimate, since its role is effectively to parametrise one's ignorance.

Replacing the variation of $H[\tilde{f}]$ in Eq. (6.8) by the variation of $Q[\tilde{f}]$ from Eq. (6.10), we obtain

$$\tilde{f}_{i+1}(r) = \tilde{f}_i(r) \left\{ \int \mathrm{d}s\, \frac{g(s)}{\tilde{g}_i(s)} K(s|r) \right. \tag{6.14}$$
$$\left. + \alpha \left[1 + S[\tilde{f}_i] + \ln\left(\frac{\tilde{f}_i(r)}{\chi_i(r)}\right) - \int \mathrm{d}r'\, \frac{\tilde{f}_i(r')}{\chi_i(r')} P(r|r') \right] \right\} ,$$

---

[4]For a panorama of suitable penalty functions, we refer the reader to Titterington 1985 [172].

which we use henceforth. Since we work with discretised data sets, the integrals in Eq. (6.14) need to be approximated by sums.

*Any coincidence is always worth notic-
ing. You can throw it away later if it is
only a coincidence.*

<div align="right">Miss J. Marple</div>

Spherical reconstruction of the lensing potential

In this chapter, we extend the reconstruction method described in Chapter 5 towards including information from galaxy kinematics. We assume that the motion of cluster member galaxies is solely determined by the dark-matter (DM) gravitational potential. The observables here are the line-of-sight velocity dispersions of the cluster galaxies as a function of cluster-centric radius. The relation between three-dimensional galaxy velocity dispersions and the dark-matter gravitational potential is governed in equilibrium by the Jeans equation (Eq. (7.5)). It resembles the equation of hydrostatic equilibrium (Eq. (5.4)), but contains an additional term that takes a possible anisotropy in the velocity distribution into account. We describe the galaxy velocity dispersions here as an effective, possibly anisotropic pressure related to the matter density by an effective polytropic relation. Under this assumption, which we find well satisfied in simulations, the effective galaxy pressure is related to the gravitational potential by a Volterra integral equation of the second kind (Eq. (6.2)), which can be solved iteratively. We can then proceed as in Sect. 5.3 and [87]: We apply the Richardson-Lucy deprojection to the observable line-of-sight velocity dispersions to obtain a three-dimensional effective galaxy-pressure profile. This is then converted to the three-dimensional potential, from which the two-dimensional potential is found by projection.

This chapter is organised as follows: We review in Sect. 7.1 the basic relations underlying our analysis, in particular our treatment of the Jeans equation. The implementation of the Richardson-Lucy deprojection method in the case of galaxy kinematics was presented in Sect. 6.2. Numerical tests of our method based on kinematic data of a numerically simulated cluster and applications to observational data are described in Sect. 7.2.

The contents of this chapter almost entirely reproduce the paper *Reconstructing the projected gravitational potential of galaxy clusters from galaxy kinematics* [Sarli et al 2014] [149]. Parts of Sect. 7.3 will be published in Stock et al. 2015 [165].
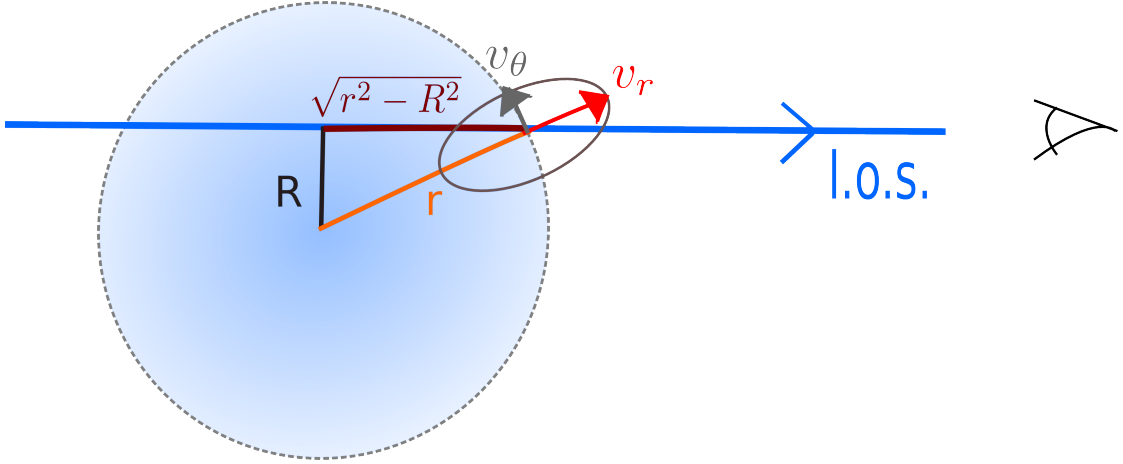
Figure 7.1: Cluster geometry (see [26]).

7.1 Recovering the projected gravitational potential from the projected velocity dispersions

7.1.1 Basic relations

To incorporate measurements of the kinematics of cluster galaxies into reconstructions of the two-dimensional gravitational potential, we first require a relation between galaxy velocity dispersions and the three-dimensional gravitational potential. The velocity dispersions are generally defined (see [26, 155]) as the mean squared deviations of the velocities of the cluster members from the mean velocity $\langle v_i \rangle$ of the population in each radial bin i:

$$\sigma_i^2 = \langle v_i^2 \rangle - \langle v_i \rangle^2 \, . \tag{7.1}$$

Measured velocity dispersions are density-weighted projections of the three-dimensional velocity dispersions along lines of sight through the cluster. Throughout this chapter, we orient the coordinate system such that the z-axis coincides with the line of sight. A projected velocity dispersion profile is constructed by averaging over concentric cylindrical shells drilled around the line of sight as a symmetry axis. This profile represents the input of our method.

The final output of our algorithm is the projected Newtonian potential of the lens, defined by

$$\psi(\vec{\theta}) = \int \phi(D_\mathrm{d}\vec{\theta}, z) \, \mathrm{d}z \, , \tag{7.2}$$

where ϕ is the three-dimensional gravitational potential of the cluster at distance D_d from the observer. The projected potential is given as a function of the two-dimensional position coordinate $\vec{\theta}$ on the sky.
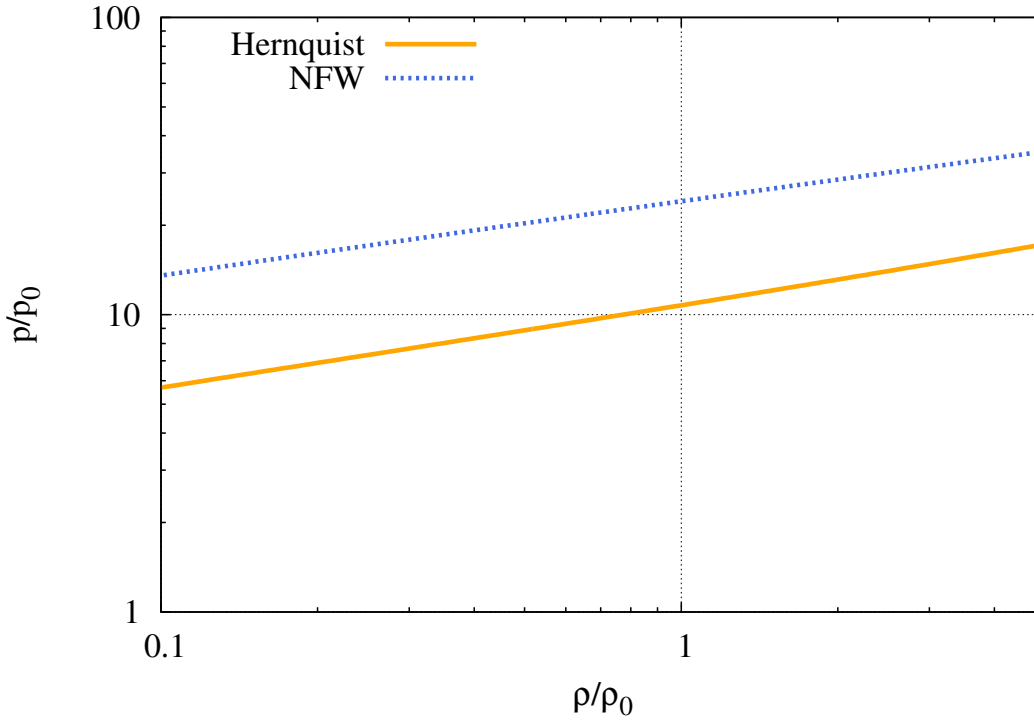
Figure 7.2: Relation (7.8) between the effective pressure and the density shown for the Hernquist (Eq. (3.8)) and NFW (Eq. (3.9)) density profiles and adopting the anisotropy parameter proposed by [79]. The very nearly straight lines (note the logarithmic axes) demonstrate that the assumption of a polytropic relation is justified.

The geometry of the problem is sketched in Fig. 7.1 (see also [26]). For simplicity during the construction of our method, we adopt a spherically-symmetric cluster model. All equations derived in the following are thus formulated in spherical coordinates.

The possible anisotropy of the velocity distribution is described by the conventional anisotropy parameter β (Eq. (4.30)) introduced in Sect. 4.2.1 and in [26],

$$\beta = 1 - \frac{\sigma_\theta^2}{\sigma_r^2} \, . \tag{7.3}$$

Our algorithm consists of three main steps:

- We deproject the observable, i.e. the velocity dispersions along the line of sight, into a deprojected quantity that, for reasons to be clarified later, is called the effective galaxy pressure P.

<div align="center">(a)   (b)</div>

Figure 7.3: (a) Surface-mass density of the simulated cluster *g1* in the *x-y* plane. (b) Two-dimensional gravitational potential obtained from the surface-density map solving Poisson's equation via fast-Fourier transform. Both images show regions with $10\,h^{-1}$Mpc side length.

- Since this effective pressure P is related to the DM gravitational potential ϕ, we can solve the Jeans equation using symmetry assumptions and a formal analogy to a polytropic gas stratification. We thus obtain a relation between the DM gravitational potential ϕ and the effective galaxy pressure. This equation is a Volterra integral equation of the second kind (Eq. (6.2)) for ϕ, which can be solved iteratively.

- Having obtained the gravitational potential, we simply project it to find the two-dimensional potential ψ.

We described our deprojection method in Sect. 6.2. The relevant three-dimen-sional quantities are the galaxy density ρ, the dark-matter density ρ_{DM}, the mean radial velocity dispersion σ_r^2 and the dark-matter gravitational potential ϕ. They are related via the Poisson and Jeans equations. In spherical symmetry, the Poisson and Jeans equations are

$$\frac{1}{r^2}\frac{\partial}{\partial r}\left(r^2\frac{\partial\phi}{\partial r}\right) = 4\pi G\rho_{DM}(r)\,, \tag{7.4}$$

and

$$\frac{1}{\rho}\frac{\partial(\rho\sigma_r^2)}{\partial r} + 2\beta\frac{\sigma_r^2}{r} = -\frac{\partial\phi}{\partial r}\,, \tag{7.5}$$

respectively. We note here that the second term on the left-hand side of Eq. (7.5) is the only formal difference to the hydrostatic equation for the hot intracluster gas (Eq. (5.4)). This difference is important because it complicates the solution of the Jeans equation considerably.

For solving the Jeans equation, we formally identify the density-weighted radial velocity dispersion $\rho\sigma_r^2$ with an effective galaxy pressure P and assume that it is related
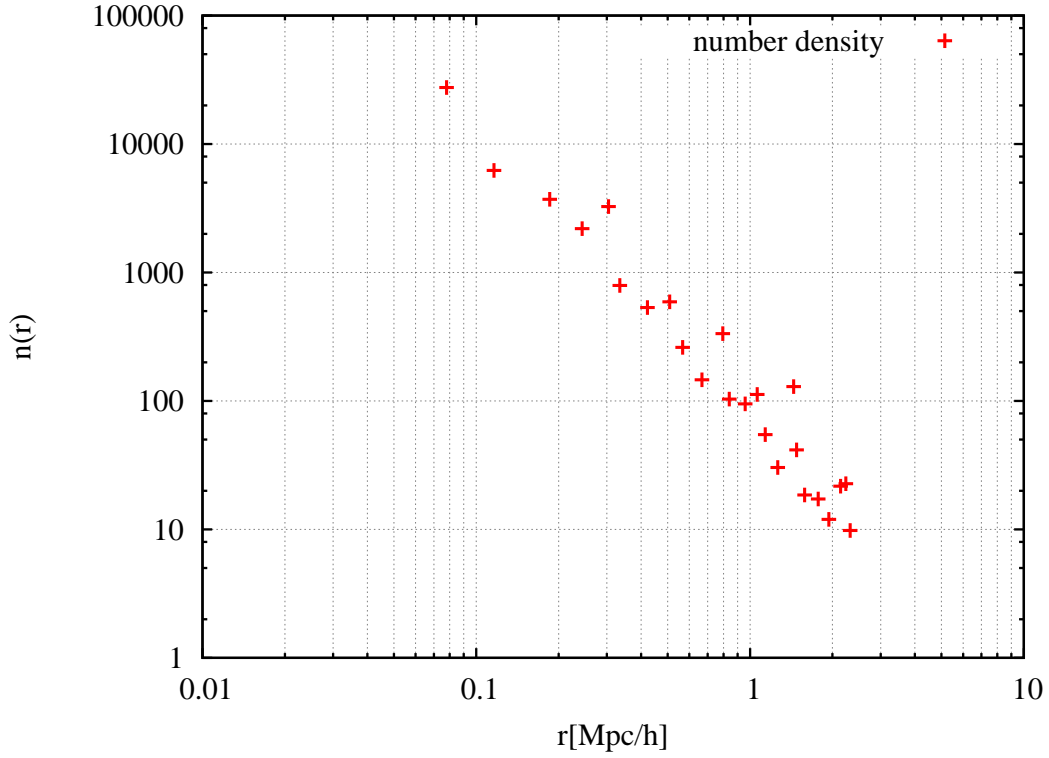
Figure 7.4: Number density profile of the simulated cluster galaxies vs. the radius. It is obtained by galaxy number counts in spherical shells.

to the density by a polytropic relation. This assumption can be justified by the following calculation.

A given radial density profile $\rho_{DM}(r)$ implies the mass profile

$$M(r) = 4\pi \int_0^r x^2 \rho_{DM}(x) \mathrm{d}x \tag{7.6}$$

and, by Poisson's equation, the gravitational-potential gradient

$$\frac{\partial \phi(r)}{\partial r} = \frac{GM(r)}{r^2} \; . \tag{7.7}$$

With this expression, the Jeans equation has the solution

$$P(r) = P_0 \exp\left(-\int_{r_0}^r \frac{2\beta}{x} \mathrm{d}x\right)$$
$$- \int_{r_0}^r \mathrm{d}y \frac{GM(y)\rho(y)}{y^2} \exp\left(\int_{r_0}^y \frac{2\beta(x)}{x} \mathrm{d}x\right), \tag{7.8}$$

where the boundary conditions are set by the pressure P_0 at the fiducial radius r_0. The fiducial pressure P_0 can be related to a fiducial density ρ_0 via the virial theorem,

$$\frac{P_0}{\rho_0} = \langle v^2 \rangle = -\phi(r_0) \quad \Rightarrow \quad P_0 = \rho_0 \int_\infty^{r_0} \frac{GM(y)}{y^2} \mathrm{d}y \, . \tag{7.9}$$

This way, the effective pressure profile of the cluster galaxies can be expressed in terms of the density and anisotropy profiles. At this point, we devise a simple way to test our assumption in which we restrict ourselves to a dissipationless case study. We evaluate Eq. (7.8) for two different mass density profiles, the Hernquist [80] and NFW [119] profiles (Eqs. (3.8) and (3.9)) described in Sect. 3.2.2, adopting the anisotropy profile derived by [79] from detailed numerical studies. As Fig. 7.2 shows, the effective pressure-density relation is nearly polytropic, i.e. an approximate power law. Thus, our assumption of an effectively polytropic galaxy stratification,

$$P = P_0 \left(\frac{\rho}{\rho_0} \right)^\gamma \, , \tag{7.10}$$

seems appropriate. In the numerical tests (see Sect. 7.2), we do not make use of the [79] profile. We instead use the anisotropy profile directly obtained from the data.

With this result, we return to the Jeans equation (7.5), where we express the density by the effective pressure by means of Eq. (7.10). For brevity, we further abbreviate

$$\epsilon = \frac{\gamma - 1}{\gamma} \, , \quad p = \frac{P}{P_0} \, , \quad \varphi = \frac{\rho_0 \epsilon}{P_0} \phi \, , \tag{7.11}$$

to cast the Jeans equation (Eq. (7.5)) into the form

$$\frac{\mathrm{d}p^\epsilon}{\mathrm{d}r} + \frac{2\epsilon\beta}{r} p^\epsilon = -\frac{\mathrm{d}\varphi}{\mathrm{d}r} \, . \tag{7.12}$$

This linear, inhomogeneous, first-order differential equation with non-constant coefficients can be solved straightforwardly, e.g. by variation of constants. The solution

$$p^\epsilon = -\varphi(r) + \exp\left(-2 \int_{r_0}^r \frac{\epsilon\beta}{x} \mathrm{d}x \right)$$
$$+ 2 \int_{r_0}^r \mathrm{d}y \frac{\epsilon\beta}{y} \varphi(y) \exp\left(2 \int_r^y \frac{\epsilon\beta}{x} \mathrm{d}x \right) \tag{7.13}$$

is the unique relation between the effective pressure and the gravitational potential we were aiming at.

Equation (7.13) is a Volterra integral equation of the second kind [2] that can be solved iteratively. In this way, we find a relation between the effective pressure p and the gravitational potential φ. Projection along the line of sight leads to the two-dimensional potential ψ.
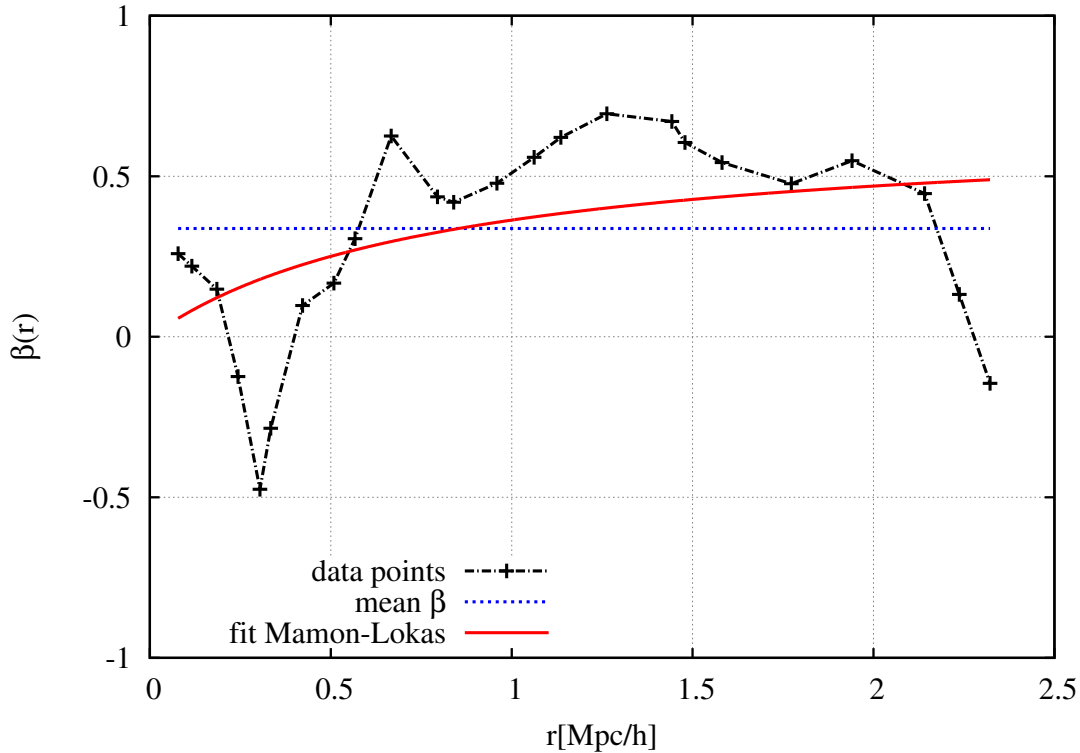
Figure 7.5: Radial profile of the anisotropy parameter $\beta(r)$ defined in Eq. (7.3), obtained from the simulated cluster data. The two-parameter model by [103] is fitted to the data points. We find $\beta_\infty = 0.66 \pm 0.36$ and $r_\beta = 0.82 \pm 1.11$.

7.2 Numerical tests

We now proceed to demonstrate that it is possible to recover the projected gravitational potential ψ of a galaxy cluster from the measured velocity dispersions projected along the line of sight. The algorithm described in Sect. 7.1.1 assumes spherical symmetry and a polytropic relation between the effective galaxy pressure and the density.

If we feed the projected velocity dispersions into the Richardson-Lucy deprojection described in Sect. 6.2, we obtain the effective pressure P related to the gravitational potential ϕ by Eq. (7.13). Once this is achieved, the gravitational potential just needs to be projected along the line of sight. We perform the reconstruction for three distinct lines of sight, chosen to be parallel to the x-, y- and z-axes respectively.
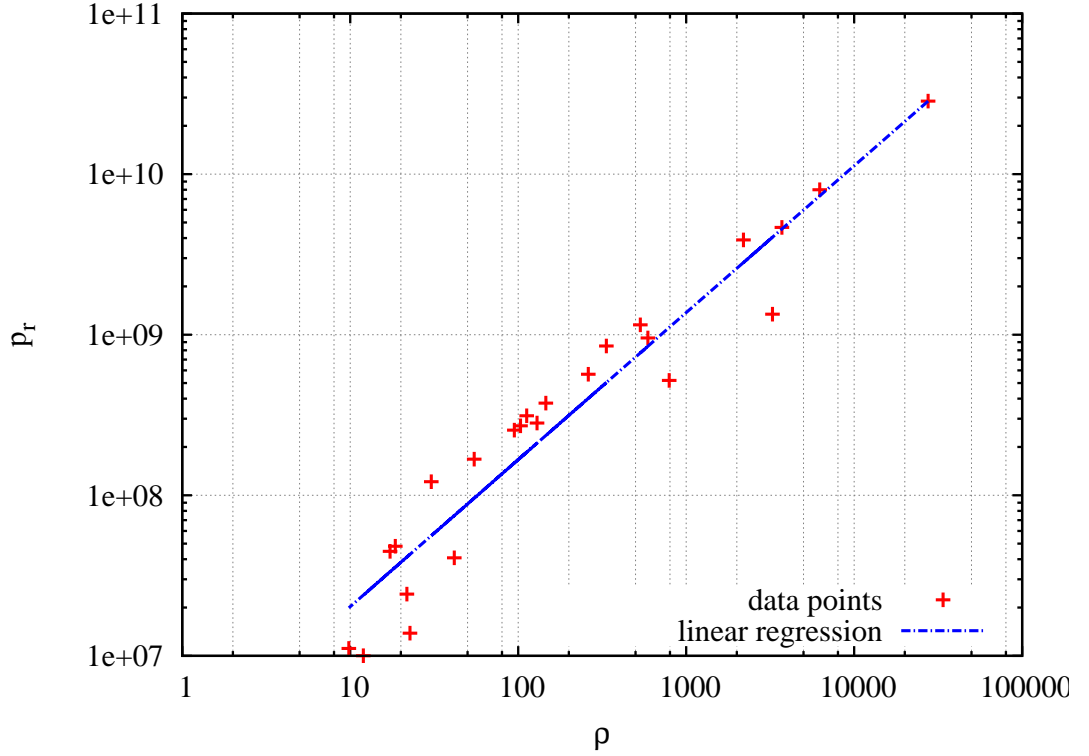
Figure 7.6: Effective galaxy pressure vs. the density. The relation is represented by a power law, supporting our assumption of an effective polytropic relation. The mean polytropic index, as derived by linear regression, is $\gamma = 0.915 \pm 0.022$.

7.2.1 The data

For testing our algorithm with simulated data, we require a velocity-dispersion profile projected along the line of sight and a two-dimensional gravitational potential obtained independently. We obtain such data from one of the clusters (denoted *g1*) in the hydrodynamically simulated sample described in [150] and used previously in [106]. The *g1* cluster has a virial mass $M_{200} = 1.14 \times 10^{15} \, h^{-1} M_\odot$ and is located at a redshift z = 0.297. We start from a catalogue listing the Cartesian coordinates and the three Cartesian velocity components of simulation particles tracking the motion of cluster galaxies. All information necessary for the kinematic analysis described in Sect. 7.2.2 can be extracted from this catalogue.

In addition, we convert the surface-mass density of the cluster into the two-dimensional potential, solving Poisson's equation by means of a fast-Fourier transform. The surface-density map and the two-dimensional gravitational potential are shown in Fig. 7.3. Evidently, the potential is considerably smoother than the mass density.
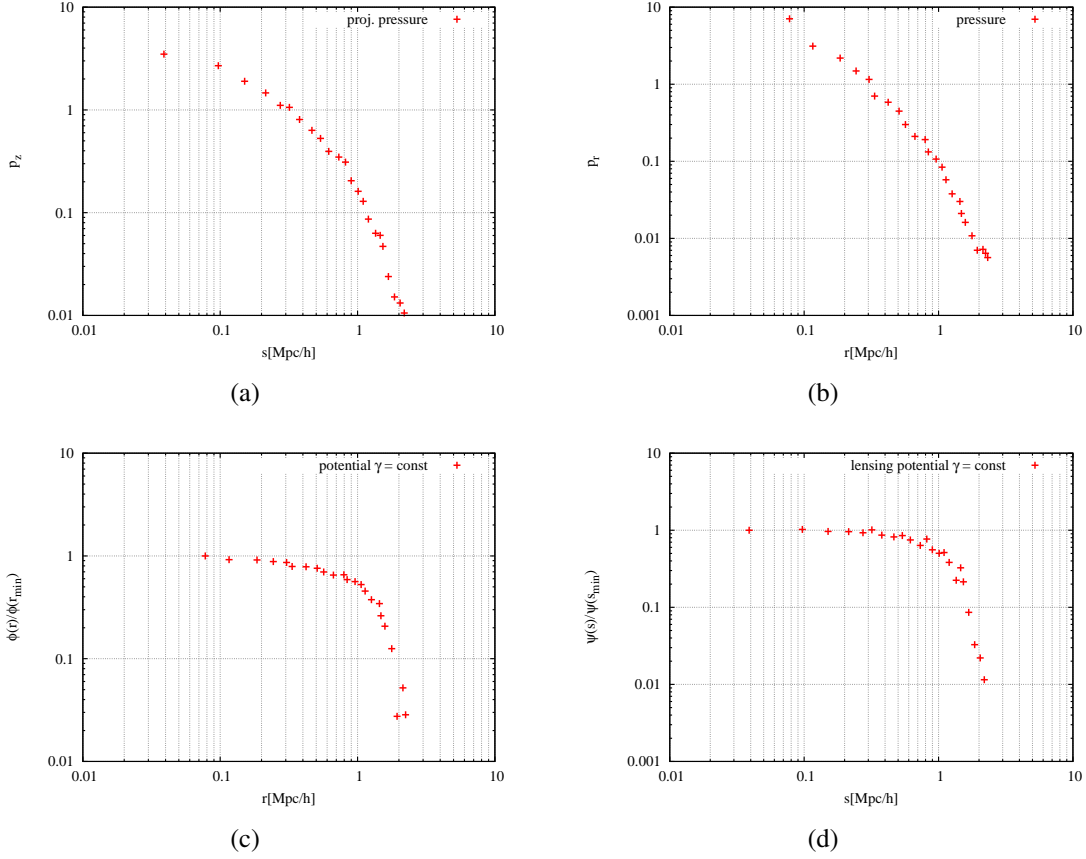
Figure 7.7: Results of the four different steps comprising our algorithm. (a) The input to our pipeline is the normalised, line-of-sight projected velocity-dispersion profile as a function of the projected radius and weighted by the galaxy number density. (b) The Richardson-Lucy deprojection algorithm yields an effective galaxy-pressure profile. (c) Solving the Volterra integral equation (Eq. (7.13)), we obtain the three-dimensional, Newtonian potential. (d) The last step consists in projecting the gravitational potential of panel (c) to find the two-dimensional potential. s_{min} is set to $0.1\,h^{-1}$Mpc, s_{max} is chosen to be $2.0\,h^{-1}$Mpc.

To enforce axial symmetry, we azimuthally average the projected gravitational potential shown in Fig. 7.3 (b) around the centre, chosen to be the point with the deepest (most negative) potential. To make it comparable to the three-dimensional gravitational potential that we reconstruct from the kinematic data, it can be passed into the RL deprojection (with $\beta = 0$) yielding the gravitational potential which can then be appropriately shifted and normalised.

7.2.2 Testing the algorithm

The assumption of spherical symmetry suggests spherical polar coordinates as a natural choice for describing the system. After transforming the velocity components to this coordinate frame, the number-density profile of the cluster galaxies is obtained within radial bins r_i centred on the cluster centre chosen to contain equal numbers of galaxies. The number counts are then converted to a number-density profile by weighting with the inverse volume of each radial shell,

$$n(r) \propto \frac{\text{counts}}{r_{i+1}^3 - r_i^3} \, .$$ (7.14)

Figure 7.4 reveals that the number-density profile for this particular cluster essentially follows a power law. In a first-order approximation that is sufficient for our purposes, galaxy biasing and variations of the galaxy mass function are neglected, allowing us to adopt the number density as a direct tracer of the mass density.

Given the number-density profile and the radial bins, a mean galaxy velocity can be obtained in each radial shell. The variance of the velocities about this mean yields the galaxy velocity-dispersion profiles σ_r^2, σ_ϕ^2 and σ_θ^2 in the radial, azimuthal and polar directions. These quantities enable us to derive the profile of the anisotropy parameter according to the definition in Eq. (7.3). The result is shown in Fig. 7.5, where we fit the two-parameter model

$$\beta(r) = \beta_\infty \frac{r}{r + r_\beta}$$ (7.15)

proposed by [103], generalised by [171] and used in [101]. This fitted profile is the best option available in the literature but the substantial scatter (also noted by [101, 182]) convinced us to use the profile-averaged mean value of β. We have also considered a linear interpolation of the data points, but this leads to unconvincing results for the gravitational potential, because the scatter in the interpolated anisotropy profile strongly affects the results of the Volterra equation.

The observed velocity dispersions are quantities projected along the line of sight and are thus implicitly weighted by the number density of galaxies along the line of sight. Therefore, we weigh the radial velocity dispersions σ_r^2 with the number density and obtain in this way the effective galaxy pressure. Projecting this quantity along the line
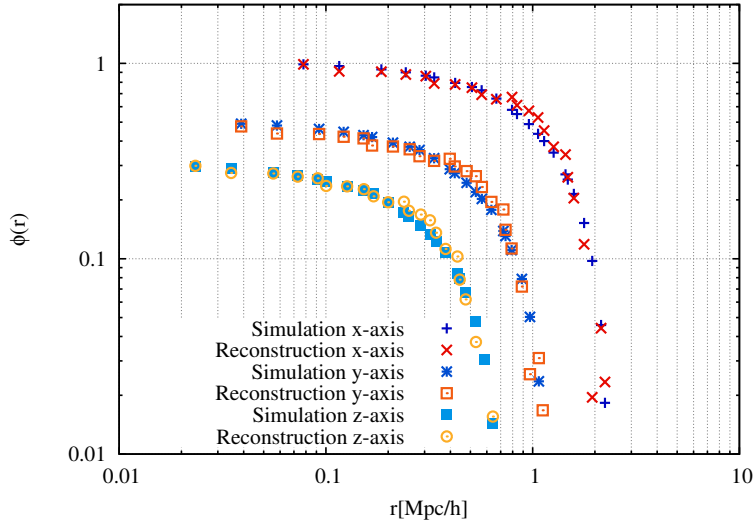
(a)
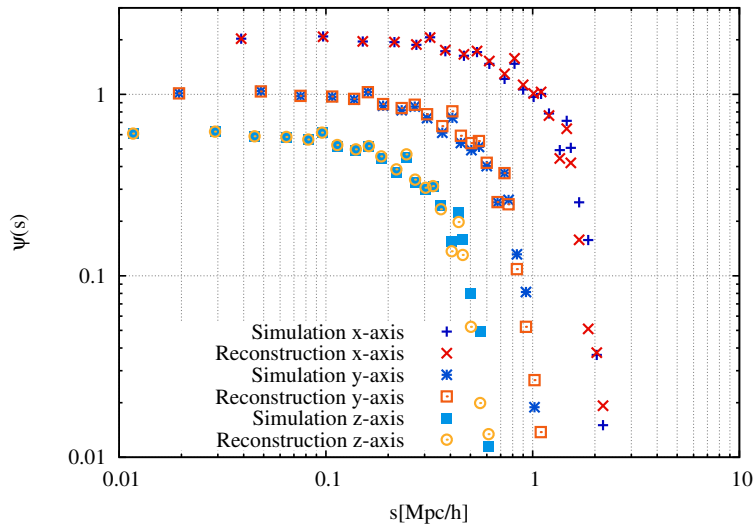
(b)

Figure 7.8: Reconstructed gravitational potentials in (a) three and (b) two dimensions are plotted as functions of radius and compared with the true potentials. In each panel, the blue, light blue and sky blue points show the true potential determined from the convergence map, while the red, orange and yellow points show the result of our reconstruction method. For better visibility, the additional point sets are multiplied by factors of 0.5 for the *y*-axis case and 0.3 for the *z*-axis case. The corresponding relative deviation as a function of radius assuming the z-axis as a line of sight is shown in Fig. 7.9.
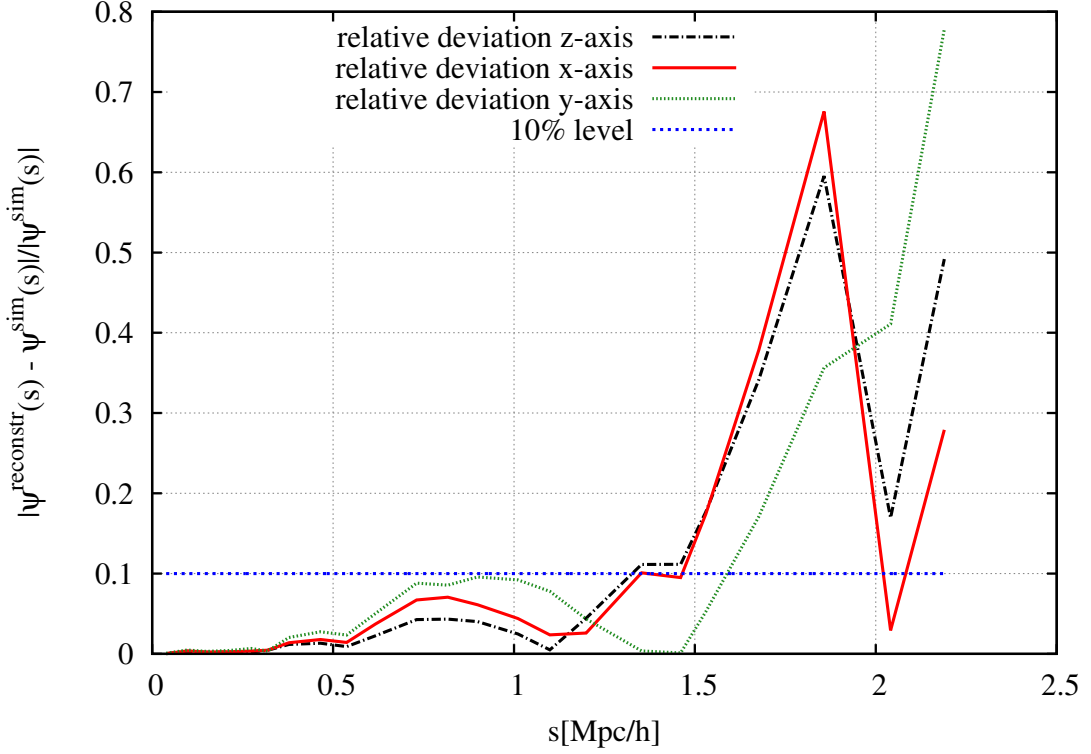
Figure 7.9: The relative deviation between the reconstructed and true two-dimensional gravitational potentials where the line of sight is taken along the z-axis is shown here as a function of distance from the cluster center. The deviation remains moderate (below 10%) within a radius of approximately $1.5\,h^{-1}$Mpc.

of sight,

$$p_z = \int_s^{r_{\max}} \mathrm{d}r\, p_r(r) K(s|r)\,, \tag{7.16}$$

with the projection kernel $K(s|r)$ defined in Eq. (6.5), we finally complete the input for our method which would be a proper observable provided by observations.

Figure 7.6 is a double-logarithmic plot of the effective galaxy pressure vs. the density, confirming that our polytropic assumption is reasonable. The mean polytropic index γ, introduced in Sect. 7.1.1, is estimated from it by linear regression.

Figure 7.7 illustrates our complete algorithm. In the top left-hand panel, we show the normalised, line-of-sight projected velocity dispersions as a function of the projected radius and weighted with the galaxy number density. In the top right-hand panel, the normalised effective pressure profile obtained from the Richardson-Lucy deprojection algorithm is displayed. We then invert Eq. (7.13) to obtain the three-dimensional, Newtonian gravitational potential shown in the bottom left-hand panel. In the bottom
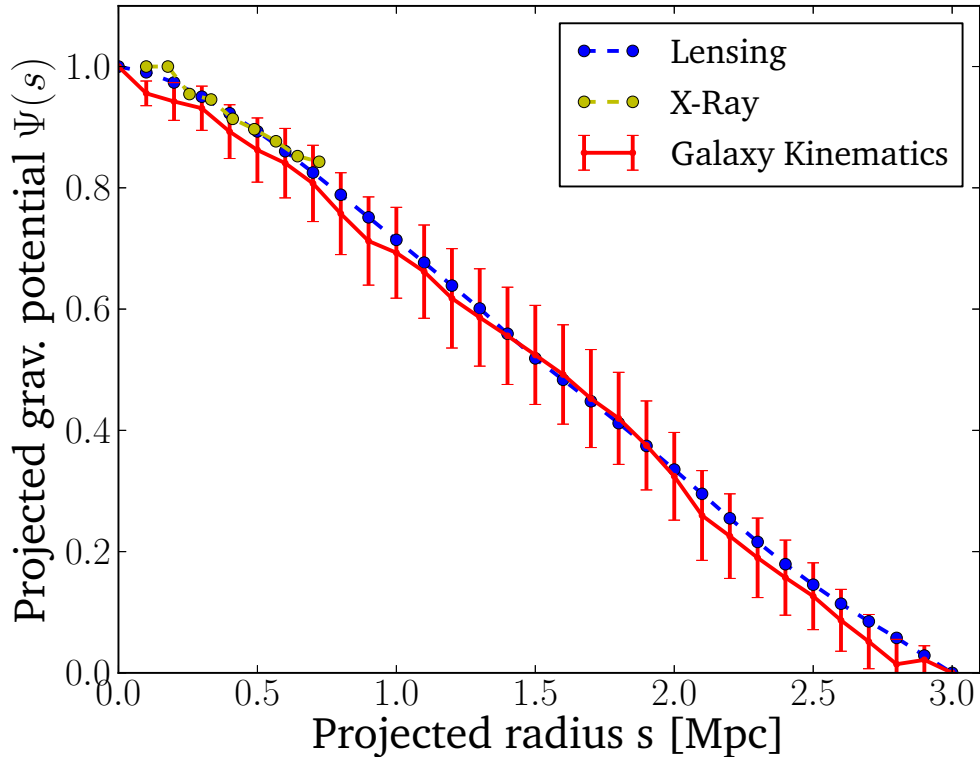
Figure 7.10: Radial profiles of the gravitational potential of MACS *J*1206, reconstructed from combined strong and weak gravitational lensing (blue), X-ray emission (yellow) and from galaxy kinematics (red) with the parameters $\alpha = 0.3$, $L = 0.6$, $\gamma = 1.1$ and β as in Eq. (7.18). [165]

right-hand panel, we finally show the derived two-dimensional gravitational potential.

Figure 7.7 provides an overview of the first test we performed on our algorithm and shows all steps needed to reconstruct the two-dimensional potential from the line-of-sight projected velocity dispersions. A comparison between our reconstructed profiles and the true three- and two-dimensional gravitational potentials is now in order. We define as "true" the potentials extracted directly from the numerically simulated cluster.

Figure 7.8 (a) shows the comparison between the reconstructed and the true gravitational potentials, while Fig. 7.8 (b) compares the reconstructed and the true projected potentials. The reconstruction was performed three times with the line of sight axis chosen to be in turn the *x*-, the *y*- and the *z*-axis. For easier comparison of both potentials, their zero points and normalisations are adjusted[1]. To be consistent with [87], we

---

[1]Note that due to the normalisation constraint of the Richardson-Lucy deprojection, we obtain a func-

decided to normalise both functions to unity and fix $\phi(r_{\max}) = 0$. In Fig. 7.9, the relative deviation

$$\Delta\psi(s) = \frac{\left|\psi^{\mathrm{reconstr}}(s) - \psi^{\mathrm{sim}}(s)\right|}{\left|\psi^{\mathrm{sim}}(s)\right|} , \tag{7.17}$$

between the reconstructed and the true two-dimensional potentials is shown as a function of projected radius. The deviation strongly increases at large radii, although it remains below 10% within $1.5\,h^{-1}\mathrm{Mpc}$, which is similar to the virial radius of the cluster.

7.3   Application to MACS $J1206.2 - 0847$

The numerical tests presented above were run on line-of-sight projected data extracted from a simulated galaxy cluster. Starting from spatial Cartesian coordinates and velocity components of a sample of member galaxies, the effective galaxy pressure was obtained by weighting the squared radial velocity dispersion with the number density. Afterwards, the required observable was constructed by projection along the line of sight. The effective polytropic index γ and the profile $\beta(r)$ of the anisotropy parameter could be easily obtained from the simulated sample. Unfortunately, neither of the last two quantities is directly accessible to observations. Therefore a method needs to be proposed that allows modelling the effective polytropic index and the anisotropy profile.

An application of the algorithm described in this chapter to the galaxy cluster MACS $J1206.2 - 0847$ was performed by Stock et al. 2015 [165].

As we have seen in the previous sections, the reconstruction method requires the setting of three parameters: the regularisation amplitude α, the smoothing scale L and the polytropic index γ. In addition, the radial profile of the anisotropy parameter $\beta(r)$ has to be modelled.

Fig. 7.10 shows the reconstructed projected gravitational potential from galaxy kinematics (in red) with the parameters $\alpha = 0.3$, $L = 0.6$, $\gamma = 1.1$. The value chosen for the polytropic index γ is motivated by the results of [149] that γ would usually be around unity, discussed in Sect. 7.2. The regularisation and reconstruction parameters are chosen such that the agreement with the lensing reconstruction is best. The $\beta(r)$ is chosen to be in agreement with the one presented in [27]:

$$\beta(r) = \begin{cases} 0.1, & \text{if } r < 0.2. \\ 0.4, & \text{if } 0.2 < r < 0.5. \\ 0.6, & \text{if } 0.5 < r < 3.0. \end{cases} \tag{7.18}$$

tion proportional to ϕ. The potential extracted from the simulation has to be normalised in the same way. Since both potentials are obtained from different datasets providing different spatial boundaries, they need to be appropriately shifted (gauged) by adding an appropriate constant.

In Sect. 4.4, we introduced the concept of *mass-anisotropy degeneracy* between the anisotropy parameter β and the gravitational potential that ensues when only kinematic data are used for the potential reconstruction. This degeneracy was lifted by fixing the β-profile in order to obtain a non-parametric estimate for the gravitational potential. To avoid an arbitrary, unmotivated guess for $\beta(r)$, it was chosen such that the reconstructed potential agrees best with a reconstruction based on gravitational-lensing data. Alternative methods for breaking the anisotropy-mass degeneracy and for recovering the gravitational potential using galaxy kinematics have been discussed in Chapter 4.

Major efforts have been undertaken in recent years to either constrain the anisotropy profile from observational and simulated data [92, 101] or to identify a general relation describing it [103, 79]. The main objective of our work is to reconstruct the projected gravitational potential of a galaxy cluster. However, we can envisage an inverse application of our algorithm. By adopting a technique similar to the one proposed in [92], it is possible to constrain $\beta(r)$ using simultaneously information from gravitational lensing and galaxy kinematics. The existence of multiple constraints on the two-dimensional potential ψ also allows developing an iterative method for constraining $\beta(r)$ and γ.

8

Ellipsoidal reconstruction of the lensing potential

In Chapter 7 we presented a method for reconstructing the projected gravitational potential of a galaxy cluster starting from a catalogue of the velocity dispersions of its members along the line-of-sight. Its main limitation lies in the assumption of sphericity of the cluster. In this chapter we present the extension of this reconstruction method to the case of a triaxial galaxy cluster.

8.1 Introduction and motivation

The main difficulty in extending our method to the case of a triaxial ellipsoid rests in the form assumed by the Jeans equation (Eq.(4.24)). Whilst in the spherical approximation presented in Chapter 7, the Jeans equation can be reduced to one radial component (Eq.(4.29)), in the ellipsoidal approximation, one has to work with a set of three components of the Jeans equation.

We have explored several possible approaches on how to further simplify the treatment of this problem. Following Chandrasekhar [40], we described a heterogeneous ellipsoid via an ellipsoidal coordinate, λ, and formulated an expression for the gravitational potential as a function of λ, with the goal of reducing our problem to one component of the Jeans equation. The major difficulty that arose is that one should assume a triaxial system in order to be able to correctly apply the definition of the ellipsoidal coordinate λ and this would further complicate the set of equations rather than simplify it. Another idea that we have investigated involves the use of methods from differential geometry: we transformed the line element of the Euclidean space to prolate spheroidal coordinates and formulated the Vlasov equation from the metric calculated in this way. By taking velocity moments of this equation we obtained the Jeans equation in the new set of coordinates (ρ, λ, φ). This procedure, though, yielded a set of two equations that appeared to be more complicated than the classic ones in cylindrical coordinates. Probably a numerical solution could be set up for the Jeans equation for a spheroid, i.e.

a rotational ellipsoid that forms when an ellipse is rotated along its major axis. This procedure would make sense if one wanted to investigate stellar kinematics in a galaxy containing millions of stars. In our case, though, it would very likely not be worth the effort since we are dealing with clusters of galaxies, which contain hundreds to thousand members in the case of rich clusters. In this case, we could calculate the velocity dispersions in at most few tens of radial bins and the resulting resolution would be too poor to solve a partial differential equation in an acceptable way.

8.2   Description of the method

A third and more successful approach is a perturbative expansion making use of the general result for the gravitational potential of a body whose equidensity surfaces are similar, coaxial ellipsoids, as presented in Binney and Tremaine [25] and Chandrasekhar [40].

On the isodensity surfaces, the variable m^2 is defined by:

$$m^2 := a_1^2 \sum_{i=1}^{3} \frac{x_i^2}{a_i^2}, \tag{8.1}$$

where $\vec{x} = (x_1, x_2, x_3)$ are Cartesian coordinates and (a_1, a_2, a_3) are the semi-axes of the ellipsoid. Without loss of generality, we set $a_3 \leq a_2 \leq a_1$. We start considering the *homoeoid theorem* extended to the case of heterogeneous ellipsoids:

Extended homoeoid theorem. *A thin shell of uniform density (homoeoid), whose inner and outer skins are the surfaces m and m + δm, generates an external potential that is constant on the ellipsoidal surfaces:*

$$m^2 := a_1^2 \sum_{i=1}^{3} \frac{x_i^2}{a_i^2 + u}, \tag{8.2}$$

where u labels the surfaces. By breaking the gravitational potential of any body in which the density is a function of m^2 only, $\rho = \rho(m^2)$, into a series of thin triaxial shells, it is thus possible to find [25]:

$$\phi(\vec{x}) = -\pi G \frac{a_2 a_3}{a_1} \int_0^{\infty} \mathrm{d}u \frac{\psi(\infty) - \psi(m^2)}{\sqrt{(u + a_1^2)(u + a_2^2)(u + a_3^2)}}, \tag{8.3}$$

where $\psi(m^2)$ is the integrated density:

$$\psi(m^2) := \int_0^{m^2} \rho(x^2)\mathrm{d}x^2. \tag{8.4}$$

We change the variable that labels the isodensity shells:

$$\tau := u/a_1^2, \tag{8.5}$$

and define the two ellipticities e_1 and e_2:

$$e_1 := \sqrt{1 - \frac{a_2^2}{a_1^2}}, \quad e_2 := \sqrt{1 - \frac{a_3^2}{a_1^2}}, \tag{8.6}$$

which are well defined for $a_3 \leq a_2 \leq a_1$. We can then rewrite the potential ϕ in the following way:

$$\phi(\vec{x}) = -\pi G \sqrt{(1 - e_1^2)(1 - e_2^2)} \int_0^\infty d\tau \frac{\psi(\infty) - \psi(m^2)}{\sqrt{(1 + \tau)(1 + \tau - e_1^2)(1 + \tau - e_2^2)}}. \tag{8.7}$$

The aim of our treatment is to find an approximate solution of the Jeans equation by expanding the gravitational potential ϕ (Eq. (8.7)) to second order in the ellipticities e_1, e_2. For readability, we define three auxiliary quantities T_1, T_2 and A:

$$T_1 := \int_0^\infty d\tau \frac{\psi(\infty)}{\sqrt{(1 + \tau)(1 + \tau - e_1^2)(1 + \tau - e_2^2)}}, \tag{8.8}$$

$$T_2(\vec{x}) := \int_0^\infty d\tau \frac{\psi(m^2)}{\sqrt{(1 + \tau)(1 + \tau - e_1^2)(1 + \tau - e_2^2)}}, \tag{8.9}$$

$$A := \sqrt{(1 - e_1^2)(1 - e_2^2)}, \tag{8.10}$$

and we rewrite the gravitational potential as:

$$\phi(\vec{x}) = -\pi G A (T_1 - T_2). \tag{8.11}$$

Since our goal is to obtain an expression of the form:

$$\phi \approx \phi|_{e_{1,2}=0} + e_1 \left. \frac{\partial \phi}{\partial e_1} \right|_{e_{1,2}=0} + e_2 \left. \frac{\partial \phi}{\partial e_2} \right|_{e_{1,2}=0}$$
$$+ \frac{e_1^2}{2} \left. \frac{\partial^2 \phi}{\partial e_1^2} \right|_{e_{1,2}=0} + \frac{e_2^2}{2} \left. \frac{\partial^2 \phi}{\partial e_2^2} \right|_{e_{1,2}=0} + e_1 e_2 \left. \frac{\partial^2 \phi}{\partial e_1 \partial e_2} \right|_{e_{1,2}=0}, \tag{8.12}$$

many terms need to be calculated to proceed further.

We start with $\phi|_{e_{1,2}=0}$:

$$\phi|_{e_{1,2}=0} = -\pi G \left[2\psi(\infty) - \int_0^\infty d\tau \frac{\psi(m^2)}{(1 - \tau)^{3/2}} \right]. \tag{8.13}$$

After some algebra, one can see that the first-order derivatives of A, T_1 and T_2 (and therefore of ϕ) with respect to the ellipticities vanish in the limit for $e_{1,2} = 0$. The same happens for the mixed derivative, i.e. the last term in the Taylor expansion.

We now want to compute the second derivatives of A, T_1 and T_2 with respect to the ellipticities in the limit for $e_{1,2} = 0$. In this limit, the second derivative of A with respect to e_1 is:

$$\frac{\partial^2 A}{\partial e_1^2}\bigg|_{e_{1,2}=0} = \frac{\partial}{\partial e_1}\left(\frac{-e_1\sqrt{1-e_2^2}}{\sqrt{1-e_1^2}}\right)\bigg|_{e_{1,2}=0} = -1, \tag{8.14}$$

In the case of T_1 we have:

$$\frac{\partial^2 T_1}{\partial e_1^2}\bigg|_{e_{1,2}=0} = \frac{2}{3}\psi(\infty), \tag{8.15}$$

and

$$\frac{\partial^2 T_1}{\partial e_2^2}\bigg|_{e_{1,2}=0} = \frac{2}{3}\psi(\infty). \tag{8.16}$$

In the case of T_2 we have:

$$\frac{\partial^2 T_2}{\partial e_1^2}\bigg|_{e_{1,2}=0} = \int_0^\infty d\tau\frac{\psi(m^2)}{(1+\tau)^{5/2}} + 2\int_0^\infty d\tau\frac{\rho(m^2)x_2^2}{(1+\tau)^{7/2}}, \tag{8.17}$$

and

$$\frac{\partial^2 T_2}{\partial e_2^2}\bigg|_{e_{1,2}=0} = \int_0^\infty d\tau\frac{\psi(m^2)}{(1+\tau)^{5/2}} + 2\int_0^\infty d\tau\frac{\rho(m^2)x_3^2}{(1+\tau)^{7/2}}. \tag{8.18}$$

Therefore, the second derivatives of ϕ with respect to the ellipticities in the limit for $e_{1,2} = 0$ are:

$$\frac{\partial^2 \phi}{\partial e_1^2}\bigg|_{e_{1,2}=0} = \pi G \int_0^\infty d\tau\frac{\psi(\infty) - \psi(m^2)}{(1+\tau)^{3/2}}$$

$$- \pi G\left(\frac{2}{3}\psi(\infty) - \int_0^\infty d\tau\frac{\psi(m^2)}{(1+\tau)^{5/2}} - 2\int_0^\infty d\tau\frac{x_2^2\rho(m^2)}{(1+\tau)^{7/2}}\right), \tag{8.19}$$

and, in a similar way,

$$\frac{\partial^2 \phi}{\partial e_2^2}\bigg|_{e_{1,2}=0} = \pi G \int_0^\infty d\tau \frac{\psi(\infty) - \psi(m^2)}{(1+\tau)^{3/2}}$$
$$- \pi G \left(\frac{2}{3}\psi(\infty) - \int_0^\infty d\tau \frac{\psi(m^2)}{(1+\tau)^{5/2}} - 2 \int_0^\infty d\tau \frac{x_3^2 \rho(m^2)}{(1+\tau)^{7/2}} \right), \tag{8.20}$$

A combination of these results with Eq. (8.13) in Eq. (8.12) gives the expansion for the gravitational potential ϕ at the second order in the ellipticities e_1, e_2:

$$\phi(\vec{x}) = \left(1 - \frac{e_1^2}{3} - \frac{e_2^2}{3} \right) \phi|_{e_{1,2}=0} + \pi G \left(\frac{e_1^2}{2} + \frac{e_2^2}{2} \right) \int_0^\infty d\tau \frac{(2-\tau)\psi(m^2)}{3(1+\tau)^{5/2}}$$
$$+ \pi G e_1^2 \int_0^\infty d\tau \frac{\rho(m^2)x_2^2}{(1+\tau)^{7/2}} + \pi G e_2^2 \int_0^\infty d\tau \frac{\rho(m^2)x_3^2}{(1+\tau)^{7/2}}, \tag{8.21}$$

where the first block incorporates the reconstruction in spherical symmetry formulated in Chapter 7, $\phi|_{e_{1,2}=0}$, and the second, third and fourth blocks represent the expansion terms.

8.3 Numerical tests

As detailed in the previous chapter, we aim at a reconstruction algorithm that takes a catalogue of velocity dispersions as an input and gives the projected gravitational potential along the line-of-sight as an output. Our main objective in this chapter is to extend the method we elaborated there for a spherical galaxy cluster to a triaxial object. Our algorithm consists of the following steps:

- Starting from a catalogue of velocity dispersions, we first reconstruct the gravitational potential ϕ of the object of interest while assuming that it has spherical symmetry with the reconstruction technique presented in Chapter 7.

- At this point, we are ready to use the expansion of the gravitational potential ϕ described by Eq. (8.21).

- The last step of our algorithm consists in projecting the gravitational potential ϕ obtained in this way along the line-of-sight to get the output we were aiming for, the two-dimensional gravitational potential ψ of the cluster.
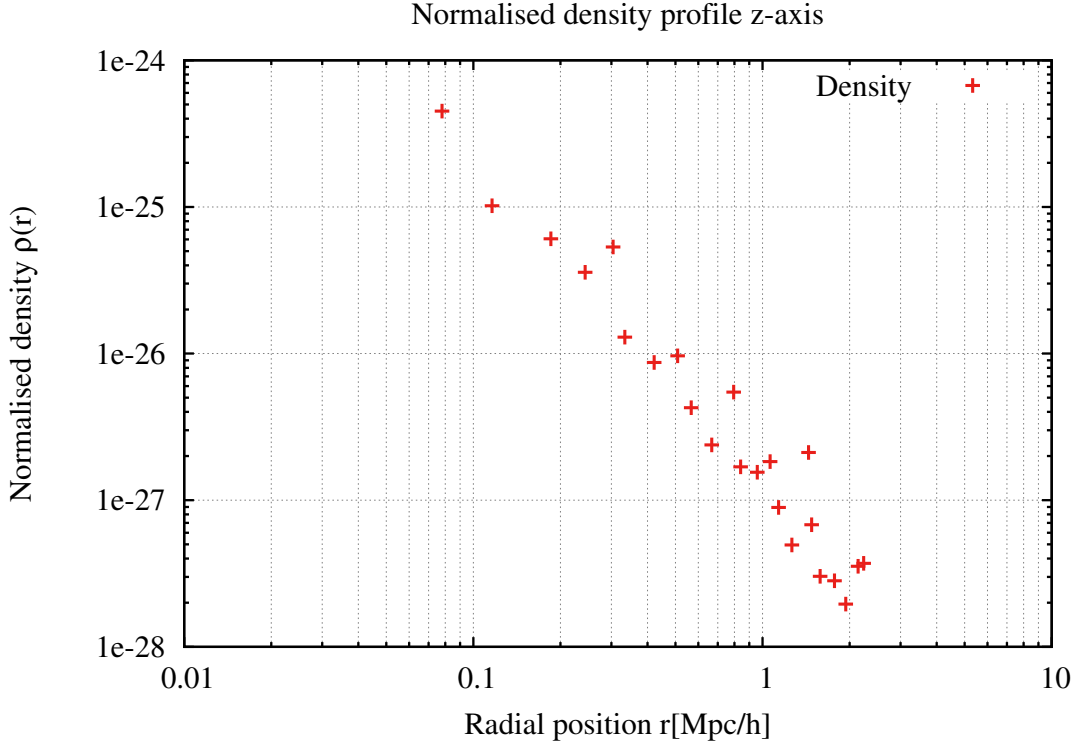
Figure 8.1: Mass density profile of the simulated cluster galaxies vs. the radius. The normalisation accounts for M_{200} of the cluster at the given redshift. It is obtained following the procedure described by Eqs. (8.22) to (8.26). The values for r_{200} and the redshift for the $g1$ cluster are specified in Table 8.1.

8.3.1 The data

In order to test our algorithm with simulated data, we need a velocity-dispersion profile projected along the line of sight and a two-dimensional gravitational potential obtained independently. We use the same data sample we adopted for testing the method in spherical approximation: we take the $g1$ cluster from [150] and [106]. All information regarding the data is presented in Sect. 7.2.1.

We perform the reconstruction for three distinct lines of sight, chosen to be parallel to the x-, y- and z-axes respectively.

8.3.2 Testing the algorithm

As mentioned at the beginning of this section, there is a number of objects that we must define before being able to implement our algorithm, the very first of which being the density of the galaxies. For our cluster of interest we are provided with the value of
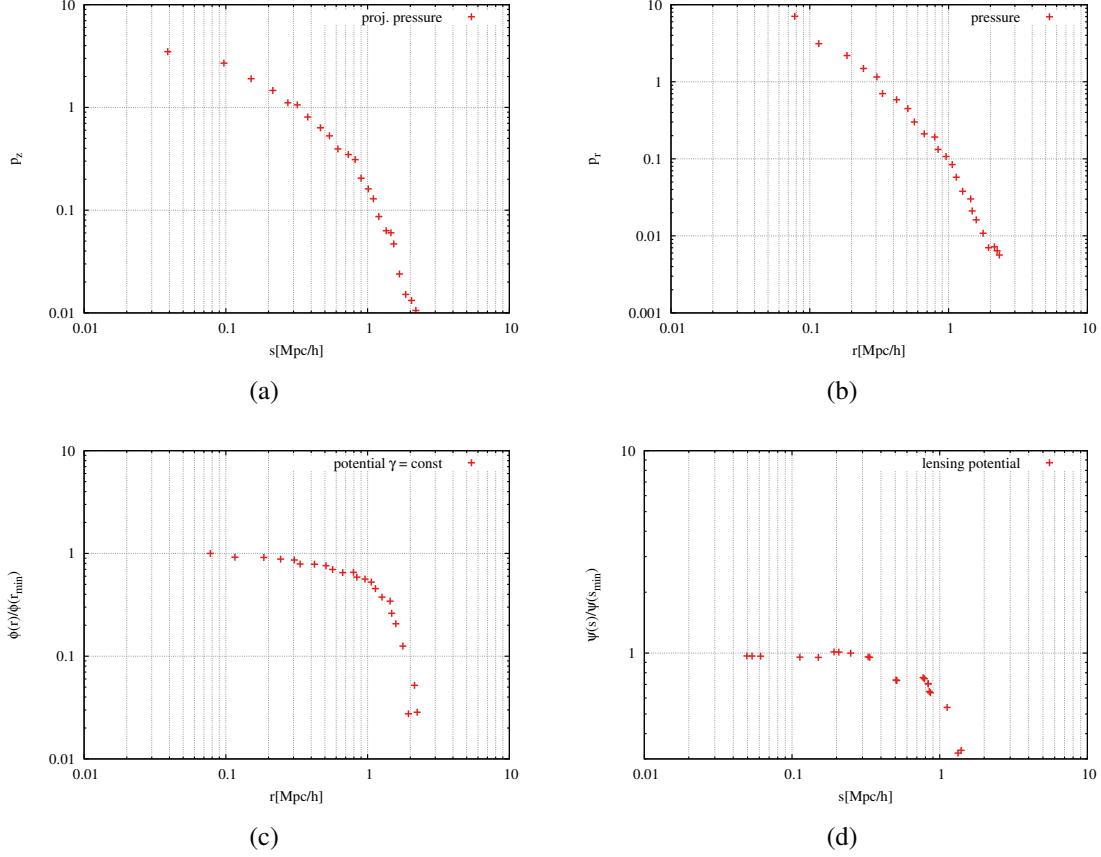
Figure 8.2: Results of the four different steps comprising our algorithm. (a) The input to our pipeline is the normalised, line-of-sight projected velocity-dispersion profile as a function of the projected radius and weighted by the galaxy number density. (b) The Richardson-Lucy deprojection algorithm yields an effective galaxy-pressure profile. (c) By solving the Volterra integral equation (Eq. (7.13)), we obtain the three-dimensional, Newtonian potential for a spherical galaxy cluster. We use the spherical gravitational potential of panel (c) in Eq. (8.21), from which we obtain the three-dimensional, Newtonian potential for a triaxial ellipsoid. (d) The last step consists in projecting the gravitational potential described by Eq. (8.21) to find the two-dimensional gravitational potential assuming an ellipsoidal geometry for the galaxy cluster.

r_{200}, i.e. the radius where the mean matter density is 200 times the critical background density of the Universe, ρ_b. We are therefore in the condition of computing the mass of the cluster contained within this radius, M_{200}:

$$M_{200} = 4\pi \int_0^{r_{200}} \mathrm{d}r r^2 \rho(r) = 4\pi\mu \int_0^{r_{200}} \mathrm{d}r r^2 \rho_{\mathrm{gal}}(r), \tag{8.22}$$

where μ is the proportionality factor that accounts for the dark-matter fraction in the cluster matter density budget and ρ_{gal} is the galaxy mass density.

Since our potential is normalised, we can assume that the galaxy density is proportional to the number density described by Eq. (7.14) taken from the spherical reconstruction and analysed in Sect. 7.2.2.

We know that by definition:

$$M_{200} = 200 \int_0^{r_{200}} \mathrm{d}r 4\pi r^2 \rho_b(r) = 200\frac{4\pi}{3} r_{200}^2 \rho_b, \tag{8.23}$$

where ρ_b is the mean density of the background and is spatially constant in a FLRW Universe:

$$\rho_b(z) = \rho_b^{(0)}(z)(1+z)^3 = \frac{3H_0^2}{8\pi\mathrm{G}}(1+z)^3, \tag{8.24}$$

with $\rho_b^{(0)}(z)$ the background density today and z the redshift of the cluster given in Table 8.1.

Equating Eqs. (8.22) and (8.23), one can solve for the proportionality factor, μ, as:

$$\mu = \frac{200\frac{4\pi}{3} r_{200}^2 \rho_b}{4\pi \int_0^{r_{200}} \mathrm{d}r r^2 \rho_{\mathrm{gal}}(r)}, \tag{8.25}$$

which allows us to compute the total dark-matter density, ρ:

$$\rho(r) = \mu\rho_{\mathrm{gal}}(r). \tag{8.26}$$

Fig. 8.1 shows the normalised density profile that we later insert into Eq. (8.21).

In order to find a suitable expression for the ellipticities e_1 and e_2, we define the inertia tensor I component-wise:

$$I_{xx} = \Sigma_{\alpha=0}^n (x_\alpha)^2 \cdot w_\alpha, \tag{8.27}$$
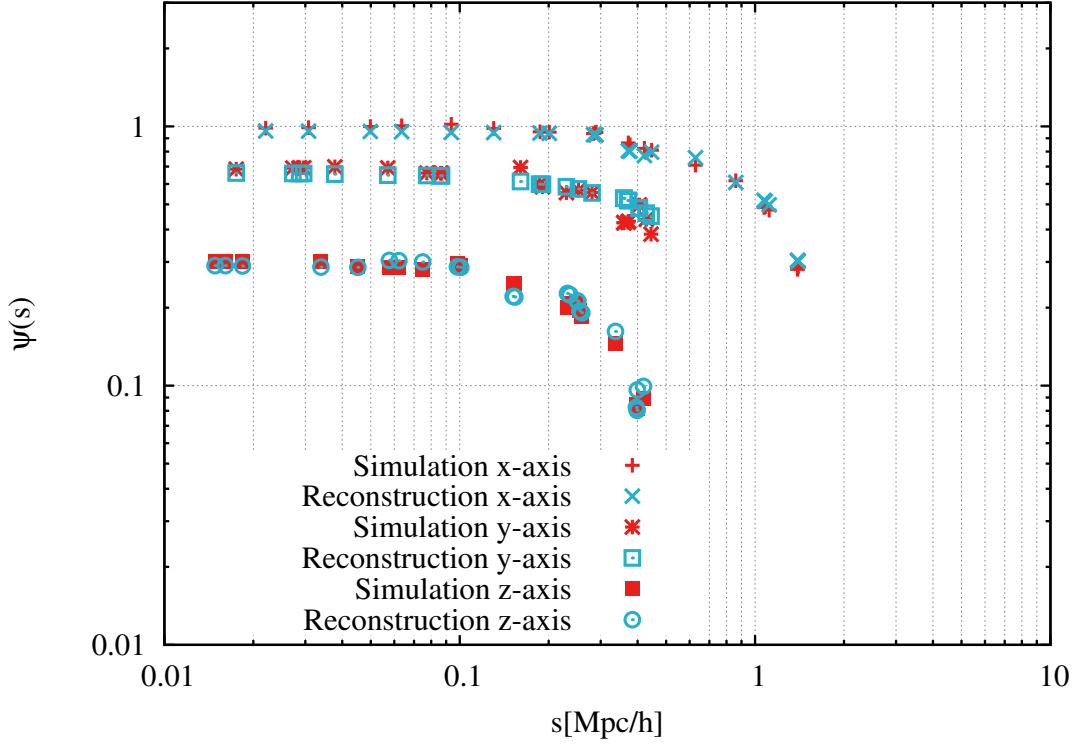$$I_{xy} = \Sigma_{\alpha=0}^n x_\alpha y_\alpha \cdot w_\alpha,$$
$$\dots$$

Figure 8.3: Reconstructed gravitational potentials in two dimensions are plotted as functions of radius and compared with the true potentials. The red points show the true potential, labeled "simulation", determined from the convergence map, while the blue points show the result of our reconstruction method. For better visibility, the additional point sets are multiplied by factors of 0.5 for the y-axis case and 0.3 for the z-axis case. The corresponding relative deviation as a function of radius assuming in turn the x-, y- and z-axis as a line of sight is shown in Fig. 8.4.

where α denotes the particle and n is the number of particles and the weight function, w_α, is chosen to be[1]:

$$w_\alpha = \exp\left\{-\frac{1}{2}\frac{r_\alpha^2}{(\frac{\text{cutoff}}{4})^2}\right\}, \tag{8.28}$$

where $r_\alpha^2 = x_\alpha^2 + y_\alpha^2 + z_\alpha^2$. The cluster parameters and their values are summarised in Tab. 8.1.

We then calculate the eigenvalues a_1, a_2, a_3 of the inertia tensor and we use them to define the ellipticities e_1, e_2 for the matter distribution according to the Eqs. (8.6). We

---

[1] We need for w_α a function that goes like a density distribution. We chose a Gaussian of the form of Eq. (8.28) and obtained a very good agreement with the axis-ratios listed in [106].

Parameter	Value
cutoff	1.5 Mpc/h
e_1	0.73382
e_2	0.934301
redshift	0.297
r_{200}	1.5 Mpc/h

Table 8.1: Values of cluster parameters.

can see in Tab. 8.1 that the values obtained for them are rather large. We can though notice that, even in case of very elliptic matter distributions, thanks to Poisson's equation and to the form of the isopotential surfaces given by the extended homoeoid theorem (Eq. (8.2)), gravitational potentials are considerably less elliptic than their sourcing density distributions.

At this stage we are ready to apply our algorithm to the sample of simulated data described in Sect. 8.3.1.

Fig. 8.2 illustrates the four different steps of our algorithm for the z-axis in the assumption of a triaxial galaxy cluster. The first three steps coincide with the procedure we adopted in Chapter 7 for a spherical cluster. The top left panel shows the input of our algorithm: the normalised, line-of-sight projected velocity dispersions as a function of the projected radius and weighted with the galaxy number density, specified by Eq. (7.16). In the top right panel, the normalised effective pressure profile obtained from the Richardson-Lucy deprojection method described in Chapter 6 is displayed. The next stage of the procedure involves inverting Eq. (7.13) to obtain the three-dimensional, Newtonian gravitational potential shown in the bottom left panel. The reconstruction of the gravitational potential we obtain in this way is then inserted into the first block of Eq. (8.21) as $\phi|_{e_{1,2}=0}$. At this point we can use all the objects obtained so far to implement the expansion of the gravitational potential to second order in the ellipticities, as detailed in Eq. (8.21). The bottom left panel displays its projection along the line-of-sight and the final goal of our work, the projected potential ψ in the assumption of a triaxial galaxy cluster.

Figure 8.2 gives an overview of the logic behind our algorithm and shows the single steps that are to be taken to reconstruct the two-dimensional potential from the line-of-sight projected velocity dispersions. A comparison between our reconstructed profiles and the true two-dimensional gravitational potentials is now in order. We call "true" the potentials extracted directly from the numerically simulated cluster. Fig. 8.3 compares the reconstructed (blue points) and the true (red points) projected potentials. The reconstruction was performed three times with the line-of-sight axis chosen to be in turn the x-, the y- and the z-axis. For easier comparison of both potentials, their zero points and normalisations are adjusted as in Chapter 7. To be consistent with [87] and [149], we
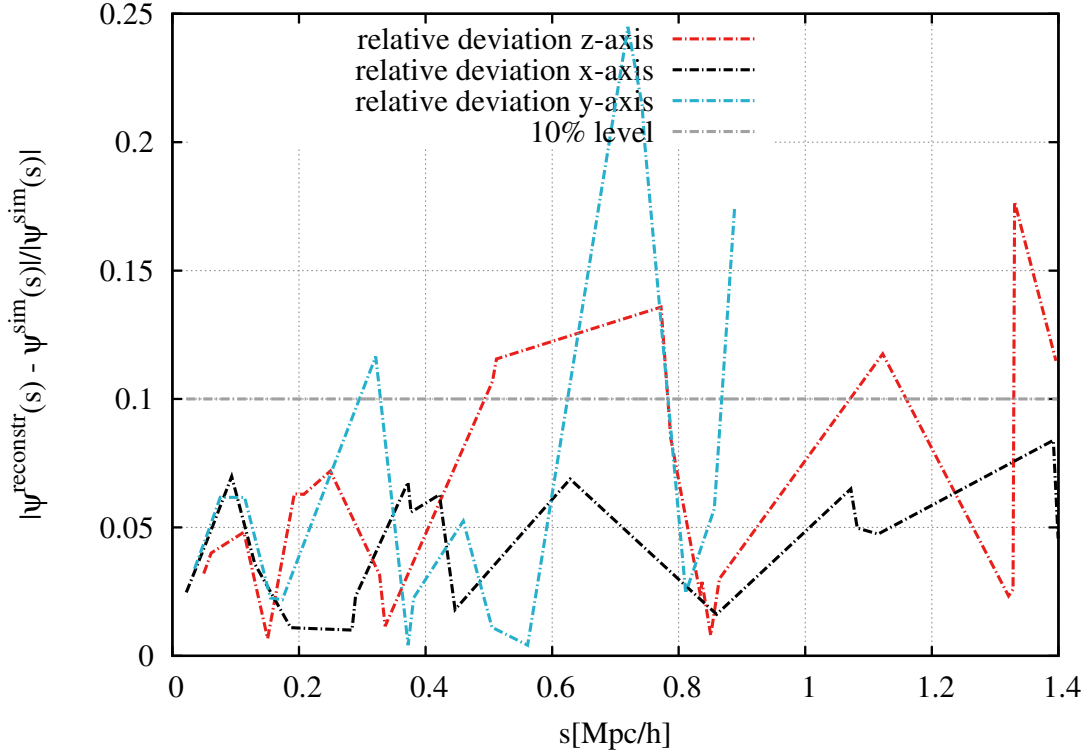
Figure 8.4: The relative deviation between the reconstructed and true two-dimensional gravitational potentials where the line of sight is taken along the x-, y- and z-axis is shown here as a function of distance from the cluster center. The deviation remains moderate (below $10\% - 25\%$) within a radius of approximately the virial radius of the cluster $1.5\,h^{-1}$Mpc for all the three cases.

decided to normalise both functions to unity and to set $\phi(r_{\max}) = 0$.

In Fig. 8.4, the relative deviation, Eq. (7.17), between the reconstructed and the true two-dimensional potentials is shown as a function of the projected radius. The deviation increases at large radii, although it remains below 25% within the virial radius of the cluster $1.5\,h^{-1}$Mpc for all the three axes and mostly below 10%. It is possible to observe a fluctuation in the reconstruction around $0.7\,h^{-1}$Mpc when taking the y-axis as the line of sight.

9

Summary and conclusions

The central question addressed in this thesis is the problem of how to reconstruct the projected gravitational potential of a galaxy cluster from the observed line-of-sight projected velocity dispersions of the cluster galaxies. We started by assuming spherical symmetry in Chapter 7 and relaxed this assumption in Chapter 8, where we presented a reconstruction algorithm valid for mildly elliptical, triaxial ellipsoids.

Chapter 5 begins by introducing the main argument on which we based our reconstruction method: clusters of galaxies exhibit a wealth of observational properties on a wide range of scales and these properties can be used to obtain further insights into the nature, structure and formation mechanisms of clusters as well as the nature of the dark matter.

It was shown that a number of these cluster observables (X-ray emission due to thermal bremsstrahlung, thermal SZ effect and galaxy kinematics) can be used to constrain the two-dimensional gravitational potential of the cluster, a quantity proportional to the lensing potential. The essential goal of our approach is to construct individual algorithms for each of these observables and to combine them at a later stage in a joint method for the reconstruction of the lensing potential of galaxy clusters that incorporates information from all the available cluster observables.

A model-free, maximum-likelihood reconstruction method, called SaWLens, combining strong- and weak-lensing information is already available and was developed in [18, 37, 109]. It is based on the minimisation of a χ^2-function composed of two contributions, one for strong and one for weak lensing. Since the individual χ^2-functions are statistically independent, they can be combined and the method extended to incorporate terms for all the cluster observables.

In Sect. 5.3 and in [87, 170], we have shown how the reconstruction of the projected gravitational potential can be achieved with one of the two cluster observables based on the hot intracluster gas, i.e. X-ray emission. An extension of our method to the thermal Sunyaev-Zel'dovich effect can be formulated in an analogous way and the fundamental steps to implement it are outlined in Sect. 5.4.

This thesis primarily focused on the formulation of an algorithm for the reconstruction of the projected gravitational potential starting from a catalogue containing the

observed line-of-sight projected velocity dispersions of the cluster members. In Chapter 7 we proposed a solution for spherical clusters that closely follows our interpretation of the observables provided by the intracluster plasma described in Sect. 5.3, but necessarily differs from it in the crucial aspect that the velocity dispersion of the cluster galaxies, unlike the gas pressure, can be anisotropic.

The algorithm we proposed rests on the following crucial assumptions. First, we assumed that the effective galaxy pressure, by which we mean the product of the galaxy number density and the local, squared radial velocity dispersion, can be related to the density itself by a polytropic relation, i.e. a power law. We tested this assumption with different density profiles and functional forms of the anisotropy parameter and found it to be satisfied. Second, by adopting this polytropic relation, we solved the radial component of the Jeans equation, relating the effective galaxy pressure to the dark-matter potential gradient. This solution can be analytically given in the form of a Volterra integral equation of the second kind for the three-dimensional gravitational potential, which can be inverted by iteration. Thus, we established a relation between the three-dimensional gravitational potential and the effective galaxy pressure.

The effective galaxy pressure itself can be obtained from the observable, density-weighted line-of-sight projected galaxy velocity dispersions by means of the Richardson-Lucy deprojection introduced in Chapt. 6. The two-dimensional gravitational potential can finally be found by straightforward projection along the line of sight.

We have tested this algorithm on a simulated galaxy cluster in which galaxies have been identified. This cluster is part of a sample of numerical hydrodynamical simulations described in [150] and used in [106]. The anisotropy profile $\beta(r)$, as well as the mean effective polytropic index γ, were obtained directly from the given member galaxy catalogue. Although these quantities can hardly be directly measured from observations, and it has up to now been impossible to give general prescriptions of their behaviour, it may well be justified to calibrate them on numerical simulations without introducing an unacceptable bias.

Fig. 7.5 shows that the anisotropy profile may be poorly constrained. The fit performed by the model suggested by [103] covers a wide range of possible behaviour. Reconstructing the two-dimensional potential based on the nominal mean value of the anisotropy profile yields a result that closely follows the numerical expectation out to $\approx 1.5\,h^{-1}$Mpc, as demonstrated by the relative deviation of the reconstructed projected gravitational potential from the true one (see Fig. 7.9). The deviation remains below 10 % in this radial range. Figure 7.6 confirms the approximate treatment of our system as a polytropic stratification.

Up to this point, we have always worked on simulated data, so we have not applied error propagation methods to our algorithm yet.

In Sect. 7.3 we showed the results of the application of the algorithm assuming spherical symmetry to the galaxy cluster MACS $J1206.2 - 0847$ performed by Stock et

al. 2015 [165] on data provided by the CLASH-VLT collaboration (see Fig. 7.10). In this publication, the propagation of errors through the Richardson-Lucy deconvolution and through our reconstruction method is investigated numerically. Within the error bars, the reconstructed potential profile is indistinguishable from the potential profile obtained from the combination of weak- and strong-gravitational lensing and from the X-ray analysis.

The main limitation of the algorithm exposed in Chapter 7 lies in the assumption of spherical symmetry. Observations and numerical simulations, instead, suggest that a triaxial ellipsoid would represent a more realistic hypothesis on the geometry of clusters of galaxies [23, 12, 77] and of the velocity field of cluster members [85, 151, 159, 173, 179].

In Chapter 8, we relaxed the assumption of sphericity and extended it to the case of an ellipsoidal body.

In contrast to stellar kinematics studies in galactic environments, the sample size of objects is considerably smaller in galaxy clusters since, in the case of spectroscopic studies of member galaxies, only a few hundred gravitationally-bound galaxies can be identified. Furthermore, in the case of a triaxial ellipsoid, we cannot yet formulate a suitable form of a polytropic equation of state for the effective pressure. We have therefore decided to approach the problem with perturbative techniques rather than pursuing a rigorous modelling in ellipsoidal geometry. Our results seem to indicate that a thorough ellipsoidal analysis might not be necessary.

Expanding the gravitational potential in the cluster's geometrical ellipticities yields second-order corrections to the spherical reconstruction. Due to Poisson's equation, gravitational potentials are considerably less elliptic than their sourcing density distributions and thus this approach seems applicable even in case of rather elliptic mass distributions.

In particular, the effects of ellipticity on the cluster potential have been investigated in the bachelor thesis of Dmitri Suharev and they were found to be minimal: the deviation from sphericity of a potential reconstructed from velocity dispersions in an axially-symmetric (rather than radially-symmetric) cluster is below $10-15\%$ for a radius larger than $0.5\,h^{-1}$Mpc for an ellipticity $e \sim 0.2-0.3$.

We tested the extended algorithm by comparing our results with the projected gravitational potential directly extracted from the surface mass density of the cluster by inverting the Poisson equation in Fourier space. The data used for this comparison are shown in Fig. 7.3. Fig. 8.3 displays the results of our comparison for the three x-, y-, z-axes taken in turn as lines of sight and Fig. 8.4 shows the corresponding relative deviation as a function of radius. From them we can see that the deviation between the reconstructed and the simulated projected potential remains moderate (below $10\%-25\%$) within a radius of approximately the virial radius $1.5\,h^{-1}$Mpc for the x-, y- and z-axis.

From the analysis presented here we can conclude that we can reconstruct the two-

dimensional, gravitational potential of a galaxy cluster starting from a catalogue of the projections along the line of sight of the velocity dispersions of its member galaxies and from the assumption of a spherical body, as discussed in Chapter 7. We can relax the assumption of sphericity later on and extend our reconstruction to the case of an ellipsoidal galaxy cluster by expanding the gravitational potential in the ellipticities for the purposes of a comparison with the projected potential derived from other observables, as detailed in Chapter 8.

As mentioned in Sect. 5.1, the final goal of the work exposed here and in the publications of several members of our group [87, 149, 170] is the combination of the algorithms presented in Chapters 5, 7 and 8 to allow a single, joint reconstruction of the two-dimensional potential of galaxy clusters using lensing, X-ray, thermal SZ effect and kinematic data.

A quantitative statement about the relative performance of the individual and joint methods we propose is intrinsically bound to the quality of the data sets that will be used to do the analysis and to the assumptions entering in the model. However, we can envisage at least three possible applications of the combination of potentials derived from them. First, especially in clusters at low redshift, the gravitational potential obtained from galaxy dynamics will extend to larger scales than the potential from gravitational lensing. In order to recover the radial profile of the matter distribution and to measure scale radii accurately, long lever arms are needed, and galaxy dynamics adds information from intermediate to large radii. Second, the dynamics of mass-less compared to the dynamics of massive particles tests the theory of gravity. Therefore, combinations of potentials reconstructed from lensing and from galaxy dynamics may be particularly important for this purpose if the individual potentials can be reconstructed accurately enough. Third, among the observables which cluster potentials can be recovered from, strong and weak lensing neither need mechanical nor hydrostatic nor thermal equilibrium, galaxy dynamics needs mechanical equilibrium, and the X-ray emission and the thermal SZ effect additionally need hydrodynamical and thermal equilibrium. Comparing the results will directly allow testing these equilibrium conditions.

Acknowledgements

You'll need coffee shops and sunsets and roadtrips. Airplanes and passports and new songs and old songs, but people more than anything else. You will need other people and you will need to be that other person to someone else - a living, breathing, screaming invitation to believe better things.

J. Tworkowski

When I began working on my Ph.D. project in July 2011, I knew it would have been a long journey. I knew that in the following three years I would have many exciting moments and I guessed I would also live many, many frustrating days. This is somehow what one expects from a Ph.D. programme: to learn a lot of new things and to learn that it takes a good deal of patience and determination to obtain some results. What I did not fully take into consideration was life. It did not take me three years to complete my Ph.D. It will take me four years and a half. In this amount of time my life changed forever several times.

Even though only my name appears on its cover, this thesis owes its existence to the collaboration, help, support and inspiration of many people.

First and foremost, I would like to express my gratitude to my supervisor, Matthias Bartelmann. Four years are a long time and many things have happened. Matthias' door was always open. I could not have imagined having a better supervisor, from the scientific or the personal point of view. In particular, I have to thank him for supporting me in my decision to change the direction of my thesis when I realised I did not want to continue working on the topic we had originally agreed on. His continuous guidance was precious and he was a constant source of encouragement and inspiration. He supported my visits to the University of Bologna and my research interests. His scientific curiosity, patience and enthusiasm have been an incredible example and taught me a great deal about what it means to be a scientist. On a more personal note, six years ago he introduced me to the man that later became my husband and, when I decided to take a break of fifteen months after the birth of my son, he supported me and helped me with additional funding to complete my Ph.D. thesis once I came back to work, things I am very grateful for.

I wish to thank Luca Amendola for kindly accepting to be the second referee of my thesis and for having me as a tutor in his course on general relativity a couple of years ago.

I would like to thank as well Karlheinz Meier and Volker Springel for being examiners in my Ph.D. defence and Andrea Macciò for being a member of my IMPRS thesis committee, together with Matthias and Luca.

Part of the work presented in this thesis has been carried out at the Observatory of

Acknowledgements

I would especially like to thank my dear friend and office mate, Agnese, who has been sharing all the highs and lows of the Ph.D. with me, an incredible amount of coffee and recently a good number of blank pages to write. These four years would have been way harder without her company, friendship and support.

My years at ITA have been accompanied by many enjoyable breaks. Emanuela, Anna, Agnese and Arianna made them very special moments.

Over the years, I met many good friends at ITA and ARI. Some of them are still here, some now live in other countries. I wish to thank Federica for always being there and for providing philosophical analyses of the Ph.D. life and support in written form when she cannot do it in person, Alessandra because she knows that sometimes all you need is a picture with a fluffy and furry animal, Ana for the uncountable chats and Massimo for offering me soothing words (and alcohol) when I most needed them.

Eventually I would like to thank some non-cosmologists. I thank James and Felicity for welcoming me in their home in Wales, for trying to elucidate the mystery of English punctuation rules and for initiating me to some embarassing yet legendary BBC productions.

A big thank you to the generalised Teodolinda group: Valentina, because she is always there and she shares my unhealthy passion for American TV shows; Chiara, because she made a crazy trip to Germany in order to be at my wedding; Sara, Martina and Teresa, because despite the distance they are still supporting me; Salvo, Matteo, Andrea, ing. Pensini and Massimo, because they are Teodolinde, no matter what.

A dear thought goes to my former flatmate, Maria, for all the time spent together, the support and the encouragement she always gives me.

Deep thanks also go to Mary, who is there for me since the very first day of high school, and to Daniela, who was always my friend.

Ringrazio i miei genitori, Grazia e Renato, mia sorella Giulia e mia nonna Gina che mi hanno sostenuto in questi anni di studio e di lontananza da casa.

My last words are for my two boys. Jean-Claude, I would like to say many things that don't belong here. The past years have been wonderful, full of joy, laughter and adventures. You have been close to me in the hardest and saddest moments of my life and never lost your sense of humour, even when mine was long gone. We have lived in different countries and in the same tiny village. We got married, we crossed Cuba on a not so solid-looking Chinese car, spent breakfasts talking about manifolds, literature and art and now have the funniest, loveliest baby. Waking up every morning with you two makes me immensely happy.

Bibliography

[1] L. F. Abbott and P. Sikivie. A cosmological bound on the invisible axion. *Physics Letters B*, 120:133–136, January 1983.

[2] M. Abramowitz and I. A. Stegun. *Handbook of Mathematical Functions*. 1972.

[3] R. J. Adler. *The Geometry of Random Fields*. 1981.

[4] Andreas Albrecht, Gary Bernstein, Robert Cahn, Wendy L. Freedman, Jacqueline Hewitt, Wayne Hu, John Huth, Marc Kamionkowski, Edward W. Kolb, Lloyd Knox, John C. Mather, Suzanne Staggs, and Nicholas B. Suntzeff. Report of the dark energy task force. *arXiv:astro-ph/0609591*, January 2006.

[5] R. A. Alpher, H. Bethe, and G. Gamow. The Origin of Chemical Elements. *Physical Review*, 73:803–804, April 1948.

[6] R. A. Alpher and R. C. Herman. On the Relative Abundance of the Elements. *Physical Review*, 74:1737–1742, December 1948.

[7] K. E. Andersson and G. M. Madejski. Complex Structure of Galaxy Cluster A1689: Evidence for a Merger from X-Ray Data? *ApJ*, 607:190–201, May 2004.

[8] C. Angrick and M. Bartelmann. Statistics of gravitational potential perturbations: A novel approach to deriving the X-ray temperature function. *A&A*, 494:461–470, February 2009.

[9] H. W. Babcock. The rotation of the Andromeda Nebula. *Lick Observatory Bulletin*, 19:41–51, 1939.

[10] R. Bacon, F. Simien, and G. Monnet. Anisotropic models of elliptical galaxies. I - The case of circular isophotes. *A&A*, 128:405–410, December 1983.

[11] J. N. Bahcall and C. L. Sarazin. Parameters and predictions for the X-ray emitting gas of Coma, Perseus, and Virgo. *ApJL*, 213:L99–L103, May 1977.

[12] J. Bailin and M. Steinmetz. Internal and External Alignment of the Shapes and Angular Momenta of ΛCDM Halos. *ApJ*, 627:647–665, July 2005.

[13] J. M. Bardeen, J. R. Bond, N. Kaiser, and A. S. Szalay. The statistics of peaks of Gaussian random fields. *ApJ*, 304:15–61, May 1986.

[14] M. Bartelmann. Theoretical Astrophysics: An Introduction. Wiley, September 2013.

[15] M. Bartelmann, M. Limousin, M. Meneghetti, and R. Schmidt. Internal Cluster Structure. *Space Science Reviews*, 177:3–29, August 2013.

[16] M. Bartelmann and P. Schneider. Weak gravitational lensing. *Physics Reports*, 340:291–472, January 2001.

[17] Matthias Bartelmann. TOPICAL REVIEW gravitational lensing. *Classical and Quantum Gravity*, 27:3001, December 2010.

[18] Matthias Bartelmann, Ramesh Narayan, Stella Seitz, and Peter Schneider. Maximum-likelihood cluster reconstruction. *ApJL*, 464:L115, June 1996.

[19] C. L. Bennett, D. Larson, J. L. Weiland, N. Jarosik, G. Hinshaw, N. Odegard, K. M. Smith, R. S. Hill, B. Gold, M. Halpern, E. Komatsu, M. R. Nolta, L. Page, D. N. Spergel, E. Wollack, J. Dunkley, A. Kogut, M. Limon, S. S. Meyer, G. S. Tucker, and E. L. Wright. Nine-year Wilkinson Microwave Anisotropy Probe (WMAP) Observations: Final Maps and Results. *ApJS*, 208:20, October 2013.

[20] G. Berkeley. *Berkeley's Philosophical Writings - De Motu*. New York: Collier, 1974.

[21] B. Bertotti, R. Balbinot, S. Bergia, and A. Messina. *Modern Cosmology in Retrospect*. May 1991.

[22] F. Bessell. On the variations of the proper motions of Procyon and Sirius. *MNRAS*, 6:136–141, December 1844.

[23] B. Binggeli. The shape and orientation of clusters of galaxies. *A&A*, 107:338–349, March 1982.

[24] J. Binney and G. A. Mamon. M/L and velocity anisotropy from observations of spherical galaxies, or must M87 have a massive black hole. *MNRAS*, 200:361–375, July 1982.

[25] J. Binney and S. Tremaine. *Galactic dynamics*. 1987.

[26] James Binney and Scott Tremaine. *Galactic dynamics*. 1987.

[27] A. Biviano, P. Rosati, I. Balestra, A. Mercurio, M. Girardi, M. Nonino, C. Grillo, M. Scodeggio, D. Lemze, D. Kelson, K. Umetsu, M. Postman, A. Zitrin, O. Czoske, S. Ettori, A. Fritz, M. Lombardi, C. Maier, E. Medezinski, S. Mei, V. Presotto, V. Strazzullo, P. Tozzi, B. Ziegler, M. Annunziatella, M. Bartelmann, N. Benitez, L. Bradley, M. Brescia, T. Broadhurst, D. Coe, R. Demarco,

M. Donahue, H. Ford, R. Gobat, G. Graves, A. Koekemoer, U. Kuchner, P. Melchior, M. Meneghetti, J. Merten, L. Moustakas, E. Munari, E. Regős, B. Sartoris, S. Seitz, and W. Zheng. CLASH-VLT: The mass, velocity-anisotropy, and pseudo-phase-space density profiles of the $z = 0.44$ galaxy cluster MACS J1206.2-0847. *A&A*, 558:A1, October 2013.

[28] A. Biviano and P. Salucci. The radial profiles of the different mass components in galaxy clusters. *A&A*, 452:75–81, June 2006.

[29] G. R. Blumenthal, H. Pagels, and J. R. Primack. Galaxy formation by dissipationless particles heavier than neutrinos. *Nature*, 299:37, September 1982.

[30] J. R. Bond, S. Cole, G. Efstathiou, and N. Kaiser. Excursion set mass functions for hierarchical Gaussian fluctuations. *ApJ*, 379:440–460, October 1991.

[31] J. R. Bond and G. Efstathiou. The statistics of cosmic background radiation fluctuations. *MNRAS*, 226:655–687, June 1987.

[32] J. R. Bond, A. S. Szalay, and M. S. Turner. Formation of galaxies in a gravitino-dominated universe. *Physical Review Letters*, 48:1636–1639, June 1982.

[33] M. Bradač, P. Schneider, M. Lombardi, and T. Erben. Strong and weak lensing united. *A&A*, 437:39–48, July 2005.

[34] M. Bradač, M. Lombardi, and P. Schneider. Mass-sheet degeneracy: Fundamental limit on the cluster mass reconstruction from statistical (weak) lensing. *A&A*, 424:13–22, September 2004.

[35] T. J. Broadhurst, A. N. Taylor, and J. A. Peacock. Mapping cluster mass distributions via gravitational lensing of background galaxies. *ApJ*, 438:49–61, January 1995.

[36] E. M. Burbidge, G. R. Burbidge, W. A. Fowler, and F. Hoyle. Synthesis of the Elements in Stars. *Reviews of Modern Physics*, 29:547–650, 1957.

[37] M. Cacciato, M. Bartelmann, M. Meneghetti, and L. Moscardini. Combining weak and strong lensing in cluster potential reconstruction. *A&A*, 458:349–356, November 2006.

[38] M. Cappellari, R. Bacon, M. Bureau, M. C. Damen, R. L. Davies, P. T. de Zeeuw, E. Emsellem, J. Falcón-Barroso, D. Krajnović, H. Kuntschner, R. M. McDermid, R. F. Peletier, M. Sarzi, R. C. E. van den Bosch, and G. van de Ven. The SAURON project - IV. The mass-to-light ratio, the virial mass estimator and the Fundamental Plane of elliptical and lenticular galaxies. *MNRAS*, 366:1126–1150, March 2006.

[39] S. M. Carroll, W. H. Press, and E. L. Turner. The cosmological constant. *Annual review of astronomy and astrophysics*, 30:499–542, 1992.

[40] S. Chandrasekhar. *Ellipsoidal figures of equilibrium*. 1969.

[41] Samuel Clarke and Gottfried Wilhelm Leibniz. *The Leibniz-Clarke Correspondence: Together Wiith Extracts from Newton's Principia and Opticks*. Manchester University Press, 1998.

[42] C. Clarkson and R. Maartens. Inhomogeneity and the foundations of concordance cosmology. *Classical and Quantum Gravity*, 27(12):124008, June 2010.

[43] Dan Coe, Keiichi Umetsu, Adi Zitrin, Megan Donahue, Elinor Medezinski, Marc Postman, Mauricio Carrasco, Timo Anguita, Margaret J. Geller, Kenneth J. Rines, Antonaldo Diaferio, Michael J. Kurtz, Larry Bradley, Anton Koekemoer, Wei Zheng, Mario Nonino, Alberto Molino, Andisheh Mahdavi, Doron Lemze, Leopoldo Infante, Sara Ogaz, Peter Melchior, Ole Host, Holland Ford, Claudio Grillo, Piero Rosati, Yolanda JimÃ©nez-Teja, John Moustakas, Tom Broadhurst, Begoña Ascaso, Ofer Lahav, Matthias Bartelmann, Narciso BenÃtez, Rychard Bouwens, Or Graur, Genevieve Graves, Saurabh Jha, Stephanie Jouvel, Daniel Kelson, Leonidas Moustakas, Dan Maoz, Massimo Meneghetti, Julian Merten, Adam Riess, Steve Rodney, and Stella Seitz. CLASH: precise new constraints on the mass profile of the galaxy cluster a2261. *ApJ*, 757:22, September 2012.

[44] M. Colless, G. Dalton, S. Maddox, W. Sutherland, P. Norberg, S. Cole, J. Bland-Hawthorn, T. Bridges, R. Cannon, C. Collins, W. Couch, N. Cross, K. Deeley, R. De Propris, S. P. Driver, G. Efstathiou, R. S. Ellis, C. S. Frenk, K. Glazebrook, C. Jackson, O. Lahav, I. Lewis, S. Lumsden, D. Madgwick, J. A. Peacock, B. A. Peterson, I. Price, M. Seaborne, and K. Taylor. The 2dF Galaxy Redshift Survey: spectra and redshifts. *MNRAS*, 328:1039–1063, December 2001.

[45] N. Cretton, P. T. de Zeeuw, R. P. van der Marel, and H.-W. Rix. Axisymmetric Three-Integral Models for Galaxies. *ApJS*, 124:383–401, October 1999.

[46] J. T. A. de Jong, G. A. Verdoes Kleijn, K. H. Kuijken, and E. A. Valentijn. The Kilo-Degree Survey. *Experimental Astronomy*, 35:25–44, January 2013.

[47] F. de Lorenzi, V. P. Debattista, and O. E. Gerhard. Dynamics of Rotating Elliptical Galaxies. In L. Stanghellini, J. R. Walsh, and N. G. Douglas, editors, *Planetary Nebulae Beyond the Milky Way*, page 311, January 2006.

[48] W. de Sitter. Einstein's theory of gravitation and its astronomical consequences. Third paper. *MNRAS*, 78:3–28, November 1917.

[49] W. de Sitter. Erratum: On Einstein's theory of gravitation and its astronomical consequences. Second paper. *MNRAS*, 77:481, March 1917.

[50] G. de Vaucouleurs. Recherches sur les Nebuleuses Extragalactiques. *Annales d'Astrophysique*, 11:247, January 1948.

[51] A. Diaferio and M. J. Geller. Infall Regions of Galaxy Clusters. *ApJ*, 481:633–643, May 1997.

[52] F. I. Diakogiannis, G. F. Lewis, and R. A. Ibata. Resolving the mass-anisotropy degeneracy of the spherically symmetric Jeans equation - I. Theoretical foundation. *MNRAS*, 443:598–609, September 2014.

[53] F. I. Diakogiannis, G. F. Lewis, and R. A. Ibata. Resolving the mass-anisotropy degeneracy of the spherically symmetric Jeans equation - II. Optimum smoothing and model validation. *MNRAS*, 443:610–623, September 2014.

[54] R. H. Dicke, P. J. E. Peebles, P. G. Roll, and D. T. Wilkinson. Cosmic Black-Body Radiation. *ApJ*, 142:414–419, July 1965.

[55] K. Dolag, M. Bartelmann, F. Perrotta, C. Baccigalupi, L. Moscardini, M. Meneghetti, and G. Tormen. Numerical study of halo concentrations in dark-energy cosmologies. *A&A*, 416:853–864, March 2004.

[56] J. Einasto. On the Construction of a Composite Model for the Galaxy and on the Determination of the System of Galactic Parameters. *Trudy Astrofizicheskogo Instituta Alma-Ata*, 5:87–100, 1965.

[57] J. Einasto, A. Kaasik, and E. Saar. Dynamic evidence on massive coronas of galaxies. *Nature*, 250:309–310, July 1974.

[58] A. Einstein. Zur Elektrodynamik bewegter Körper. *Annalen der Physik*, 322:891–921, 1905.

[59] A. Einstein. Die Feldgleichungen der Gravitation. *Sitzungsberichte der Königlich Preußischen Akademie der Wissenschaften (Berlin), Seite 844-847.*, pages 844–847, 1915.

[60] A. Einstein. Die Grundlage der allgemeinen Relativitätstheorie. *Annalen der Physik*, 354:769–822, 1916.

[61] A. Einstein. Kosmologische Betrachtungen zur allgemeinen Relativitätstheorie. *Sitzungsberichte der Königlich Preußischen Akademie der Wissenschaften (Berlin), Seite 142-152.*, pages 142–152, 1917.

[62] A. Einstein. Dialog über Einwände gegen die Relativitätstheorie. *Naturwissenschaften*, 6:697–702, November 1918.

[63] A. Einstein. Letter to Wilhelm Wien, Prague, 10 July 1912. In *Published in The Collected Papers of Albert Einstein*, volume vol. 5, page 82. Princeton, Princeton University Press, 1993.

[64] I. M. H. Etherington. On the Definition of Distance in General Relativity. *Philosophical Magazine*, 15:761, 1933.

[65] A. E. Evrard. Formation and evolution of X-ray clusters - A hydrodynamic simulation of the intracluster medium. *ApJ*, 363:349–366, November 1990.

[66] D. Fabricant, M. Lecar, and P. Gorenstein. X-ray measurements of the mass of M87. *ApJ*, 241:552–560, October 1980.

[67] E. E. Falco, M. V. Gorenstein, and I. I. Shapiro. On model-dependent bounds on H(0) from gravitational images Application of Q0957 + 561A,B. *ApJL*, 289:L1–L4, February 1985.

[68] A. Finoguenov, T. H. Reiprich, and H. Böhringer. Details of the mass-temperature relation for clusters of galaxies. *A&A*, 368:749–759, March 2001.

[69] D. J. Fixsen. The Temperature of the Cosmic Microwave Background. *ApJ*, 707:916–920, December 2009.

[70] W. Forman, C. Jones, and W. Tucker. Clusters of galaxies as a probe of the intergalactic medium. *ApJ*, 277:19–26, February 1984.

[71] B. Fort, Y. Mellier, and M. Dantel-Fort. Distribution of galaxies at large redshift and cosmological parameters from the magnification bias in CL 0024+1654. *A&A*, 321:353–362, May 1997.

[72] A. Friedmann. Über die Krümmung des Raumes. *Zeitschrift fur Physik*, 10:377–386, 1922.

[73] A. Friedmann. Über die Möglichkeit einer Welt mit konstanter negativer Krümmung des Raumes. *Zeitschrift fur Physik*, 21:326–332, December 1924.

[74] J. G. Galle. Account of the discovery of Le Verrier's planet Neptune, at Berlin, Sept. 23, 1846. *MNRAS*, 7:153, November 1846.

[75] G. Gamow. Expanding Universe and the Origin of Elements. *Physical Review*, 70:572–573, October 1946.

[76] L. Gao, J. F. Navarro, C. S. Frenk, A. Jenkins, V. Springel, and S. D. M. White. The Phoenix Project: the dark side of rich Galaxy clusters. *MNRAS*, 425:2169–2186, September 2012.

[77] S. Gottlöber and G. Yepes. Shape, Spin, and Baryon Fraction of Clusters in the MareNostrum Universe. *ApJ*, 664:117–122, July 2007.

[78] A. H. Guth. Inflationary universe: A possible solution to the horizon and flatness problems. *Phys. Rev. D*, 23:347–356, January 1981.

[79] Steen H. Hansen and Ben Moore. A universal density slope velocity anisotropy relation for relaxed structures. *New Astronomy*, 11:333–338, March 2006.

[80] Lars Hernquist. An analytical model for spherical galaxies and bulges. *ApJ*, 356:359–364, June 1990.

[81] K. Horne. Maximum entropy reconstruction of accretion disk images from eclipse data. In P. P. Eggleton and J. E. Pringle, editors, *NATO ASIC Proc. 150: Interacting Binaries*, pages 327–348, 1985.

[82] E. Hubble. A Relation between Distance and Radial Velocity among Extra-Galactic Nebulae. *Proceedings of the National Academy of Science*, 15:168–173, March 1929.

[83] A. Jenkins, C. S. Frenk, S. D. M. White, J. M. Colberg, S. Cole, A. E. Evrard, H. M. P. Couchman, and N. Yoshida. The mass function of dark matter haloes. *MNRAS*, 321:372–384, February 2001.

[84] Milan Kalal and Keith A. Nugent. Abel inversion using fast fourier transforms. *Applied Optics*, 27:1956–1959, May 1988.

[85] S. F. Kasun and A. E. Evrard. Shapes and Alignments of Galaxy Cluster Halos. *ApJ*, 629:781–790, August 2005.

[86] L. A. Kofman and A. A. Starobinskii. Effect of the Cosmological Constant on Largescale Anisotropies in the Microwave Background. *Soviet Astronomy Letters*, 11:271–274, September 1985.

[87] S. Konrad, C. L. Majer, S. Meyer, E. Sarli, and M. Bartelmann. Joint reconstruction of galaxy clusters from gravitational lensing and thermal gas. I. Outline of a non-parametric method. *A&A*, 553:A118, May 2013.

[88] PS. Laplace. Exposition du système du monde. 1795.

[89] R. Laureijs, J. Amiaux, S. Arduini, J. L. AuguÃ¨res, J. Brinchmann, R. Cole, M. Cropper, C. Dabin, L. Duvet, A. Ealet, B. Garilli, P. Gondoin, L. Guzzo, J. Hoar, H. Hoekstra, R. Holmes, T. Kitching, T. Maciaszek, Y. Mellier, F. Pasian, W. Percival, J. Rhodes, G. Saavedra Criado, M. Sauvage, R. Scaramella, L. Valenziano, S. Warren, R. Bender, F. Castander, A. Cimatti, O. Le FÃ¨vre, H. Kurki-Suonio, M. Levi, P. Lilje, G. Meylan, R. Nichol, K. Pedersen, V. Popa, R. Rebolo Lopez, H. W. Rix, H. Rottgering, W. Zeilinger, F. Grupp, P. Hudelot, R. Massey, M. Meneghetti, L. Miller, S. Paltani, S. Paulin-Henriksson, S. Pires, C. Saxton, T. Schrabback, G. Seidel, J. Walsh, N. Aghanim, L. Amendola, J. Bartlett, C. Baccigalupi, J. P. Beaulieu, K. Benabed, J. G. Cuby, D. Elbaz, P. Fosalba, G. Gavazzi, A. Helmi, I. Hook, M. Irwin, J. P. Kneib, M. Kunz, F. Mannucci, L. Moscardini, C. Tao, R. Teyssier, J. Weller, G. Zamorani, M. R. Zapatero Osorio, O. Boulade, J. J. Foumond, A. Di Giorgio, P. Guttridge, A. James, M. Kemp, J. Martignac, A. Spencer, D. Walton, T. BlÃ¼mchen, C. Bonoli, F. Bortoletto, C. Cerna, L. Corcione, C. Fabron, K. Jahnke, S. Ligori, F. Madrid, L. Martin, G. Morgante, T. Pamplona, E. Prieto, M. Riva, R. Toledo, M. Trifoglio, F. Zerbi, F. Abdalla, M. Douspis, C. Grenet, S. Borgani, R. Bouwens, F. Courbin, J. M. Delouis, P. Dubath, A. Fontana, M. Frailis, A. Grazian, J. KoppenhÃ¶fer, O. Mansutti, M. Melchior, M. Mignoli, J. Mohr, C. Neissner, K. Noddle, M. Poncet, M. Scodeggio, S. Serrano, N. Shane, J. L. Starck, C. Surace, A. Taylor, G. Verdoes-Kleijn, C. Vuerli, O. R. Williams, A. Zacchei, B. Altieri, I. Escudero Sanz, R. Kohley, T. Oosterbroek, P. Astier, D. Bacon, S. Bardelli, C. Baugh, F. Bellagamba, C. Benoist, D. Bianchi, A. Biviano, E. Branchini, C. Carbone, V. Cardone, D. Clements, S. Colombi, C. Conselice, G. Cresci, N. Deacon, J. Dunlop, C. Fedeli, F. Fontanot, P. Franzetti, C. Giocoli, J. Garcia-Bellido, J. Gow, A. Heavens, P. Hewett, C. Heymans, A. Holland, Z. Huang, O. Ilbert, B. Joachimi, E. Jennins, E. Kerins, A. Kiessling, D. Kirk, R. Kotak, O. Krause, O. Lahav, F. van Leeuwen, J. Lesgourgues, M. Lombardi, M. Magliocchetti, K. Maguire, E. Majerotto, R. Maoli, F. Marulli, S. Maurogordato, H. McCracken, R. McLure, A. Melchiorri, A. Merson, M. Moresco, M. Nonino, P. Norberg, J. Peacock, R. Pello, M. Penny, V. Pettorino, C. Di Porto, L. Pozzetti, C. Quercellini, M. Radovich, A. Rassat, N. Roche, S. Ronayette, E. Rossetti, B. Sartoris, P. Schneider, E. Semboloni, S. Serjeant, F. Simpson, C. Skordis, G. Smadja, S. Smartt, P. Spano, S. Spiro, M. Sullivan, A. Tilquin, R. Trotta, L. Verde, Y. Wang, G. Williger, G. Zhao, J. Zoubian, and E. Zucca. Euclid definition study report. *ArXiv e-prints*, 1110:3193, October 2011.

[90] G. Lemaître. Un Univers homogène de masse constante et de rayon croissant rendant compte de la vitesse radiale des nébuleuses extra-galactiques. *Annales de la Société Scientifique de Bruxelles*, 47:49–59, 1927.

[91] G. Lemaître. Expansion of the universe, A homogeneous universe of constant mass and increasing radius accounting for the radial velocity of extra-galactic nebulae. *MNRAS*, 91:483–490, March 1931.

[92] Doron Lemze, Tom Broadhurst, Yoel Rephaeli, Rennan Barkana, and Keiichi Umetsu. Dynamical study of a1689 from wide-field VLT/VIMOS spectroscopy: Mass profile, concentration parameter, and velocity anisotropy. *ApJ*, 701:1336–1346, August 2009.

[93] E. L. Łokas and G. A. Mamon. Dark matter distribution in the Coma cluster from galaxy kinematics: breaking the mass-anisotropy degeneracy. *MNRAS*, 343:401–412, August 2003.

[94] E. L. Łokas, F. Prada, R. Wojtak, M. Moles, and S. Gottlöber. The complex velocity distribution of galaxies in Abell 1689: implications for mass modelling. *MNRAS*, 366:L26–L30, February 2006.

[95] L. B. Lucy. An iterative technique for the rectification of observed distributions. *The Astronomical Journal*, 79:745, June 1974.

[96] L. B. Lucy. Astronomical Inverse Problems. In G. Klare, editor, *Reviews in Modern Astronomy*, volume 7 of *Reviews in Modern Astronomy*, pages 31–50, 1994.

[97] L. B. Lucy. Optimum strategies for inverse problems in statistical astronomy. *A&A*, 289:983–994, September 1994.

[98] J.-P. Luminet. Editorial note to: Georges Lemaître, A homogeneous universe of constant mass and increasing radius accounting for the radial velocity of extra-galactic nebulae. *General Relativity and Gravitation*, 45:1619–1633, August 2013.

[99] E. Mach. *The science of mechanics: A critical and historical account of its development.* 1960.

[100] Ernst Mach. Die geschichte und die wurzel des satzes von der erhaltung der arbeit. pages 23–29. Springer Vienna, 1964.

[101] G. A. Mamon, A. Biviano, and G. Boué. MAMPOSSt: Modelling Anisotropy and Mass Profiles of Observed Spherical Systems - I. Gaussian 3D velocities. *MNRAS*, 429:3079–3098, March 2013.

[102] G. A. Mamon and G. Boué. Kinematic deprojection and mass inversion of spherical systems of known velocity anisotropy. *MNRAS*, 401:2433–2450, February 2010.

[103] Gary A. Mamon and Ewa L. Łokas. Dark matter in elliptical galaxies - II. estimating the mass within the virial radius. *MNRAS*, 363(n):705–722, November 2005.

[104] I. G. McCarthy, R. G. Bower, and M. L. Balogh. Revisiting the baryon fractions of galaxy clusters: a comparison with WMAP 3-yr results. *MNRAS*, 377:1457–1463, June 2007.

[105] E. Medezinski, K. Umetsu, M. Nonino, J. Merten, A. Zitrin, T. Broadhurst, M. Donahue, J. Sayers, J.-C. Waizmann, A. Koekemoer, D. Coe, A. Molino, P. Melchior, T. Mroczkowski, N. Czakon, M. Postman, M. Meneghetti, D. Lemze, H. Ford, C. Grillo, D. Kelson, L. Bradley, J. Moustakas, M. Bartelmann, N. Benítez, A. Biviano, R. Bouwens, S. Golwala, G. Graves, L. Infante, Y. Jiménez-Teja, S. Jouvel, O. Lahav, L. Moustakas, S. Ogaz, P. Rosati, S. Seitz, and W. Zheng. CLASH: Complete Lensing Analysis of the Largest Cosmic Lens MACS J0717.5+3745 and Surrounding Structures. *ApJ*, 777:43, November 2013.

[106] M. Meneghetti, E. Rasia, J. Merten, F. Bellagamba, S. Ettori, P. Mazzotta, K. Dolag, and S. Marri. Weighing simulated galaxy clusters using lensing and x-ray. *A&A*, 514:93, May 2010.

[107] D. Merritt, A. W. Graham, B. Moore, J. Diemand, and B. Terzić. Empirical Models for Dark Matter Halos. I. Nonparametric Construction of Density Profiles and Comparison with Parametric Models. *The Astronomical Journal*, 132:2685–2700, December 2006.

[108] J. Merten. *An advanced method to recover the mass distribution of galaxy clusters*. PhD thesis, University of Heidelberg, 2010.

[109] J. Merten, M. Cacciato, M. Meneghetti, C. Mignone, and M. Bartelmann. Combining weak and strong cluster lensing: applications to simulations and MS 2137. *A&A*, 500:681–691, June 2009.

[110] J. Miralda-Escude and A. Babul. Gravitational Lensing in Clusters of Galaxies: New Clues Regarding the Dynamics of Intracluster Gas. *ApJ*, 449:18, August 1995.

[111] A. Monna, S. Seitz, N. Greisel, T. Eichner, N. Drory, M. Postman, A. Zitrin, D. Coe, A. Halkola, S. H. Suyu, C. Grillo, P. Rosati, D. Lemze, I. Balestra, J. Snigula, L. Bradley, K. Umetsu, A. Koekemoer, U. Kuchner, L. Moustakas, M. Bartelmann, N. Benítez, R. Bouwens, T. Broadhurst, M. Donahue, H. Ford, O. Host, L. Infante, Y. Jimenez-Teja, S. Jouvel, D. Kelson, O. Lahav, E. Medezinski, P. Melchior, M. Meneghetti, J. Merten, A. Molino, J. Moustakas, M. Nonino, and W. Zheng. CLASH: z = 6 young galaxy candidate quintuply lensed by

the frontier field cluster RXC J2248.7-4431. *MNRAS*, 438:1417–1434, February 2014.

[112] A. Morandi, K. Pedersen, and M. Limousin. Reconstructing the Triaxiality of the Galaxy Cluster A1689: Solving the X-ray and Strong Lensing Mass Discrepancy. *ApJ*, 729:37, March 2011.

[113] V. F. Mukhanov and G. V. Chibisov. Quantum fluctuations and a nonsingular universe. *ZhETF Pisma Redaktsiiu*, 33:549–553, May 1981.

[114] Ramesh Narayan and Matthias Bartelmann. Lectures on gravitational lensing. *ArXiv Astrophysics e-prints*, page 6001, June 1996.

[115] J. F. Navarro, C. S. Frenk, and S. D. M. White. Simulations of X-ray clusters. *MNRAS*, 275:720–740, August 1995.

[116] J. F. Navarro, C. S. Frenk, and S. D. M. White. The Structure of Cold Dark Matter Halos. *ApJ*, 462:563, May 1996.

[117] J. F. Navarro, C. S. Frenk, and S. D. M. White. A Universal Density Profile from Hierarchical Clustering. *ApJ*, 490:493, December 1997.

[118] J. F. Navarro, A. Ludlow, V. Springel, J. Wang, M. Vogelsberger, S. D. M. White, A. Jenkins, C. S. Frenk, and A. Helmi. The diversity and similarity of simulated cold dark matter haloes. *MNRAS*, 402:21–34, February 2010.

[119] Julio F. Navarro, Carlos S. Frenk, and Simon D. M. White. The structure of cold dark matter halos. *ApJ*, 462:563, May 1996.

[120] C. Neumann. *Ueber die Principien der Galilei-Newtonâschen Theorie.* Leipzig: B. G. Teubner, 1870.

[121] A. B. Newman, T. Treu, R. S. Ellis, and D. J. Sand. The Density Profiles of Massive, Relaxed Galaxy Clusters. II. Separating Luminous and Dark Matter in Cluster Cores. *ApJ*, 765:25, March 2013.

[122] Isaac Newton. *The Principia : Mathematical Principles of Natural Philosophy.* University of California Press, October 1999.

[123] J. H. Oort. The force exerted by the stellar system in the direction perpendicular to the galactic plane and some related problems. *Bulletin of the Astronomical Institutes of the Netherlands*, 6:249, August 1932.

[124] J. P. Ostriker, P. J. E. Peebles, and A. Yahil. The size and mass of galaxies, and the mass of the universe. *ApJL*, 193:L1–L4, October 1974.

Bibliography

[125] J. A. Peacock. *Cosmological Physics*. January 1999.

[126] P. J. E. Peebles. Large-scale background temperature and mass fluctuations due to scale-invariant primeval perturbations. *ApJL*, 263:L1–L5, December 1982.

[127] P. J. E. Peebles. Tests of cosmological models constrained by inflation. *ApJ*, 284:439–444, September 1984.

[128] P. J. E. Peebles. *Principles of Physical Cosmology*. 1993.

[129] P. J. E. Peebles. Seeing Cosmology Grow. *Annual Review of Astronomy and Astrophysics*, 50:1–28, September 2012.

[130] P. J. E. Peebles and J. T. Yu. Primeval Adiabatic Perturbation in an Expanding Universe. *ApJ*, 162:815, December 1970.

[131] E.-H. Peng, K. Andersson, M. W. Bautz, and G. P. Garmire. Discrepant Mass Estimates in the Cluster of Galaxies Abell 1689. *ApJ*, 701:1283–1299, August 2009.

[132] A. A. Penzias and R. W. Wilson. A Measurement of Excess Antenna Temperature at 4080 Mc/s. *ApJ*, 142:419–421, July 1965.

[133] S. Perlmutter, G. Aldering, G. Goldhaber, R. A. Knop, P. Nugent, P. G. Castro, S. Deustua, S. Fabbro, A. Goobar, D. E. Groom, I. M. Hook, A. G. Kim, M. Y. Kim, J. C. Lee, N. J. Nunes, R. Pain, C. R. Pennypacker, R. Quimby, C. Lidman, R. S. Ellis, M. Irwin, R. G. McMahon, P. Ruiz-Lapuente, N. Walton, B. Schaefer, B. J. Boyle, A. V. Filippenko, T. Matheson, A. S. Fruchter, N. Panagia, H. J. M. Newberg, W. J. Couch, and Supernova Cosmology Project. Measurements of Omega and Lambda from 42 High-Redshift Supernovae. *ApJ*, 517:565–586, June 1999.

[134] David L. Phillips. A technique for the numerical solution of certain integral equations of the first kind. *J. ACM*, 9(1):84–97, January 1962.

[135] Planck Collaboration, R. Adam, P. A. R. Ade, N. Aghanim, M. Arnaud, J. Aumont, C. Baccigalupi, A. J. Banday, R. B. Barreiro, J. G. Bartlett, and et al. Planck intermediate results. XXX. The angular power spectrum of polarized dust emission at intermediate and high Galactic latitudes. *ArXiv e-prints*, September 2014.

[136] Planck Collaboration, P. A. R. Ade, N. Aghanim, C. Armitage-Caplan, M. Arnaud, M. Ashdown, F. Atrio-Barandela, J. Aumont, C. Baccigalupi, A. J. Banday, and et al. Planck 2013 results. XVI. Cosmological parameters. *ArXiv e-prints*, March 2013.

126

[137] Planck Collaboration, P. A. R. Ade, N. Aghanim, C. Armitage-Caplan, M. Arnaud, M. Ashdown, F. Atrio-Barandela, J. Aumont, C. Baccigalupi, A. J. Banday, and et al. Planck 2013 results. XVI. Cosmological parameters. *A&A*, 571:A16, November 2014.

[138] Marc Postman, Dan Coe, Narciso BenÃtez, Larry Bradley, Tom Broadhurst, Megan Donahue, Holland Ford, Or Graur, Genevieve Graves, Stephanie Jouvel, Anton Koekemoer, Doron Lemze, Elinor Medezinski, Alberto Molino, Leonidas Moustakas, Sara Ogaz, Adam Riess, Steve Rodney, Piero Rosati, Keiichi Umetsu, Wei Zheng, Adi Zitrin, Matthias Bartelmann, Rychard Bouwens, Nicole Czakon, Sunil Golwala, Ole Host, Leopoldo Infante, Saurabh Jha, Yolanda Jimenez-Teja, Daniel Kelson, Ofer Lahav, Ruth Lazkoz, Dani Maoz, Curtis McCully, Peter Melchior, Massimo Meneghetti, Julian Merten, John Moustakas, Mario Nonino, Brandon Patel, EnikÃ¶ RegÃ¶s, Jack Sayers, Stella Seitz, and Arjen Van der Wel. The cluster lensing and supernova survey with hubble: An overview. *ApJS*, 199:25, April 2012.

[139] J. Preskill, M. B. Wise, and F. Wilczek. Cosmology of the invisible axion. *Physics Letters B*, 120:127–132, January 1983.

[140] W. H. Press and P. Schechter. Formation of Galaxies and Clusters of Galaxies by Self-Similar Gravitational Condensation. *ApJ*, 187:425–438, February 1974.

[141] Y. Rephaeli, S. Sadeh, and M. Shimon. The Sunyaev Zeldovich effect. *Nuovo Cimento Rivista Serie*, 29(12):1–18, December 2006.

[142] William Hadley Richardson. Bayesian-based iterative method of image restoration. *Journal of the Optical Society of America (1917-1983)*, 62:55, January 1972.

[143] A. G. Riess, A. V. Filippenko, P. Challis, A. Clocchiatti, A. Diercks, P. M. Garnavich, R. L. Gilliland, C. J. Hogan, S. Jha, R. P. Kirshner, B. Leibundgut, M. M. Phillips, D. Reiss, B. P. Schmidt, R. A. Schommer, R. C. Smith, J. Spyromilio, C. Stubbs, N. B. Suntzeff, and J. Tonry. Observational Evidence from Supernovae for an Accelerating Universe and a Cosmological Constant. *The Astronomical Journal*, 116:1009–1038, September 1998.

[144] W. Rindler. *Relativity: special, general, and cosmological.* 2001.

[145] H. P. Robertson. Kinematics and World-Structure. *ApJ*, 82:284, November 1935.

[146] M. Roncadelli. *Aspetti astrofisici della materia oscura.* Bibliopolis, 2004.

[147] Prasenjit Saha, Geoffrey V. Bicknell, and Peter J. McGregor. A varying mass-to-light ratio in the galactic center cluster? *ApJ*, 467:636, August 1996.

[148] C. L. Sarazin. X-ray emission from clusters of galaxies. *Reviews of Modern Physics*, 58:1–115, January 1986.

[149] E. Sarli, S. Meyer, M. Meneghetti, S. Konrad, C. L. Majer, and M. Bartelmann. Reconstructing the projected gravitational potential of galaxy clusters from galaxy kinematics. *A&A*, 570:A9, October 2014.

[150] A. Saro, S. Borgani, L. Tornatore, K. Dolag, G. Murante, A. Biviano, F. Calura, and S. Charlot. Properties of the galaxy population in hydrodynamical simulations of clusters. *MNRAS*, 373:397–410, November 2006.

[151] A. Saro, J. J. Mohr, G. Bazin, and K. Dolag. Toward Unbiased Galaxy Cluster Masses from Line-of-sight Velocity Dispersions. *ApJ*, 772:47, July 2013.

[152] P. Schneider. Part 1: Introduction to gravitational lensing and cosmology. In G. Meylan, P. Jetzer, P. North, P. Schneider, C. S. Kochanek, and J. Wambsganss, editors, *Saas-Fee Advanced Course 33: Gravitational Lensing: Strong, Weak and Micro*, pages 1–89, 2006.

[153] P. Schneider, J. Ehlers, and E. E. Falco. *Gravitational Lenses*. 1992.

[154] P. Schneider and C. Seitz. Steps towards nonlinear cluster inversion through gravitational distortions. 1: Basic considerations and circular clusters. *A&A*, 294:411–431, February 1995.

[155] Peter Schneider. *Extragalactic Astronomy and Cosmology: An Introduction*. Springer, 1 edition, November 2006.

[156] B. F. Schutz. *A First Course in General Relativity*. February 1985.

[157] M. Sereno, S. Ettori, K. Umetsu, and A. Baldi. Mass, shape and thermal properties of Abell 1689 using a multiwavelength X-ray, lensing and Sunyaev-Zel'dovich analysis. *MNRAS*, 428:2241–2254, January 2013.

[158] R. K. Sheth and G. Tormen. Large-scale bias and the peak background split. *MNRAS*, 308:119–126, September 1999.

[159] A. Skielboe, R. Wojtak, K. Pedersen, E. Rozo, and E. S. Rykoff. Spatial Anisotropy of Galaxy Kinematics in Sloan Digital Sky Survey Galaxy Clusters. *ApJL*, 758:L16, October 2012.

[160] V. M. Slipher. Nebulae. *Proceedings of the American Philosophical Society*, 56:403–409, 1917.

[161] S. Smith. The Mass of the Virgo Cluster. *ApJ*, 83:23, January 1936.

[162] J. Soldner. *Berliner Astron. Jahrb.*, page p. 176, 1804.

[163] J. Sommer-Larsen and M. Limousin. Moderate steepening of galaxy cluster dark matter profiles by baryonic pinching. *MNRAS*, 408:1998–2007, November 2010.

[164] V. Springel, S. D. M. White, A. Jenkins, C. S. Frenk, N. Yoshida, L. Gao, J. Navarro, R. Thacker, D. Croton, J. Helly, J. A. Peacock, S. Cole, P. Thomas, H. Couchman, A. Evrard, J. Colberg, and F. Pearce. Simulations of the formation, evolution and clustering of galaxies and quasars. *Nature*, 435:629–636, June 2005.

[165] D. Stock, S. Meyer, E. Sarli, M. Bartelmann, I. Balestra, C. Grillo, A. Koekemoer, A. Mercurio, M. Nonino, and P. Rosati. The projected gravitational potential of the galaxy cluster MACS˜J1206 derived from galaxy kinematics. *ArXiv e-prints*, July 2015.

[166] R. A. Sunyaev and I. B. Zeldovich. Microwave background radiation as a probe of the contemporary structure and history of the universe. *Annual review of astronomy and astrophysics*, 18:537–560, 1980.

[167] R. A. Sunyaev and Y. B. Zeldovich. Small scale entropy and adiabatic density perturbations - Antimatter in the Universe. *Astrophysics and Space Science*, 9:368–382, December 1970.

[168] R. A. Sunyaev and Y. B. Zeldovich. Small-Scale Fluctuations of Relic Radiation. *Astrophysics and Space Science*, 7:3–19, April 1970.

[169] A. N. Taylor, S. Dye, T. J. Broadhurst, N. Benítez, and E. van Kampen. Gravitational Lens Magnification and the Mass of Abell 1689. *ApJ*, 501:539–553, July 1998.

[170] C. Tchernin, C. L. Majer, S. Meyer, E. Sarli, D. Eckert, and M. Bartelmann. Reconstructing the projected gravitational potential of Abell 1689 from X-ray measurements. *A&A*, 574:A122, February 2015.

[171] O. Tiret, F. Combes, G. W. Angus, B. Famaey, and H. S. Zhao. Velocity dispersion around ellipticals in MOND. *A&A*, 476:L1–L4, December 2007.

[172] D. M. Titterington. General Structure of Regularization Procedures in Image Reconstruction. *A&A*, 144:381, March 1985.

[173] G. Tormen. The rise and fall of satellites in galaxy clusters. *MNRAS*, 290:411–421, September 1997.

[174] V F Turchin, V P Kozlov, and M S Malkevich. The use of mathematical-statistics methods in the solution of incorrectly posed problems. *Soviet Physics Uspekhi*, 13(6):681, 1971.

[175] S. Twomey. On the numerical solution of fredholm integral equations of the first kind by the inversion of the linear system produced by quadrature. *J. ACM*, 10(1):97–101, January 1963.

[176] A. G. Walker. On milne's theory of world-structure. *Proceedings of the London Mathematical Society*, s2-42(1):90–127, 1937.

[177] J. Wambsganss, P. Bode, and J. P. Ostriker. Gravitational Lensing in a Concordance ΛCDM Universe: The Importance of Secondary Matter along the Line of Sight. *ApJL*, 635:L1–L4, December 2005.

[178] S. Weinberg. *Gravitation and Cosmology: Principles and Applications of the General Theory of Relativity*. July 1972.

[179] M. White, J. D. Cohn, and R. Smit. Cluster galaxy dynamics and the effects of large-scale environment. *MNRAS*, 408:1818–1834, November 2010.

[180] S. D. M. White, M. Davis, G. Efstathiou, and C. S. Frenk. Galaxy distribution in a cold dark matter universe. *Nature*, 330:451–453, December 1987.

[181] S. D. M. White and R. Narayan. Maximum entropy states and the structure of galaxies. *MNRAS*, 229:103–117, November 1987.

[182] R. Wojtak, E. L. Łokas, G. A. Mamon, S. Gottlöber, A. Klypin, and Y. Hoffman. The distribution function of dark matter in massive haloes. *MNRAS*, 388:815–828, August 2008.

[183] J. Wolf, G. D. Martinez, J. S. Bullock, M. Kaplinghat, M. Geha, R. R. Muñoz, J. D. Simon, and F. F. Avedo. Accurate masses for dispersion-supported galaxies. *MNRAS*, 406:1220–1237, August 2010.

[184] S. Zibetti, S. D. M. White, D. P. Schneider, and J. Brinkmann. Intergalactic stars in z~ 0.25 galaxy clusters: systematic properties from stacking of Sloan Digital Sky Survey imaging data. *MNRAS*, 358:949–967, April 2005.

[185] A. Zitrin, W. Zheng, T. Broadhurst, J. Moustakas, D. Lam, X. Shu, X. Huang, J. M. Diego, H. Ford, J. Lim, F. E. Bauer, L. Infante, D. D. Kelson, and A. Molino. A Geometrically Supported z ~ 10 Candidate Multiply Imaged by the Hubble Frontier Fields Cluster A2744. *ApJL*, 793:L12, September 2014.

[186] F. Zwicky. Die Rotverschiebung von extragalaktischen Nebeln. *Helvetica Physica Acta*, 6:110–127, 1933.